

8-2

EXPERIMENTAL STUDY OF TWO PHASE FLOW PATTERNS
OCCURRING IN A WELL DURING PRESSURE CONTROL OPERATIONS

A Thesis

Submitted to the Graduate Faculty of the
Louisiana State University and
Agricultural and Mechanical College
in partial fulfillment of the
requirements for the degree of
Master of Science

in

The Department of Petroleum Engineering

by
Vicente Casariego G.
B.S., Universidad Nacional Autonoma de Mexico, 1969
May, 1981

TABLE OF CONTENTS

	Page
Acknowledgement	ii
List of Tables	
List of Figures	
Abstract	
Chapter	
I. Introduction	1
II. Previous Investigations	11
2.1 Flow Patterns	11
2.1.1 Extended Liquids	12
2.1.2 Tubes	13
2.1.3 Annuli	27
2.1.4 Complex Geometries	28
2.2 Bubble Rise Velocity	32
2.2.1 Extended Liquids	32
2.2.2 Tubes	43
2.2.3 Annuli	63
2.3 Liquid Holdup Correlations	72
III. Experimental Apparatus and Procedure	80
3.1 Apparatus	81
3.2 Experimental Procedure	83
3.2.1 Bubble Rise Velocity Measurements	84
3.2.2 Flow Patterns Observations	86
IV. Experimental Results	89

TABLE OF CONTENTS (continued)

	Page
4.1 Bubble Rise Velocity Measurements	91
4.1.1 Tube	91
4.1.2 Annulus	99
4.2 Flow Pattern Observations	107
4.2.1 Tube	107
4.2.2 Annulus	111
4.2.3 Annulus with Restriction	127
V. Conclusions	133
Nomenclature	134
References	139
Vita	144

LIST OF TABLES

Table		Page
4.1	Velocity of Cylindrical Bubbles in a 6.375 in Tube	92
4.2a	Velocity of Air Bubbles in an 6.375 in by 2.375 in Annulus through Quiescent Water	96
4.2b	Velocity of Air Bubbles in an 6.375 in by 2.375 in Annulus through a Quiescent 80 cp Glycerine Solution	97
4.2c	Velocity of Air Bubbles in an 6.375 in by 2.375 in Annulus through a Quiescent 146 cp Glycerine Solution	98
4.2d	Velocity of Gas Slugs in a 6.375 in by 2.375 in Annulus through a 146 cp Glycerine Solution Having an Upward Flow of 0.26 ft/sec	104
4.3	Initial Slug Length and Gas Fraction for Constant Gas Flow Rates in a Static Column of Water (6.375 in I.D. Tube)	108
4.4a	Initial Slug Length and Gas Fraction for Constant Gas Flow Rates in Static Column of Water (6.375 in by 2.375 in Annulus)	112
4.4b	Initial Slug Length and Gas Fractions for Constant Gas Flow Rates in Static Column of 80 cp Glycerine (6.375 in by 2.375 in Annulus)	113
4.4c	Initial Slug Length and Gas Fraction for Constant Gas Flow Rates in Static Column of 146 cp Glycerine (6.375 in by 2.375 in Annulus).....	114
4.5	Initial Slug Length and Gas Fraction for Constant Gas Flow Rates in a Flowing Column of 146 cp Glycerine (6.375 in by 2.375 in Annulus with $v_{sL} = .10$ ft/sec).....	115

LIST OF TABLES (continued)

Table	Page
4.6 Initial Slug Length Leaving a 4 in Restriction in an 6.375 in by 2.375 in Annulus (Static Column of 80 cp Glycerine)	130

LIST OF FIGURES

Figure		Page
1.1	History of Water Depth Record for Floating Drilling Vessels (After Harris ¹)	3
1.2	Schematic of Typical Flow Geometry Present for Deep Water Blowout Control Operations ..	4
1.3	Predicted Well Pressure Response for Example Described in Figure 1.2	7
1.4	Example of Pressure Control Training Simulators at LSU Blowout Prevention Center.	8
2.1	Typical Shapes of Air Bubbles of Several Volumes in Various Liquids (After Haberman and Morton ²)	14
2.2	Typical Shapes of Air Bubbles in Water ³	15
2.3	Flow Pattern Description for Vertical Two Phase Flow Selected by Taitel et al ⁴ ...	17
2.4	Flow Pattern Description for Vertical Two Phase Flow Used by Chierici et al ⁵	19
2.5	Flow Regime Numbers of Duns and Ross ¹⁴	22
2.6	Shape Assumed by Large Gas Bubble Rising in an Annulus ¹⁸	29
2.7	Angle Subtended of Lenticular Bubbles and Relationship between Curvature Radius and Equivalent Radius	37
2.8	Variation of Bubble Velocity with r_c/r_t After Collins	44
2.9	Values of b as a Function of Tube Diameter and Surface Tension (After Uno and Kintner ³⁴)	48
2.10	Dimensionless Constant C_1 Versus Bubble Reynolds Number (After Griffith and Wallis ⁷)	50

LIST OF FIGURES (continued)

Figure	Page
2.11 Dimensionless Constant C_2 as a Function of Liquid Reynolds Number and Bubble Reynolds Number (After Griffith and Wallis ⁷)	50
2.12 General Correlation for Velocity of Rise of Cylindrical Air Bubbles (After White and Beardmore ³⁶)	54
2.13 Bubble Velocity Vs. Surface Tension Parameter for Ranges of Reynolds Numbers (After Zukoski ¹⁷)	61
2.14 Variation of Normalized Velocity with Diameter Number for Angles of Inclination as Measured with Respect to a Horizontal Plane (After Zukoski ¹⁷)	62
2.15 Variation of $v_{bo}/v_{b\infty}$ with \bar{r}_c/r_t (After Collins).....	64
2.16 Variation of Bubble Velocity with $2 r_c/w$. (After Collins ⁴⁰)	68
2.17 Definition of Equivalent Radius and Perimeter for Plane Bubble	70
3.1 Diagram of the Model	82
3.2 Experimental Procedure Followed in Bubble Rise Velocity Measurements	85
3.3 Flow Pattern Observations	88
4.0 Definition of Velocities and Its Relationships	90
4.1 Velocity of Cylindrical Bubbles Versus Slug Length for Low and High Viscosity Liquids. Tube Diameter 6.375 in	93

LIST OF FIGURES (continued)

Figure	Page
4.2 Relationship Between v_b and v_{bo} for Ideal Slug Flow	95
4.3 Measured Bubble Velocity Versus Equivalent Diameter of the Bubbles in a 6.375 in by 2.375 in Annulus (Zero Liquid Velocity)	100
4.4 Velocity of Large Bubbles in a 6.375 in by 2.375 in Annulus. (Zero Liquid Velocity .	102
4.5 Bubble Velocity in a 6.375 in by 2.375 in Annulus through 146 cp Glycerine Solution with an Upward Flow of 0.26 ft/sec.....	105
4.6 Relationship between v_b and v_{bo} for Ideal Slug Flow in a 6.375 in by 2.375 in Annulus	106
4.7 Initial Slug Length Versus Superficial Gas Velocity in a 6.375 in Tube and Quiescent Liquids	110
4.8 Initial Gas Slug Length Versus Superficial Gas Velocity (6.375 in by 2.375 in Annulus and Quiescent Liquid)	116
4.9 Initial Gas Slug Length Versus Superficial Gas Velocity (6.375 in by 2.375 in Annulus and Liquid Velocity of 0.1 ft/sec)	118
4.10 General Plot of Initial Gas Slug Length Versus Superficial Gas Velocity. (6.375 in by 2.375 in Annulus and 6.375 in Tube)	120
4.11 Gas Fraction Versus Superficial Gas Velocity (Tube of 6.375 in I.D.)	121
4.12 Gas Fraction Versus Superficial Gas Velocity (6.375 in by 2.375 in Annulus).....	124

LIST OF FIGURES (continued)

Figure	Page
4.13 Theoretical Gas Fraction for Annular Geometries ad Predicted by Eq. 4.4	126
4.14 Flow Restriction in the 6.375 in by 2.375 in Annulus	128
4.15 Bubbles Passing through Annular Restriction	129

ABSTRACT

The control of high pressure formation fluids encountered while drilling for hydrocarbon reservoirs is one of the more expensive and potentially dangerous problems of the oil producing industry. Well control simulators are used for both evaluating well control procedures and training of drilling personnel. Unfortunately, current well control simulators assume that the gas enters a wellbore as continuous plug traveling at the same velocity of the drilling fluid, which is not always accurate. The purpose of this study is to determine bubble rise velocity relative to the drilling fluid in large annulus, gas concentration in gas contaminated region and the two phase flow patterns present when formation fluids have entered the wellbore during drilling.

The first step of the present study was a review of the literature on bubble rise velocity in both extended and bounded systems, liquid holdup correlations, and flow pattern correlations. The second step included the construction of a 22 ft long experimental model of wellbore annulus and the performance of experimental work in tubes, annulus and annulus with restriction.

As a result of the experimental work it was found that the velocity of large gas slugs relative to the liquid above the slug is not greatly influenced by viscosity; the correlation of Rader, Bourgoyne, and Ward gave good agreement with the measured gas velocities for low viscosity liquids, but underpredicted the gas slug velocities in high viscosity liquids; furthermore, a new approach was developed for computing the velocity of large gas slugs. Also, it was found that bubble flow could be the predominant flow pattern during well control operations, specially in low viscosity circulating fluids.

CHAPTER I

INTRODUCTION

One of the more expensive and potentially dangerous problems associated with the oil producing industry is the control of high pressure formation fluids encountered while drilling for hydrocarbon reservoirs. When this is not accomplished a blowout may occur. A blowout is the uncontrolled flow of formation fluids from the well during drilling operations. When this uncontrolled flow discharges to the atmosphere or seafloor, it is called a surface blowout. The uncontrolled flow of fluids from one subsurface formation, through the wellbore, to a second more shallow, subsurface formation is called an underground blowout.

Surface blowouts are extremely dangerous, frequently resulting in injury of drilling personnel, and almost always causing damage of drilling equipment and the environment. In some extreme cases, additional wells must be drilled in order to flood the high pressure formation causing the flow. On the other hand, underground blowouts are not usually as dangerous as surface blowouts, but they are more common because the flow cannot be controlled by surface blowout prevention equipment. Usually subsurface control can be

established only by sealing off the lower portion of the well. Many expensive wells have to be redrilled because of this phenomenon.

As the search for petroleum reserves has moved into the offshore environment, the blowout control problem has continued to increase in complexity. In addition, the difficulties in confining an offshore oil spill makes the environmental consequences of a blowout more important. Most modern blowout prevention equipment was largely developed for land based drilling operations. With only minor modifications, this equipment has been applied to bottom-supported exploratory drilling rigs such as jack ups and development rigs operating on an offshore platform. However, more significant modifications in blowout prevention equipment and procedures are required for floating vessels, which are used almost exclusively for deep water operations. The first major modification for deep water operation was the location of the blowout preventer stack at the seafloor rather than the surface. The current trend of the oil industry to much greater water depths (See Figure 1.1) emphasizes the importance of the blowout control problem in floating drilling vessels.

Figure 1.2 is a schematic of a typical flow geometry which would be present for blowout control operations on a floating drilling vessel in deep water. The schematic is based in part on a well drilled off the coast of Africa in

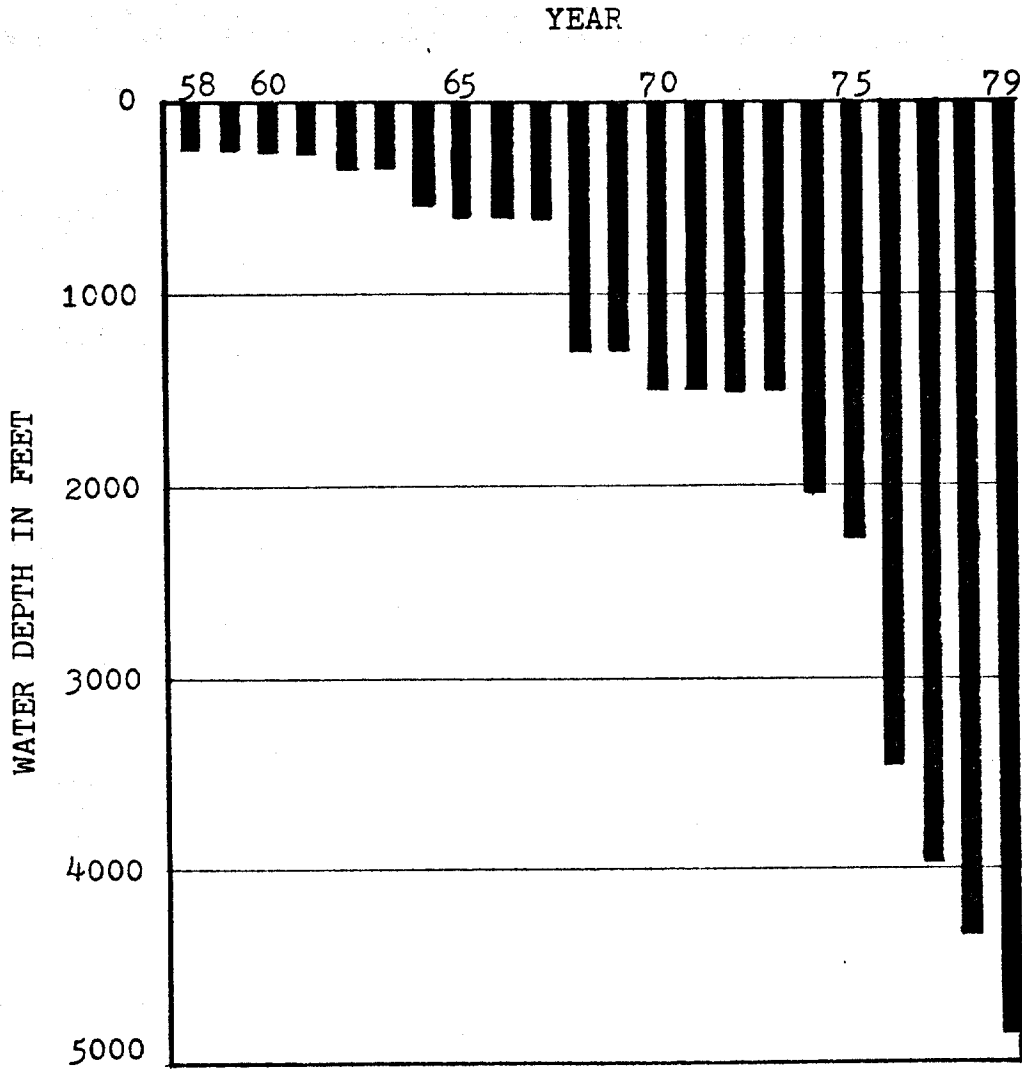


Figure 1.1 - History of Water Depth Record for Floating Drilling Vessels (After Harris¹).

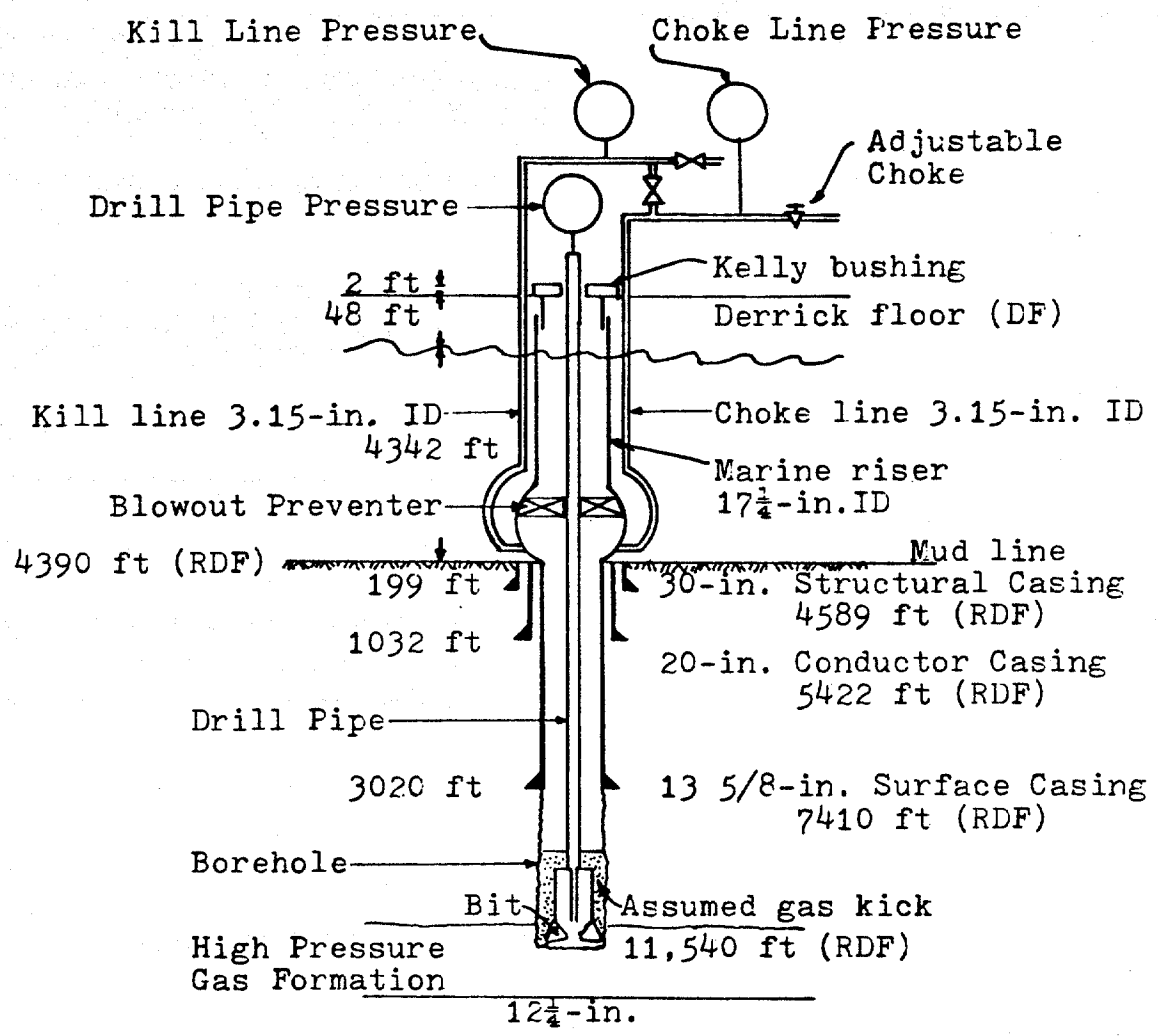


Figure 1.2 - Schematic of Typical Flow Geometry Present for Deep Water Blowout Control Operations.

1978. In this schematic it was assumed that an influx of gas into the borehole was experienced after drilling into a high pressure formation at 11,540 ft. Note that well closure is accomplished by blowout preventers located at the sea floor.

A threatened blowout or "kick" starts if the pressure exerted by the column of drilling fluid in the well is less than the formation pore pressure. The influx of formation fluid into the well can be detected at the surface because of the drilling fluid which is displaced or "kicked" from the surface wellbore annulus into the surface drilling fluid pits. Once detected, the influx of formation fluid is stopped by closing the subsea blowout preventer which seals the annular space around the drill pipe. Before normal drilling operations can be resumed, the formation fluids must be removed from the well and the density of the drilling fluid in the well increased sufficiently to prevent further influx of formation fluids. This is accomplished by circulating the well against a back-pressure provided by an emergency high pressure flow-line and an adjustable choke. The operations required to (1) close the well and (2) circulate the formation fluid from the well and higher density mud into the well are called well control procedures or pressure control procedures.

Pressure control procedures have been developed by the oil industry to provide guidance to the field personnel who must ultimately handle threatened blowouts under a wide variety of circumstances. Most of these procedures, like the blowout prevention equipment which must be employed, were

largely developed for land based drilling operations, and modified as required as the search for oil and gas moved offshore. It is anticipated that further modifications in pressure control procedures will be needed as drilling operations are extended to much greater water depths.

Most modern pressure control procedures are evaluated at least in part by computer studies predicting the pressure response of the well during various phases of the pressure control operations. Shown in Figure 1.3 is a predicted surface choke pressure for the example of Figure 1.2 for various assumed initial gas influx volumes. One major problem predicted in this example is the rapid increase in choke pressure required when the gas reaches the sea floor and enters the small diameter choke lines. Computer simulations of well control operations can give much insight both in predicting operational conditions and in evaluating alternative pressure control procedures.

Computer simulations of pressure control operations are also carried out on a real time, interactive basis to train field personnel in those pressure control procedures selected for routine applications. Several pressure control simulators are manufactured specifically for such training exercises. Two of the commercially available pressure control training simulators are shown in Figure 1.4. These simulator facilities are part of the LSU Blowout Prevention Training Center and are used in industry courses leading to

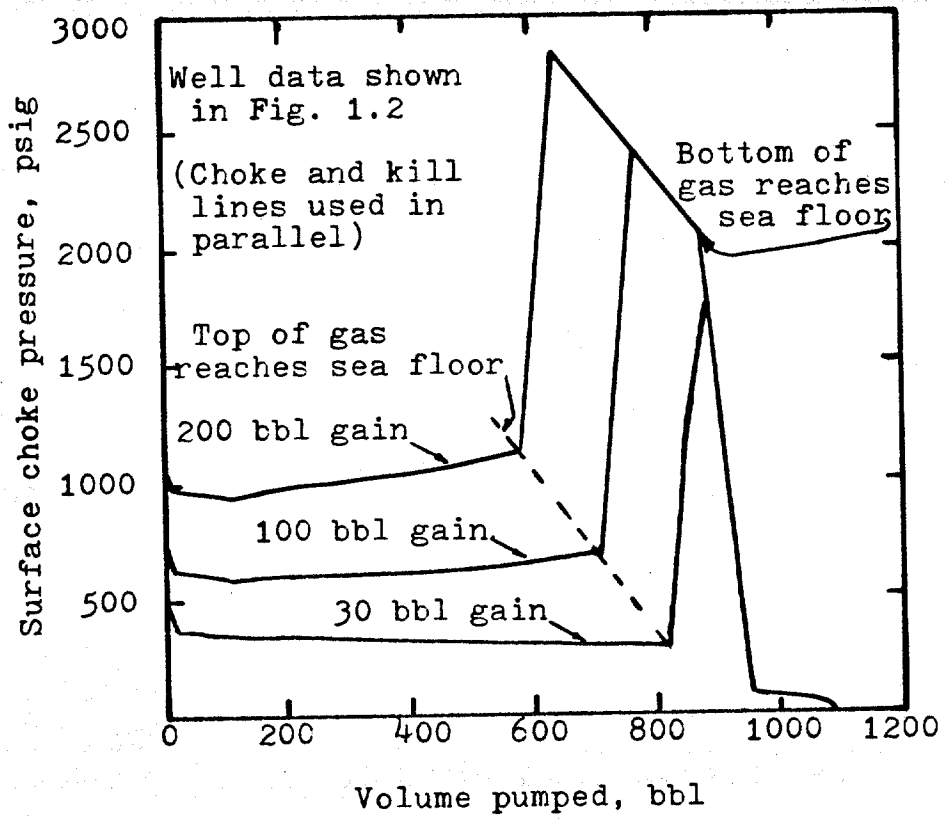


Figure 1.3 - Predicted Well Pressure Response for Example Described in Figure 1.2.

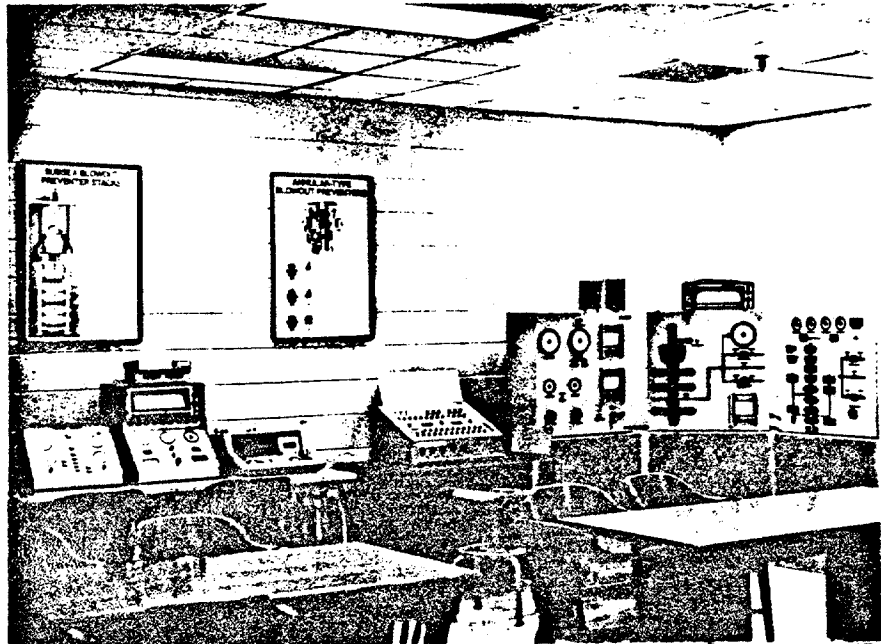


Figure 1.4 Example of Pressure Control Training Simulators at LSU Blowout Prevention Center.

certification in pressure control operations.

Accurate computer simulation of pressure control operations require an accurate knowledge of fluid behavior in the well. Preliminary research at Louisiana State University has already shown that the assumptions used at present in blowout control simulations do not always predict actual well behavior when gas is present. Two assumptions found to be at fault are (1) that gas influx enters the wellbore as a continuous slug which occupies the entire annular cross section of the well and remains in this configuration during subsequent pressure control operations and (2) that the gas zone does not migrate upward through the column of drilling fluid but moves instead at the same velocity as the circulating drilling fluid.

This study is being conducted as part of a large ongoing research effort towards the development of improved pressure control procedures for floating drilling operations. The main thrust of this study is aimed at determining a more accurate understanding of the behavior of a gas kick during pressure control operations for the flow geometry present on a floating drilling vessel. Ultimately, it is hoped that a more accurate understanding of the fluid behavior will lead to more accurate computer simulations of pressure control operations.

The primary objectives of the current study is to experimentally determine for gaseous formation fluids and

the flow geometry present on a floating drilling vessel:

- (1) the two phase flow patterns occurring during pressure control operations
- (2) the bubble rise velocity of the gas contaminated zone and
- (3) the gas concentration in the gas contaminated zone.

Both circulating and non circulating well conditions were included in the study. The flow geometry effect was considered by using segments of annuli and tubes. The combined effect of different sizes of annuli and tubes connected in series could not be studied because of size limitations of the experimental apparatus.

The pressure distribution within the gas contaminated region was not included in the scope of this experimental study. It was felt that existing two phase flow pressure gradient correlations could be employed if the flow pattern and fluid distribution could be predicted. Experimental verification of predicted pressures will be conducted in full scale wells as part of a future study.

CHAPTER II

PREVIOUS INVESTIGATIONS

It is hoped that major improvements in the accuracy of computer simulations of pressure control operations associated with gas kicks could be made through the development of more realistic algorithms for predicting:

- (1) The two phase flow patterns present in the well-bore annulus.
- (2) The upward slip velocity of the contaminated region relative to the drilling fluid.
- (3) The gas concentration in the gas contaminated region.

An extensive literature review was conducted in these three areas as a first step in the development of the needed algorithms. This chapter summarizes the results of this literature review.

2.1 Flow Patterns

Previous work on two phase flow patterns was classified in this study according to the following three geometries.

- (1) Extended liquids
- (2) Tubes
- (3) Annuli
- (4) Complex Geometries

The extended liquid case includes gas rising in a liquid media which is large enough so that no significant effect of the liquid boundaries can be observed. The next two cases investigated include the effect of bounding the liquid in a tube or in an annulus. The effect of the confining liquid conduit becomes more pronounced as the size of the individual gas bubbles approach the size of the conduit.

The last case considered previous work which may provide some insight on the effect of a complex geometry similar to that present on a floating drilling vessel. A floating drilling vessel operating in deep water typically has several long sections of different size annuli connected in series. The upper annular section is in turn connected at the sea floor with one or more vertical tubes which serve as the high pressure choke lines to the surface. Gas is introduced at the bottom of the well from porous media. Before pressure control operations can be accurately modelled, the effect of such a complex flow geometry and associated end effects on the two phase flow patterns must also be determined.

2.1.1 Extended Liquids

When gas is released in an infinite liquid media, the resulting flow pattern is generally described as bubble flow. A qualitative subclassification of this regime, based on the shape of the bubbles is generally used. This kind of

classification is useful because the geometry of the bubble is related to the forces controlling the phenomenon of bubble motion. The bubble shape classification used in this study includes:

























- (1) Spherical bubbles
- (2) Oblate spheroid bubbles
- (3) Lenticular bubbles

Bubbles of a given gas in a given liquid tend to progress from small spherical bubbles to oblate spheroid bubbles and finally to large lenticular bubbles as the bubble volume is increased. Large lenticular bubbles can be unstable, breaking into smaller spherical or oblate spheroid bubbles. Examples of typical air bubble shapes observed by Haberman and Morton² in different liquids are shown in Figure 2.1. Similar observations for air bubbles rising in water described by V.G. Levich³ are shown in Figure 2.2.

An excellent summary discussion on bubble behavior in extended liquids is given by Haberman and Morton². In addition to bubble volume, the shape of a bubble also depends upon the interfacial tension between the gaseous and liquid phases, the densities of the gaseous and liquid phases, and the viscosity of the gaseous and liquid phases.

2.1.2 Tubes

Flow conduits having a circular cross sectional area are of particular interest in this study because the flow pattern in the subsea choke lines between the blowout preventer stack at the sea floor and the floating drilling vessel at the surface can have a very large effect on the

Liquid	Equivalent radius*, cm.		
	0.05	0.2	0.7
Methyl alcohol			
Varsol			
Turpentine			
Water 6°C (filtered)			
Water 19°C (filtered)			
Mineral oil			
62% corn syrup- water			
68% corn syrup- water			

*Equivalent radius is radius of sphere of equal volume.

Figure 2.1 - Typical Shapes of Air Bubbles of Several Volumes in Various Liquids (After Haberman and Morton²).

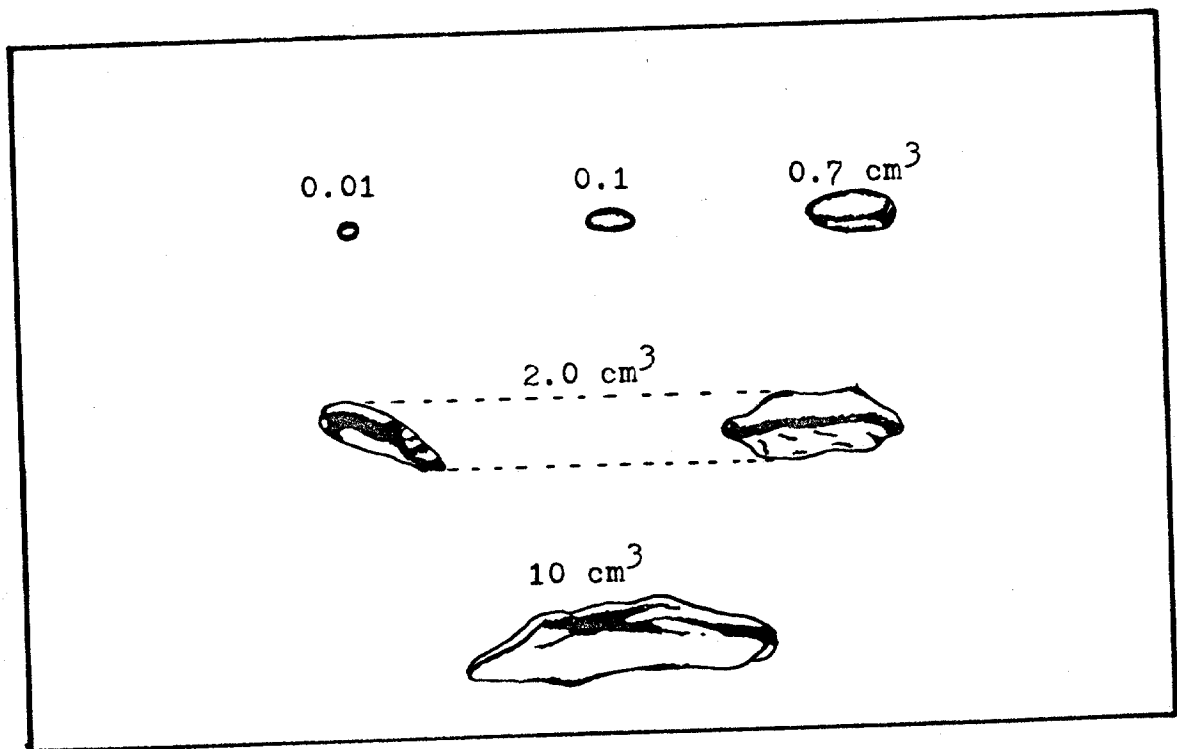


Figure 2.2 - Typical Shapes of Air Bubbles in Water³.

classifications of flow patterns. In general, the description of each flow pattern is characterized by the radial or axial distribution of liquid and gas. Taitel et al⁴ in a very recent summary publication used the following flow pattern descriptions in conjunction with the classification shown in Figure 2.3:

Bubble Flow. The gas phase is approximately uniformly distributed in the form of discrete bubbles in a continuous liquid phase.

Slug Flow. Most of the gas is located in large bullet shape bubbles which have a diameter almost equal to the pipe diameter. They move uniformly upward and are sometimes designated as "Taylor Bubbles", after one of the first investigators who studied this flow pattern.⁶ Taylor bubbles are separated by slugs of continuous liquid which bridge the pipe and contain small gas bubbles. Between the Taylor bubbles and the pipe wall liquid flows downward in the form of a thin falling film.

Churn Flow. Churn flow is somewhat similar to slug flow. It is however, much more chaotic, frothy and disordered. The bullet-shaped Taylor bubble becomes narrow and its shape is distorted. The continuity of the liquid in the slug between successive Taylor bubbles is repeatedly destroyed by a high local gas concentration in the slug. As this happens and the liquid slug falls, this liquid accumulates, forms a bridge and is again lifted by the gas. This oscillatory or alternating direction of motion of the liquid is typical of churn flow.

Annular Flow. Annular flow is characterized by the continuity of the gas phase along the pipe in the core. The liquid phase moves partly as a wavy liquid film and partly in the form of drops entrained in the gas core.

The annular flow pattern fits the assumption generally made in computer simulation of pressure control operations closer than the other three flow patterns described.

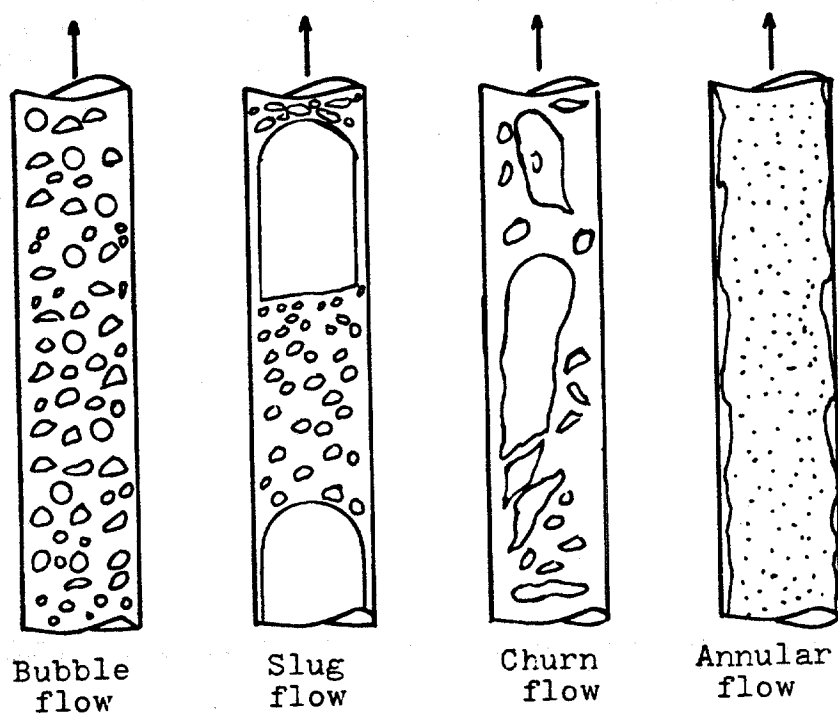


Figure 2.3 - Flow Pattern Description for Vertical Two Phase Flow Selected by Taitel et al⁴.

Steady state flow pattern prediction relies on a wide variety of flow pattern correlations. Among the published flow pattern correlations are those given by:

- (1) Griffith and Wallis (1961)⁷
- (2) Duns and Ross (1963)¹⁴
- (3) Sternling (1965)⁸
- (4) Wallis (1969)⁹
- (5) Hewitt and Roberts (1969)¹⁰
- (6) Govier and Aziz (1972)¹¹
- (7) Gould (1974)¹²
- (8) Oshinawa and Charles (1974)¹³
- (9) Chierici, Ciucci, and Schloechi (1974)⁵
- (10) Taitel, Bornea, and Dukler (1980)⁴

A typical approach has been to correlate experimental observations by plotting transitional boundary lines on a two dimensional plot called a flow pattern map. An example of this approach is shown in Figure 2.4. There has not been uniformity on the parameters selected for the coordinates of the flow pattern maps although the abscissa is often directly related to the gas flow rate and the ordinate is often related to the liquid flow rate.

Usually there is not good agreement in results obtained using the various flow pattern correlations available. This is not too surprising since maps prepared from experimental data on one pipe size and for a limited range of fluid properties are not necessarily valid for other conditions.

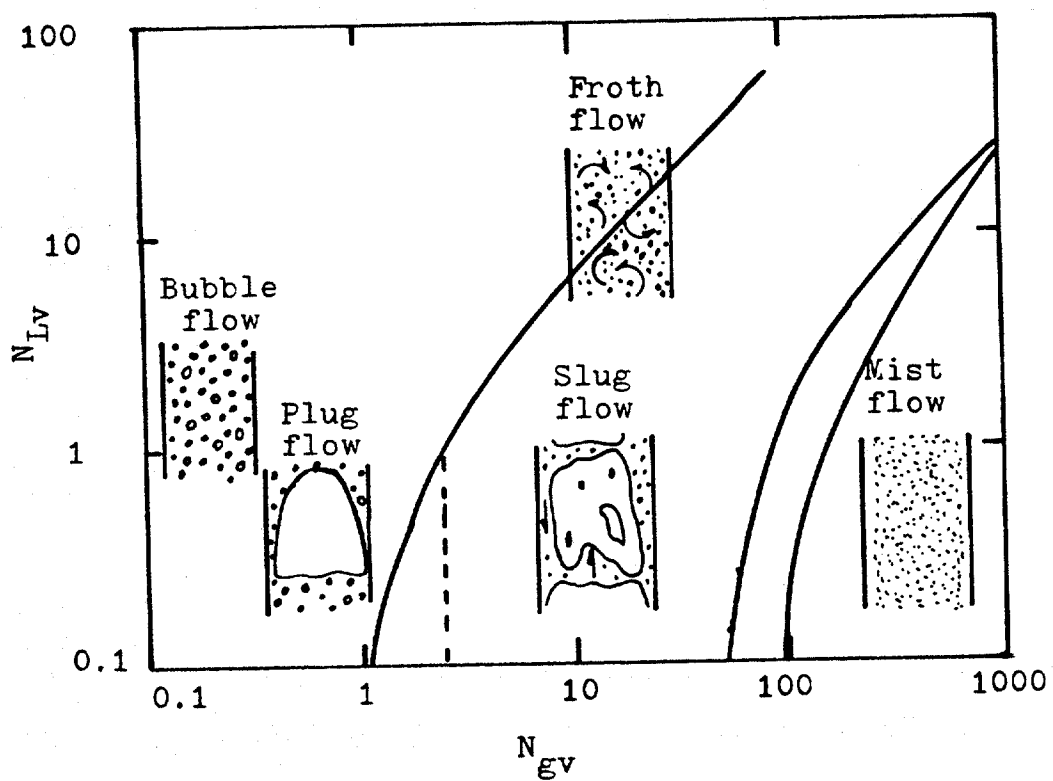


Figure 2.4 - Flow Pattern Description for Vertical Two Phase Flow Used by Chierici et al⁵.

For sake of brevity, only the correlations judged to have the most promising potential will be presented. The correlations are classified according to the flow pattern boundaries which they represent.

Transition to Slug Flow Pattern

Griffith and Wallis were the first to discuss the bubble flow to slug flow transition. They were not sure that the bubble flow pattern was a stable pattern in long systems, reasoning that since different size bubbles travel at different rates, there is a natural tendency for small bubbles to link up and form slugs. However, based on previous experimental observations by Bailey et al¹⁶, they presented a correlation for the transition from bubble flow to slug flow when the gas volume fraction, in the column surpasses 0.18 for a 1" diameter tube. This implies that slug formation is not stable for gas volume fractions below 0.18.

Taitel et al⁴ in a very recent publication make a similar recommendation but placed the limiting gas volume fraction at 0.25. Taitel pointed out that spherical bubbles could be theoretically packed so as to occupy a maximum of 52% of the volume, but bubble coalescence begins to increase sharply when the spacing between the bubbles is less than half their radius. This corresponds to a gas volume fraction of 0.25.

Duns and Ross¹⁴ presented the following criteria for the transition from bubble flow to slug flow:

$$N_{gv} = L_1 + L_2 N_{Lv} \quad (2.1a)$$

$$N_d = d \sqrt{\frac{\rho_L g}{\sigma}} \quad (2.1b)$$

$$N_{gv} = \frac{q_g}{A} \sqrt[4]{\frac{\rho_L}{g \sigma}} \quad (2.1c)$$

$$N_{Lv} = \frac{q_l}{A} \sqrt[4]{\frac{\rho_L}{g \sigma}} \quad (2.1d)$$

q_g = upward gas volume flow rate at existing conditions

q_l = upward liquid volume flow rate at existing conditions.

A = Area of tube

d = tube diameter

ρ_L = liquid density

g = acceleration of gravity

σ = interfacial tension

L_1, L_2 = parameters defined by N_d and Figure 2.5.

Use of this correlation does not require prior knowledge or calculation of the gas volume fraction. The criteria is most sensitive to the gas flow rate, the liquid flow rate, and the tube diameter, with the liquid density and interfacial tension being much less important. The criteria is completely independent of the liquid viscosity.

Orkiszewski¹⁵ suggested the transition from bubble flow to slug flow occurs when a parameter L_B becomes greater than the gas fraction in the output stream of the system. The parameter, L_B , is defined by

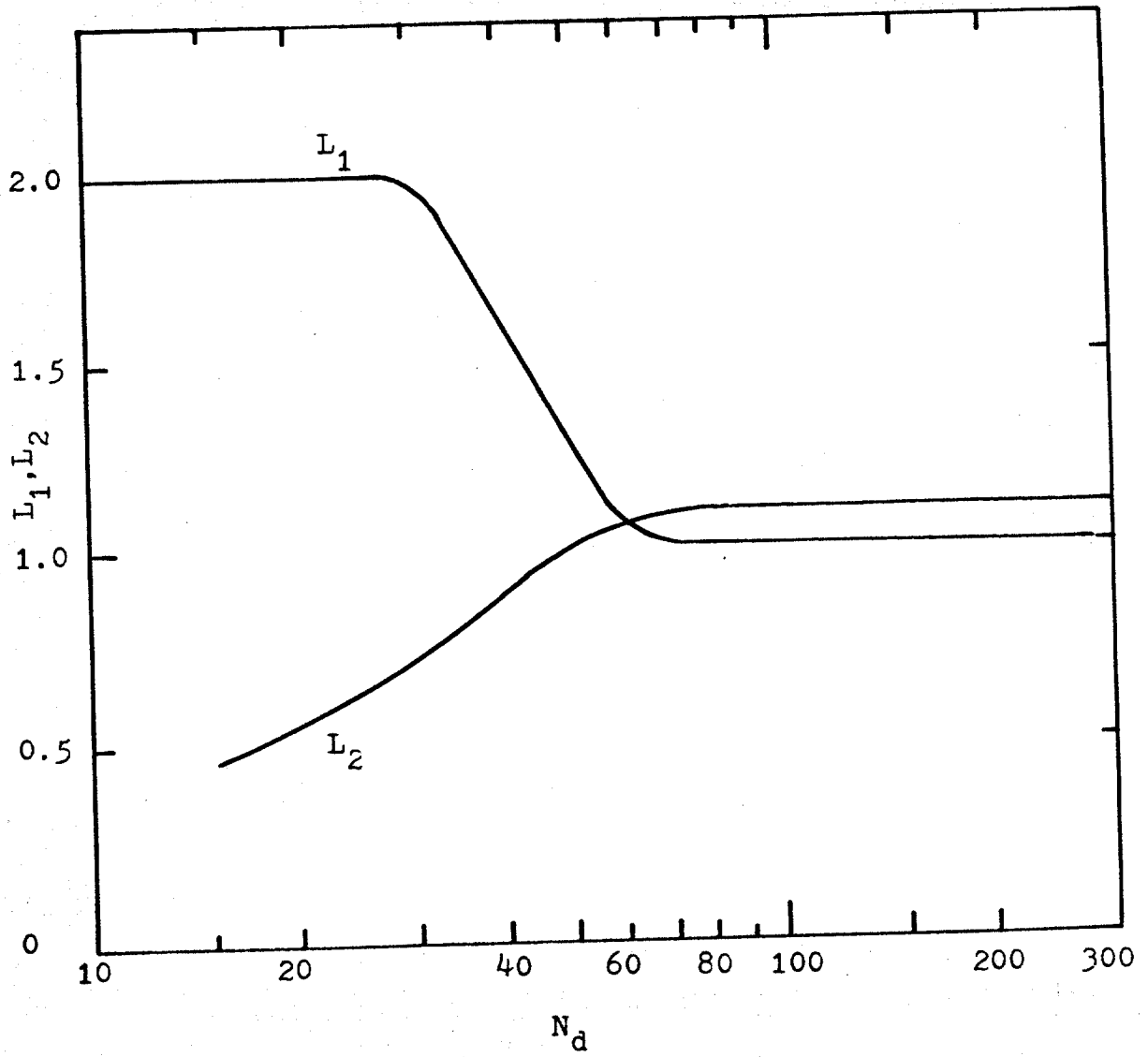


Figure 2.5 - Flow Regime Numbers of Duns and Ross.

$$L_B \approx \frac{q_g}{q_g + q_L} \quad (2.2a)$$

$$L_B = \begin{cases} 0.13 & \text{for } L_x \leq 0.13 \\ L_x & \text{for } L_x > 0.13 \end{cases} \quad (2.2b)$$

$$L_x = 1.071 - 0.2281 v_m^2 / d \quad (2.2c)$$

where:

v_m = the mixture velocity obtained by dividing the total gas and liquid volume flow rate at the existing conditions by the tube area, ft/sec.

d = the tube diameter, ft.

Chierici et al⁵ used essentially this same criteria with a limiting value of 0.18 for L_B rather than 0.13. This criteria is sensitive only to the gas and liquid flow rates and the tube diameter.

Govier and Aziz¹¹ predict the onset of a slug flow pattern when

$$N_x \geq N_1 \quad (2.3a)$$

$$N_x = \frac{q_g}{A} \left(\frac{g}{0.0764} \right)^{1/3} \left(\frac{72 \rho_L}{62.4 \sigma_L} \right)^{1/4} \quad (2.3b)$$

$$N_1 = 0.51 (100 N_y)^{0.172} \quad (2.3c)$$

$$N_y = \frac{q_l}{A} \left(\frac{72 \rho_L}{62.4 \sigma_L} \right)^{1/4} \quad (2.3d)$$

q_g = gas volume flow rate at existing conditions, ft³/sec.

q_L = liquid volume flow rate, ft³/sec

ρ_g = gas density, lb/ft³

ρ_L = liquid density, lb/ft³

σ_L = interfacial tension, dynes/cm

This criteria is primarily sensitive to gas flow rate, liquid flow rate, and tube area and has a weak dependence on liquid density and interfacial tension.

Transition to Churn Flow Pattern

It is difficult to compare different criteria for predicting the onset of churn flow because of differences as to the description of this flow pattern by different investigators. Some identify churn flow on the basis of froth that appears within the gas region. In this study, we have adopted the description of Taitel et al⁴ which is based on an oscillatory motion of the liquid region between gas slugs that are too short to remain stable.

Taitel et al provide a convincing argument backed by experimental observation that churn flow is actually due to entrance effects and if the system is long enough, eventually a stable slug flow will be produced. Churn flow is caused when a Taylor bubble breaks through a short liquid slug to another Taylor bubble above, resulting in a coalescence of two gas bubbles and two liquid slugs into one larger gas bubble and one larger liquid slug. Eventually a long enough liquid slug is created to form a stable bridge between the Taylor bubbles. A liquid slug length approximately 16 times

the tube diameter was found to be stable.

For low viscosity liquids and/or tube sizes of several inches or greater, the length of the system, l_E , above the entrance in which churn flow can exist is given approximately by:

$$l_E = 40.6 d \left(\frac{v_m}{\sqrt{gd}} + 0.22 \right) \quad (2.4)$$

where the tube diameter d , mixture velocity, v_m , and gravitational constant, g , are defined in any consistent units. For systems of finite lengths less than l_E , churn flow could exist throughout the entire system. Since we are dealing with extremely long systems in pressure control operations, churn flow is probably of significance only over the bottom several hundred feet of each section of uniform geometry.

Transition to Annular Flow Pattern

For high gas flow rates, the flow becomes annular. A liquid film flows adjacent to the wall and gas travels rapidly upward carrying entrained liquid droplets. The liquid film tends to be wavy and liquid droplets tend to be broken off the wave peaks by the upward moving gas core. For this flow pattern to be stable, the liquid droplets must be carried upward. If they are allowed to fall and accumulate into a liquid bridge, slug flow or churn flow results.

Duns and Ross¹⁴ predict the transition to the annular

flow pattern occurs when:

$$N_{gv} \geq 75 + 84 N_{Lv}^{0.75} \quad (2.5)$$

where N_{gv} and N_{gL} are given by Equations (2.1c) and (2.1d) respectively. This criteria is most sensitive to gas flow rate, liquid flow rate, and tube area, with liquid density and interfacial tension playing a much more minor role.

The criteria is independent of liquid viscosity. Orkiszewski¹⁵ as well as Chierici et al⁵ also used this same criteria for predicting the transition to annular flow.

Govier and Aziz¹¹ predict the onset of annular flow when:

$$N_x \geq \begin{cases} 70/(100 N_y)^{0.152} & \text{for } N_y < 4 \\ 26.5 & \text{for } N_y \geq 4 \end{cases} \quad (2.6)$$

where the variables N_x , N_y , q_g , A , ρ_L , and σ_L have the same units as defined for Equation (2.3). This criteria is highly sensitive to gas flow rate and tube area, with liquid flow rate, liquid density, and interfacial tension playing a more minor role.

Taitel et al⁴, developed an expression for onset of annular flow based on the slip velocity of the largest drop size felt to be stable. The critical drop size is based on a critical Weber number of 30 and a drag coefficient of 0.44 for the liquid drop. The resulting criteria is given by:

$$q_g = \frac{3.1A [\sigma_g (\rho_L - \rho_g)]^{0.25}}{\rho_g^{0.5}} \quad (2.7)$$

This criteria depends primarily on gas flow rate and tube area, with liquid density, gas density, and interfacial tension having a more minor role. the criteria is independent of liquid flow rate and liquid viscosity.

2.1.3 Annuli

Vertical two phase flow patterns have not been studied previously. The work done in tubes is sometimes extended to annuli through use of an equivalent hydraulic radius concept, but this approach has not been verified experimentally.

Zukoski¹⁷ in reporting some work on the slip velocity of long bubbles in tubes mentioned that D. Gluck and J. Gille of North American Aviation, Downey, California had observed in unpublished experiments an unsymmetric bubble shape in the emptying of an annular space between cylinders. These individuals are reported by Zukoski to have observed that gas moves up one side of the annulus with liquid falling down the opposite side. For large ratios of the outer to inner radius of the annulus, the width of the liquid fluid flow area near the bubble nose was reported approximately equal to the diameter of the inner tube.

Rader, Bourgoyne, and Ward¹⁸ worked with an annular geometry on a previous LSU study of gas slip velocity for a wide variety of tube sizes and fluid properties. However, this previous work considered only the flow pattern resulting from a very rapid gas injection into the system, attempting to be as close as possible to the conventional assumption

that the gas enters the well as a continuous plug. It was noted that in all cases, the gas did not occupy the entire cross sectional area, but instead the gas slug traveled up one side of the annulus with liquid backflow occupying an area opposite the bubble. The fractional area of the liquid backflow was found to increase as the viscosity of the fluid was increased. The observed bubble shapes are shown in Figure 2.6.

2.1.4 Complex Geometries

Although it is widely recognized that end effects due to changing geometry are important, little experimental work has been reported. Griffith and Wallis⁷ pointed out that entrance effects can persist over great lengths and long periods of time are often required to achieve steady-state two phase flow. Taitel et al⁴ reported that the churn flow pattern was due primarily to entrance effects. Flow exit conditions can also affect upstream flow patterns. For non vertical tubes, the angle of deviation has a large effect on the bubble shape and fluid distribution¹⁷.

Since a gas kick is taken from an open formation, the gas travels directly from a porous media to the wellbore. A large number of small streams of gas converging in the wellbore to form a gas kick may cause different entrance effects than a single stream of gas from a pipe. It is well known that a porous media is an excellent bubbler device.

Nicklin¹⁹ used a porous plate to generate bubble flow

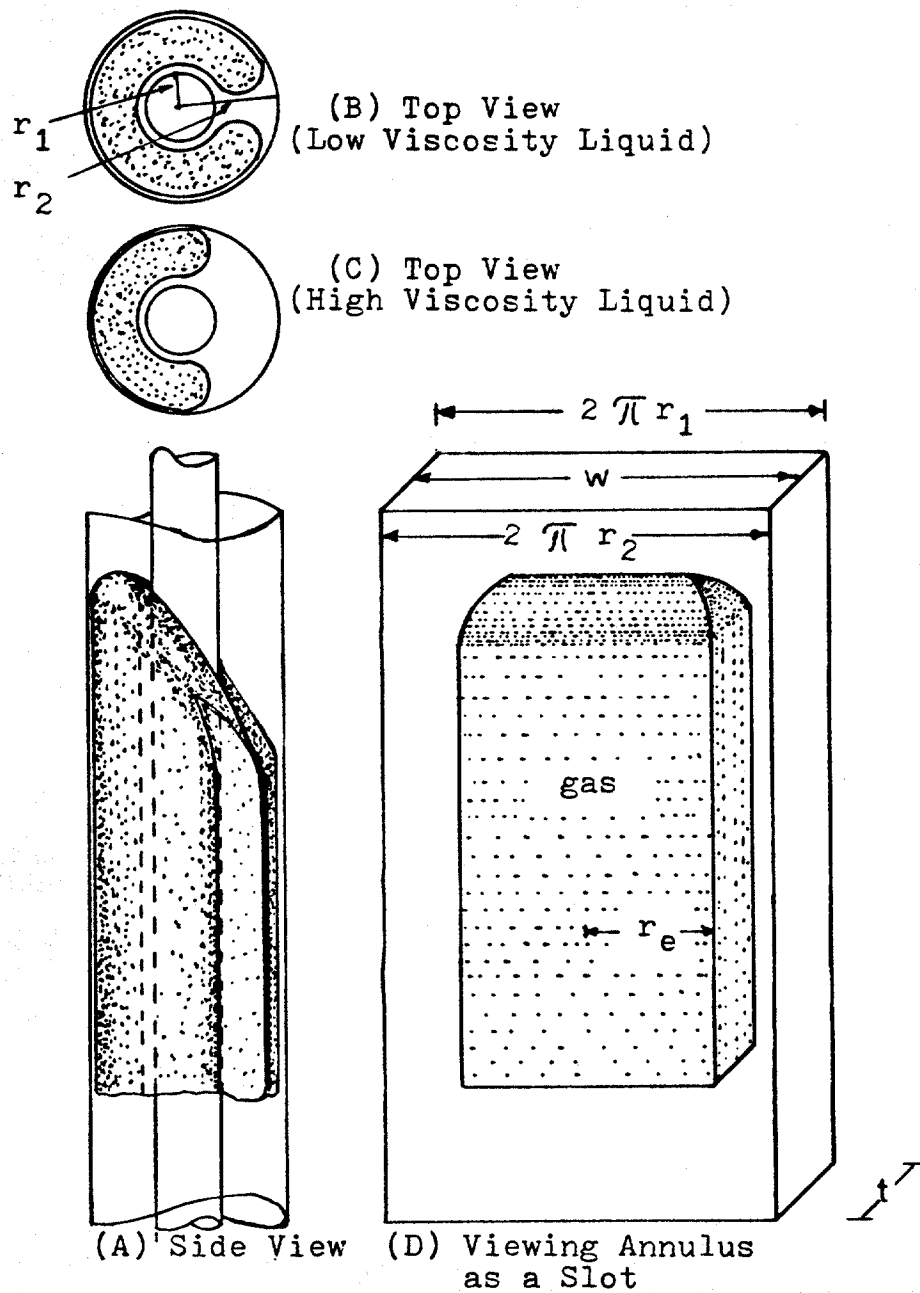


Figure 2.6 - Shape Assumed by Large Gas Bubble
Rising in an Annulus¹⁸.

patterns in a vertical tube having 3.75 in. internal diameter and 6 ft. of length he injected gas through a porous bronze disk at flow rates up to about 1.8 ft³/min measured at average test conditions. This corresponded to a superficial gas velocity of about 0.4 ft/sec. Over the short length of pipe used, bubble flow was observed up to a superficial gas velocity of about 0.2 ft/sec. At higher gas rates, the formation of gas slugs was noted.

A porous media may be represented by a large number of small diameter tubes closely packed. Some investigators have worked on the prediction of the volume of the bubbles released from a nozzle. Acharya et al²⁰ performed a review of the available models of bubble formation in newtonian fluids. They found that the models for inviscid fluids may be simplified to the form of

$$V_b = C (q_g^2 / g)^{3/5} \quad (2.8)$$

where V_b = volume of the bubble

q_g = volumetric gas flow rate

$C = 0.976$

Also, they found that this equation could be safely extended to predict the bubble sizes in highly viscous non-newtonian fluids provided the flow rates were in the order of 10^{-6} m³/sec (35.3×10^{-6} ft³/sec) per one nozzle opening.

Eizo Sada et al²¹ worked on the phenomenon of bubble formation in flowing liquids. Their work may be summarized

as follows:

- (1) The bubble size formed in flowing liquids decreases with the superficial liquid velocity.
- (2) Three types of bubble formation are observed:
 - (a) Single bubbles, (b) Coalescent bubbles, and
 - (c) Gas jets; these types depend on the fluid flow rates.
- (4) The bubble sizes in the regions of single bubbles and coalescent bubbles are correlated by the empirical equations:

$$\frac{d_{bi}}{d_N} = 1.55 N_{Frm}^{0.2} \quad \text{Single bubbles} \quad (2.9)$$

$$\frac{d_{bi}}{d_N} = 2.5 N_{Frm}^{0.2} \left(\frac{d_N}{d_{No}}\right)^{0.1} - 3.5 \quad \text{Coalescent bubbles} \quad (2.10)$$

$$\text{where } N_{Frm} = \frac{v_{gN}}{gd_{bi} + 0.33 v_{Ls}^2} \quad (2.11)$$

d_{bi} = initial diameter of the bubble, cm.

d_N = nozzle diameter, cm.

d_{No} = 0.086 cm.

v_{gN} = gas velocity through nozzle, cm/sec.

v_{Ls} = superficial liquid velocity, cm/sec.

g = gravitational constant, cm/sec².

The region of single bubbles is determined by

$$d_{bi}^2 N_{Frm} < 6$$

They did not provide a criteria for determining upper limit of the equation for coalescent bubbles.

2.2 Bubble Rise Velocity

Previous work on the velocity at which a gaseous zone moves upward through a liquid was classified in this study according to the following three geometries:

- (1) Extended liquids
- (2) Tubes
- (3) Annuli

The importance of flow pattern on the bubble rise velocity for these three geometries was also researched.

2.2.1 Extended Liquids

The velocity of gas bubbles rising through a relatively infinite liquid media has been widely studied. Some of the more significant work done in this area include those of:

1. Hadamard²²-Rybezyński (1911)²³
2. Davies and Taylor (1949)⁶
3. Peebles and Garber (1953)²⁴
4. Haberman and Morton (1956)²
5. Mendelson (1967)²⁵
6. Acharya, Mashelkar and Ulbrecht (1977)²⁶
7. Ishii and Pei (1980)²⁷

In several of these works, experimental bubble slip velocity measurements were presented in terms of a bubble drag coefficient which was correlated with a bubble Reynolds

number. Unfortunately, the correlations of drag coefficients versus bubble Reynolds number lack generality.

Recall from Section 2.1.1 that the injection of gas in an infinite liquid media results in a bubble flow pattern and that a qualitative subclassification of this regime, based on the shape of the bubbles, is generally used. The same subclassification is also useful in discussing the upward velocity of the gas bubbles except that the spherical bubble shape is further subdivided into a rigid sphere and a fluid sphere case. Very small gas bubbles behave much like a solid particle and hence the term rigid sphere is applied.

Thus, the gas bubble rise behavior will be discussed for the four following major regions:

- (1) rigid spherical bubbles
- (2) fluid spherical bubbles
- (3) oblate spheroid bubbles
- (4) lenticular bubbles

Rigid Spherical Bubbles

Several investigators have shown experimentally that very small gas bubbles rising in an extended liquid behave much like solid spherical particles in that the bubbles drag coefficient is predicted by Stokes' Law. Thus, bubble rise velocity can be developed using the following relationship for drag force F_D :

$$F_D = \frac{6\pi\mu_L r_e v_{\text{boo}}}{g_c} \quad (\text{Stokes' Law}) \quad (2.12)$$

for a bubble rising at its terminal velocity, the drag force, F_D , is also expressed by:

$$F_D = F_B - W = v_b \rho_L \frac{g}{g_c} - v_b \rho_g \frac{g}{g_c} = \frac{4}{3} \pi \frac{g}{g_c} r_e^3 (\rho_L - \rho_g) \quad (2.13)$$

where F_B = bouyancy force

W = weight of the spherical bubble

v_b = volume of the spherical bubble

ρ_L, ρ_g = liquid and gas density respectively.

μ_L = fluid viscosity

r_e = equivalent radius of shpere having the same
volume of the gas bubble

v_{boo} = velocity of the bubble in an extended liquid

g_c = gravitational constant

From equations (2.12) and (2.13), the terminal velocity results to be

$$v_{\text{boo}} = \frac{2}{9} \frac{g r_e^2 (\rho_L - \rho_g)}{\mu_L} \quad (2.14)$$

By definition, the drag coefficient is

$$f_D = \frac{F_D}{E_K \cdot A} = \frac{6\pi\mu_L r_e v_{\text{boo}}/g_c}{\left(\frac{\rho v_{\text{boo}}^2}{2 g_c}\right) (\pi r_e^2)} \quad (2.15)$$

$$\text{where } N_{Rb} = \frac{2 r_e v_{\text{boo}} \rho_L}{\mu_L} \quad (2.16)$$

Peebles and Garber²⁴ following the trend of many investigators recommended application of Stokes' Law for $N_{Rb} \leq 2$. However, Haberman and Morton proved that the transition to the fluid sphere region can happen at bubble Reynolds numbers as low as 2×10^{-6} .

Fluid Spherical Bubbles

The transition to the fluid sphere region is marked by slightly lower drag coefficients than that predicted for a solid sphere of equal volume. This occurs because of circulation patterns taking place within the gaseous phase.

Peebles and Garber²⁴ presented the following drag correlation for the fluid spherical bubble region

$$f_D = 18.7 N_{Rb}^{-0.68} \quad (2.17)$$

Also, f_D can be expressed as

$$f_D = \frac{F_D}{E_K \cdot A} = \frac{\frac{4}{3} \pi g r_e^3 (\rho_L - \rho_g) / g_c}{(\rho_L \frac{v_{b\infty}^2}{2 g_c}) (\pi r_e^2)}$$

From the former two equations, the velocity of the bubble becomes

$$v_{b\infty} = 0.33 g^{0.76} r_e^{1.28} \left(\frac{\rho_L}{\mu_L} \right)^{0.52} \left(\frac{\rho_L - \rho_g}{\rho_L} \right) \quad (2.18)$$

Equations (2.17) and (2.18) apply for the following range of bubble Reynolds numbers:

$$2 \leq N_{Rb} \leq 4.03 \left(\frac{g_L \mu_L^4}{\rho_L \sigma_L^3} \right)^{-0.214}$$

where all variables are defined as above and

σ_L = surface tension

This correlation was based on experimental work done for air bubbles rising in over 22 different liquids.

Haberman and Morton² also did experimental work in the fluid sphere region. They found that a theoretical development by Hadamard²²/Rybeznysky²³ could be applied. The Hadamard/Rybeznysky equation is defined by

$$F_D = 4 \pi \mu_L r_e v_{\text{boo}} / g_c \quad (2.19)$$

From equation (2.19) and (2.13), the terminal velocity for fluid sphere results to be

$$v_{\text{boo}} = \frac{1}{3} \frac{g r_e^2 (\rho_L - \rho_g)}{\mu_L} \quad (2.20)$$

and from equation (2.19) and the definition of drag coefficient

$$f_D = \frac{16}{N_{Rb}} \quad (2.21)$$

Oblate Spheroid Bubbles

The oblate spheroid region is marked by sharply increasing drag coefficients with increasing Reynolds number. The most extensive work done in the oblate spheroid region was presented by Peebles and Garber²⁴. They provided the following expressions to correlate the drag coefficient and the velocity of slightly deformed bubbles

$$v_{\text{boo}} = 1.35 \left(\frac{\sigma_L}{\rho_L r_e} \right)^{0.5} \quad (2.22)$$

$$f_D = 0.44 \frac{g r_e^4 v_{\text{boo}}^4 \rho_L^3}{\sigma_L^3} \quad (2.23)$$

Equations (2.22) and (2.23) apply for the following conditions

$$16.32 \frac{(g \mu_L^4)^{0.144}}{\rho_L \sigma_L^3} \leq \frac{g r_e^4 v_{\text{boo}}^4 \rho_L^3}{\sigma_L^3} \leq 5.75$$

Lenticular Bubbles

In 1949, Davies and Taylor⁶ found that the flow near the front of large lenticular bubbles in extended liquids was very close to the theoretical flow near the front of a complete sphere in an inviscid fluid. Also, they noticed that the angle subtended at the center of curvature of the stagnation point of a bubble changes during the growth of the bubble (see Fig. 2.7)

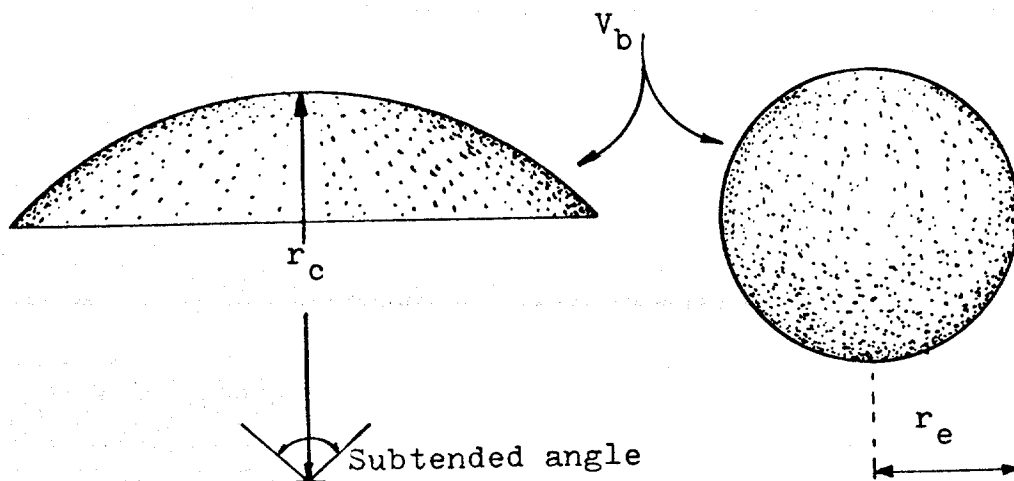


Figure 2.7 Angle subtended of lenticular bubbles and relationship between curvature radius and equivalent radius.

The following expression to calculate the slip velocity of lenticular bubbles was given by Davies and Taylor:

$$v_{\text{boo}} = \frac{2}{3} (g r_c)^{0.5} \quad (2.24)$$

where v_{boo} = velocity of the bubble
 r_c = curvature radius of the top portion of the bubble
 g = acceleration of gravity

The curvature radius, r_c , was determined from photographed bubbles.

Davies and Taylor also derived the following relationship between volume and rate of rise of a bubble.

$$v_{\text{boo}} = 24.8 V_b^{1/6} \quad (2.25)$$

where V_b = volume of the bubble, cm^3

v_{boo} = bubble velocity, cm/sec .

If we define an equivalent radius, r_e , as that of one sphere having the same volume of the lenticular bubble, we can write

$$V = \frac{4}{3} \pi r_e^3 \quad (2.26)$$

$$v_{\text{boo}} = 24.8 \left(\frac{4}{3} \pi r_e^3 \right)^{1/6} \quad (2.27)$$

Dividing equation (2.24) by equation (2.27) yields the following relationship between radius of curvature and equivalent radius

$$\frac{r_c}{r_e} = 2.275 \quad (2.28)$$

In terms of the equivalent radius, the velocity of the flattened-shape bubbles becomes

$$v_{\text{boo}} = 1.01 (g r_e)^{0.5} \quad (2.29)$$

Haberman and Morton found that for lenticular bubbles the drag coefficient is a constant, e.g., $f_D = 2.6$

since $f_D = \frac{8}{3} \frac{g r_e}{v_{\text{boo}}^2}$, the bubble rise velocity is given by

the same expression founded by Davies and Taylor, Equation (2.29).

Harvey D. Mendelson²⁵ found an equation to determine the terminal velocity of the bubbles in pure liquids of low viscosity. Based on the work of Haberman and Morton, he observed an analogy between the propagation of surface waves over deep water and the lenticular bubbles rising in pure liquids. By substituting the wave length, λ , for the perimeter of an equivalent circumference in the wave velocity equation, he arrived at the following expression:

$$v_{\text{boo}} = \left(\frac{\sigma_L}{r_e \rho_L} + g r_e \right)^{0.5} \quad (2.30)$$

where v_{boo} = velocity of the bubble

σ_L = surface tension

ρ_L = liquid density

g = acceleration of gravity

r_e = equivalent spherical radius of the bubble

Non-Newtonian Fluids

Acharya, Mashelkar, and Ulbrecht²⁶ extended the study on bubble motion in extended liquids to include non-newtonian fluid media. For the low velocity range they presented the following relationship between drag coefficient, f_D , and the modified number of Reynolds, N_{Rm}

$$f_D = \frac{24 F(n)}{N_{Rm}} \quad (\text{rigid sphere})$$

$$f_D = \frac{16 E(n)}{N_{Rm}} \quad (\text{fluid sphere})$$

$$\text{where } N_{Rm} = \frac{d_e^n v_{\text{boo}}^{2-n} \rho_L}{K}$$

the transition from rigid to fluid sphere is given by

$$r_{\text{cr}} = \left(\frac{\sigma_L}{\rho_L g} \right)^{0.5} \quad (2.31)$$

where r_{cr} = the critical sphere radius

d_e = equivalent diameter of a sphere having the same volume of the gas bubble

$F(n)$, $F_1(n)$ = function of the pseudoplasticity index

n = pseudoplasticity index

k = consistency index

For large Reynolds numbers (lenticular bubbles) they found that the Mendelson equation presented previously as equation (2.30) gave the best fit for their experimental data.

Recently, Ishii and Pei²⁷ derived a theoretical equation to obtain the drag coefficient of gas bubbles.

The theoretical values were compared with experimental ones for dilute solutions of alcohols. Their equation verified that the drag coefficient of single gas bubbles increases with the contamination of the liquid as it was observed by several previous authors. This occurs because the solid sphere region is extended to a higher Reynolds number by the collection of solid particles at the gas/liquid interface. Also they developed an expression for the drag coefficient of a swarm of bubbles which is defined by the general expression

$$(f_D)_{\text{swarm}} = (f_D)_{\text{single}} F(\alpha) \quad (2.32)$$

where $(f_D)_{\text{swarm}}$; $(f_D)_{\text{single}}$ = drag coefficient of gas bubbles and single bubbles, respectively.

$F(\alpha)$ = void function

Ishii and Pei experimentally found that the value of the void function tended to be between that predicted by Marrucci²⁸ and by Lewis and Bowerman²⁹. These void functions are defined as follows:

$$F(\alpha) = \frac{1 - (H_L)^{5/3}}{\alpha^2} \quad (\text{Marrucci}) \quad (2.33)$$

$$F(\alpha) = \alpha^{-1.97} \quad (\text{Lewis and Bowerman}) \quad (2.34)$$

where H_L is the volumetric fraction of liquid flowing in the tube

α is the volumetric fraction of gas flowing in the tube.

Fragmentation of Bubbles

The shape of the bubbles depends on the dynamic forces acting over them. These in turn, depend on the volume or size of the bubbles. As the size of the bubbles increases, the bubbles increase their velocity until they begin to deform, and finally they become unstable. At this point the bubbles go into a process of fragmentation.

Levich³ reported fragmentation of gas bubbles in water to occur at equivalent radius of around 3 cm (1.18 in). Bryn³⁰ also reported that large air bubbles in water at room temperature assume a lenticular shape, become very unstable, and finally tend to break easily into numerous smaller bubbles.

Levich also derived the following equation in an effort to predict the r_{ef} critical equivalent radius at which fragmentation of bubbles happens

$$r_{ef} = \left(\frac{3 \sigma_L}{f_D^1 v_{boo}^2 (\rho_g \rho_L^2)^{1/3}} \right)^{1/3} \quad (2.35)$$

where σ_L = surface tension, dyne/cm.

ρ_L = liquid density, gr/cc.

ρ_g = gas density, gr/cc.

v_{boo} = bubble velocity, cm/sec.

f_D^1 = drag coefficient

r_{ef} = critical equivalent radius of a lenticular bubble, cm.

For water at room temperature and assuming $f_D^1 = 0.5$, v_{boo} to be equal to the limiting velocity of rise $v_{\text{boo}} = 30$ cm/sec, and $\rho_g = 0.001$ gr/cc, Levich³ determined the critical radius to be

$$r_{\text{ef}} \doteq 1.8 \text{ cm}$$

Haberman and Morton² reported bubble rise velocities up to 60 cm/sec for lenticular bubbles (equivalent radius around 3 cm) rising in water at room temperature. With these values and assuming $f_D^1 = 0.5$, the equation (2.35) gives

$$r_{\text{ef}} \doteq 1.1 \text{ cm}$$

Unfortunately Equation (2.35) predicts critical radius lower than the maximum equivalent radius, 3 cm, reported in the literature for lenticular bubbles.

2.2.2 Tubes

When bubbles rise in a restricted media, the boundary affects their velocities. The net effect is a lower bubble rise velocity than that obtained for infinite media. The reduction in bubble rise is not important for small bubble diameters in large tubes. However, as the size of the bubbles approaches the size of the tube the boundary effect becomes significant. This phenomenon is illustrated in Figure 2.8.

Among the first works published on gas bubbles moving in restricted media was that of O'Brian and Gosline.

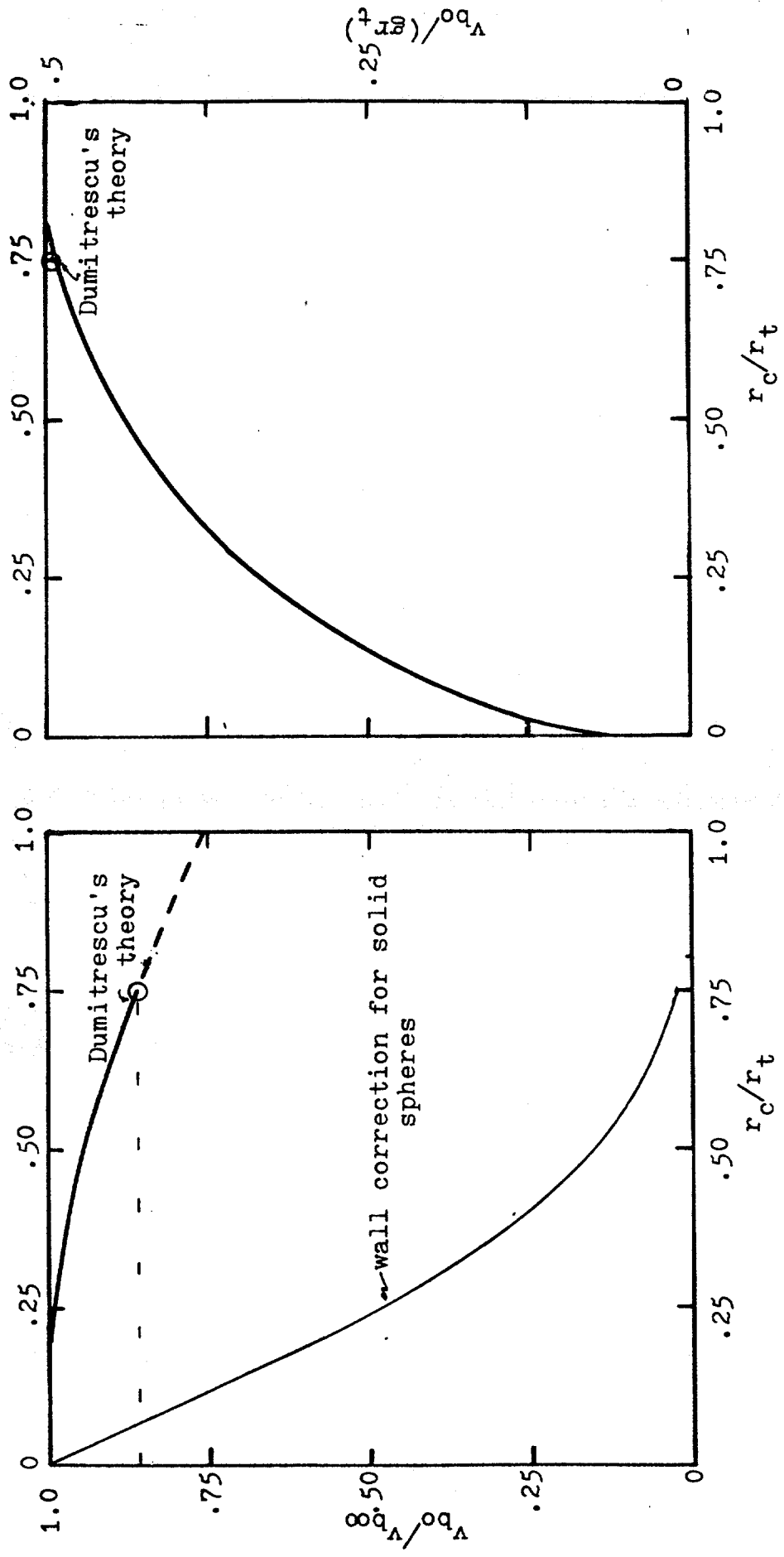


Figure 2.8 Variation of bubble velocity with r_c/r_t (After Collins).

O'Brien and Gosline³¹ made a study of the velocity of large bubbles in vertical tubes. Their experimental work was performed in three tubings having diameters of 1.18 in, 2.24 in, and 6.0 in. The properties of the fluids covered a range of viscosities from 1 to 96 cp. They found that for bubble radius greater than 3 mm the effect of the pipe walls becomes noticeable. Also they reported a limiting velocity beyond of which no increase resulted from an increase in the volume of the bubble. They also performed experiments on the velocity of stream of bubbles in a stationary liquid. They observed that the bubble velocities increased linearly with increases in air flow through the tube. The maximum velocities found for continuous gas injection was found to be far greater than the velocity of the largest single bubbles released in the same tube.

In 1943 D. T. Dumitrescu³², made a theoretical analysis of an infinitely long bubble in a tube. He arrived to the following equation for the limiting velocity of a bubble in an inviscid fluid

$$v_{bo} = 0.496 (g r_t)^{0.5} \quad (2.36)$$

Also, he supported this equation with experimental investigation. Using tubes of 0.99 cm, 2 cm, 3.76 cm, and 7 cm of diameter, he found a value of 0.49 for the constant of proportionality of his equation. The equation (2.36) is valid for larger diameters where the surface tension and

viscous forces are insignificant.

Later, Davies and Taylor⁶ also derived an equation for the velocity of slugs rising through perfect fluids contained in cylindrical tubes. They arrived to the following equation:

$$v_{bo} = 0.464 (g r_t)^{0.5} \quad (2.37)$$

They also provided experimental data to support this equation. The value 0.464 was lower than that obtained by Dumitrescu. Apparently this difference resulted from differences in the tube diameters used in the experiment.

Laird and Chisholm³³ reported measured velocities of cylindrical bubbles in vertical tubes. The values obtained were on the average 10% greater than those obtained from the equations of Davies and Taylor. Their experiments were conducted in a 2 in diameter tube with the upper end open to the atmosphere.

In 1956, Uno and Kintner³⁴ conducted a study to determine the effect of wall proximity on the velocity of air bubbles rising in a static liquid. They measured terminal velocities of bubbles rising in distilled water, 65% glycerine, diethylene glycol, and a surfactant solution in vertical cylindrical tubes, having internal diameters of 2.09, 3.64, 4.91, 6.90, 9.50 and 15.25 cm. Diethylene glycol, having a viscosity of 24.5 cp was the most viscous fluid included in the study. They obtained an empirical correlation which is

defined by the following equation:

$$\frac{v_{bo}}{v_{boo}} = \left[\frac{1}{b} \left(1 - \frac{r_e}{r_t} \right) \right]^{0.765} \quad (2.38)$$

where r_e = the equivalent spherical radius for the given
bubble volume

r_t = the tube radius

b = a function of the tube radius and the surface
tension

v_{bo} = actual terminal velocity of the bubble

v_{boo} = velocity of the bubble in a liquid of infinite
extent

Figure 2.9 gives the values of b for the liquids used by Uno and Kintner. This figure illustrates the importance of the surface tension. Note that the effect of surface tension decreases for the larger tube sizes.

In 1961, Griffith and Wallis⁷ studied experimentally the effect of water velocity on the rise velocity of large air slugs in vertical tubes with diameters of 0.5, 0.75 and 1.0 in. They presented their results in terms of a gas slip velocity defined as

$$v_{bo} = v_b - \bar{v}_m \quad (2.39)$$

where

v_b = the bubble rise velocity with respect to the
ground

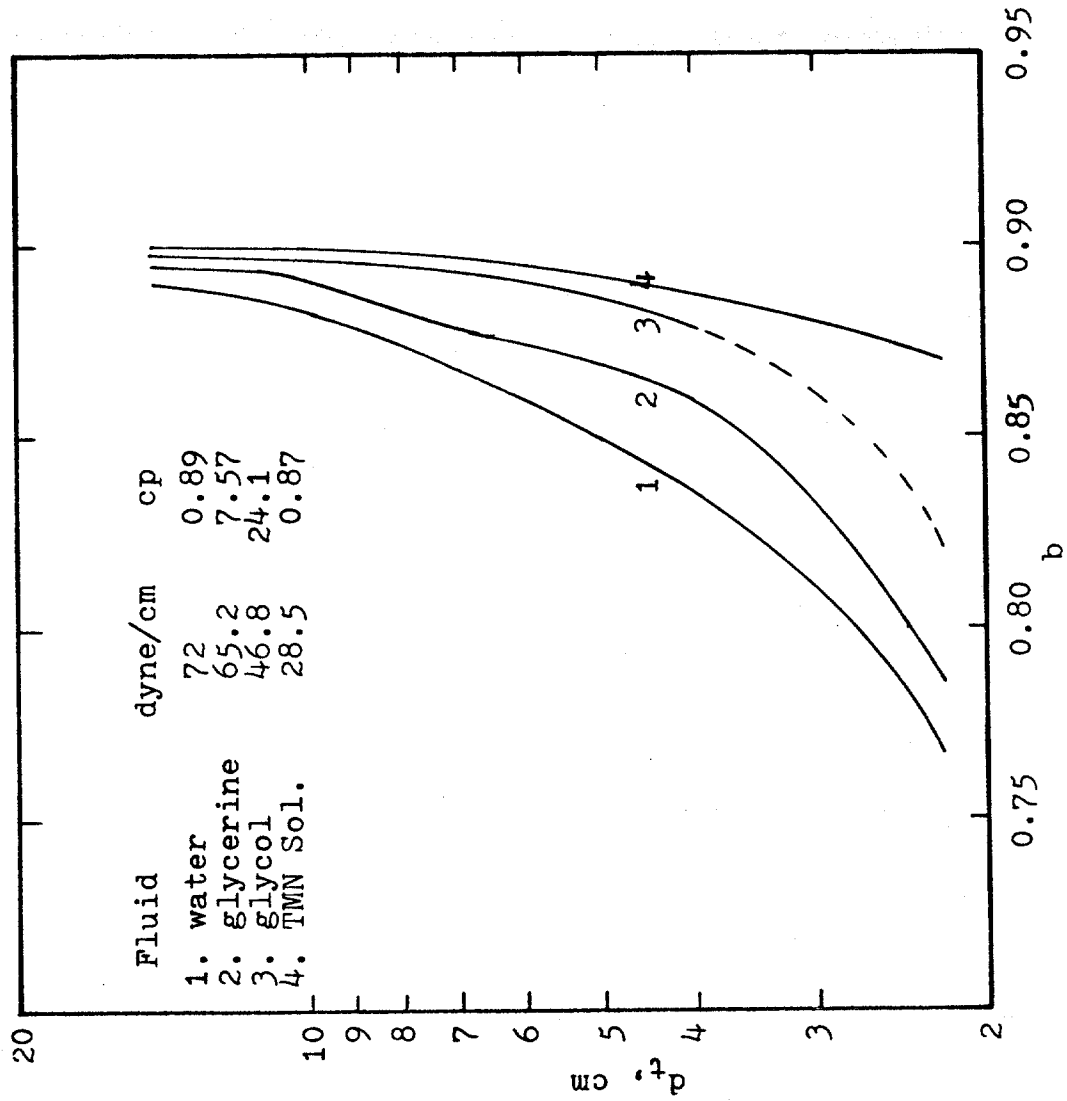


Figure 2.9 Values of b as a function of tube diameter and surface tension (After Uno and Kintner³⁴).

v_{bo} = the bubble velocity with respect to the liquid ahead of the bubble, assuming incompressible fluids

\bar{v}_m = the mean mixture velocity due to continuous injection into the tube.

The bubble velocity was found to be given by

$$v_{bo} = C_1 C_2 (g r_t)^{0.5} \quad (2.40)$$

where C_1 is a function of the bubble Reynolds number, and C_2 is a function of both the bubble Reynolds number and the liquid Reynolds number.

The bubble Reynolds number was defined by

$$N_{Rb} = \frac{d_t v_{bo} \rho_L}{\mu_L} \quad (2.41)$$

and the fluid Reynolds number by

$$N_{Rf} = \frac{d_t \bar{v}_m \rho_L}{\mu_L} \quad (2.42)$$

where d_t = tube diameter

v_{bo} = the bubble rise velocity with respect to the liquid ahead of the bubble

\bar{v}_m = the mean mixture velocity

ρ_L = the liquid density

μ_L = the liquid viscosity

The resulting correlation for C_1 and C_2 are shown in Figures 2.10 and 2.11.

Equations (2.39) and (2.40) can be combined to obtain

$$\bar{v}_b - \bar{v}_m = C_1 C_2 (g r_t)^{0.5}$$

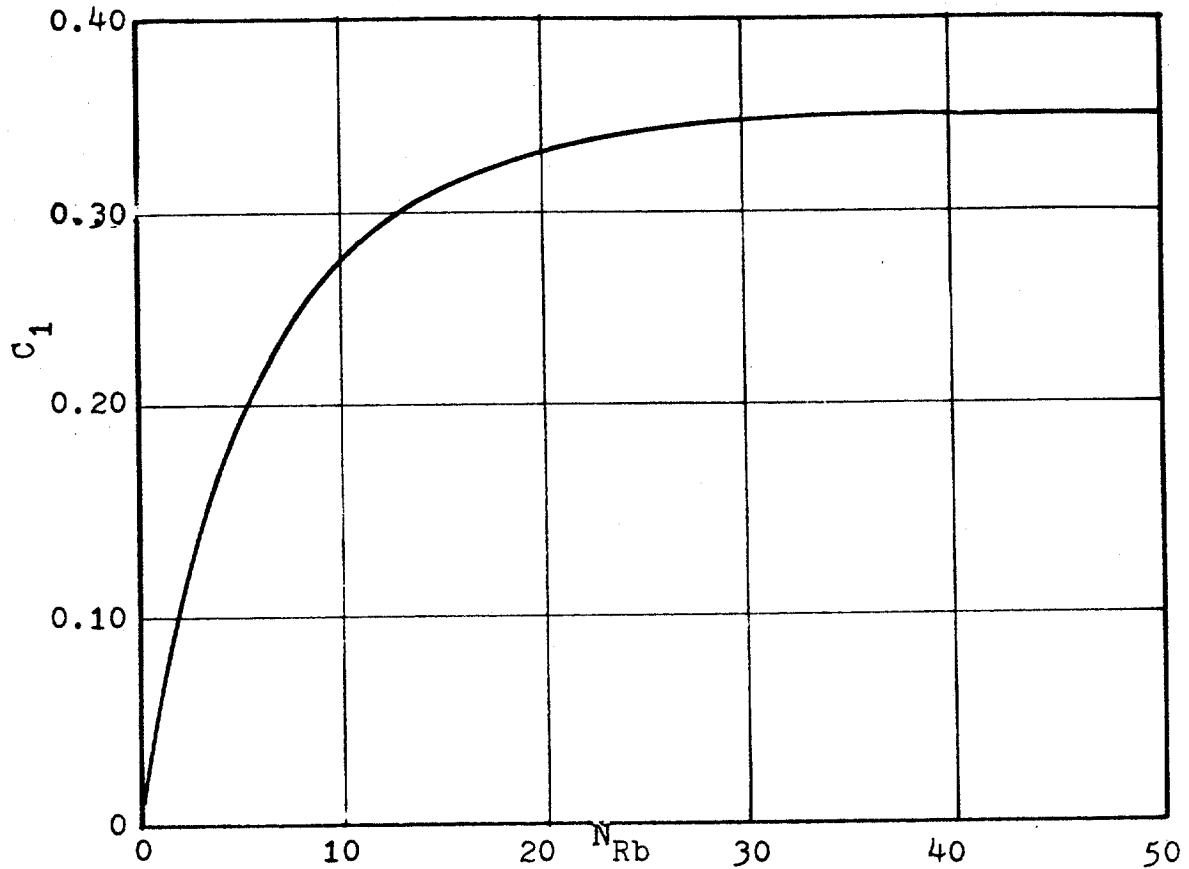


Figure 2.10 Dimensionless constant C_1 versus bubble Reynolds number (After Griffith and Wallis⁷).

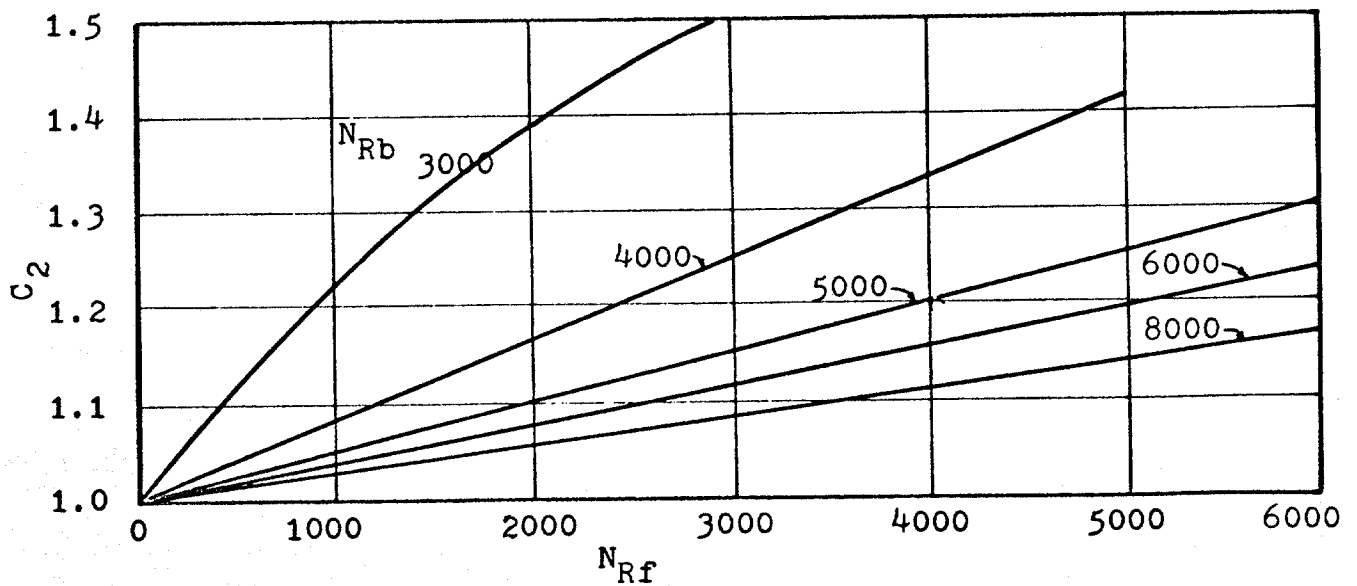


Figure 2.11 Dimensionless constant C_2 as a function of liquid Reynolds number and bubble Reynolds number (After Griffith and Wallis⁷).

solving for v_b yields

$$v_b = C_1 C_2 (g r_t)^{0.5} + \bar{v}_m \quad (2.43)$$

for inviscid liquids large diameters of tube and cylindrical bubbles C_1 reaches the value obtained by Dumitrescu, 0.496, to describe the slug velocity in closed end tubes.

In 1962 Nicklin, Wilkes and Davidson³⁵ performed a study on cylindrical bubbles flowing through either stagnant liquid or moving liquid. To prevent the viscous effects from becoming important, they used water as the liquid phase and a 1.02 in internal diameter tubing. They observed that the rising velocity of the gas slugs through stagnant liquid in an open tube increased with the length of the slugs as it has already been observed by other investigators furthermore, Nicklin et al found that increase in velocity to be related to the movement of the liquid caused by the expansion of the bubble itself. The investigators experimentally found that in a moving liquid stream the velocity of the cylindrical bubbles is given by the expressions

$$v_b = 0.496 (g r_t)^{0.5} + K_{Lv} \bar{v}_L \quad (2.44)$$

where v_b = the upward gas slug velocity

\bar{v}_L = the average upward liquid velocity

K_{Lv} = a coefficient having a value of 1.48 for liquid Reynolds number below of 2000 and a value of 1.2 for liquid Reynolds number above of 2000.

The liquid Reynolds number, N_{RL} , is given by

$$N_{RL} = \frac{d_t \bar{v}_L \rho_L}{\mu_L} \quad (2.45)$$

where d_t = internal diameter of the tube

\bar{v}_L = average velocity of the liquid

ρ_L = density of the liquid

μ_L = viscosity of the liquid

The first term of the right side of the equation is the Dumitrescu's equation for cylindrical bubbles in a static liquid. The second term accounts for the effect of the moving liquid. The factor K_{Lv} , in front of the liquid velocity is greater than one because the average liquid velocity in the central core of the tube where the gas tends to reside is greater than the average liquid velocity in the complete section of the tube. When both liquid and gas were continuously injected in the bottom of the tube, the steady state bubble rise velocity, for turbulent flow, was found to be predicted by

$$v_b = 0.496 (g r_t)^{0.5} + 1.2 (v_{sL} + v_{sg}) \quad (2.46)$$

where v_{sL} = the superficial liquid velocity

v_{sg} = the superficial gas velocity

the remaining terms are defined above.

By analogy, the authors extended the use of their equation for small bubbles.

Equation (2.44) of Nicklin et al and Equation (2.43) of Griffith and Wallis define the bubble rise velocity in a moving liquid stream. The expressions differ in the way the effect of liquid velocity on the velocity of the bubble is taken into account. Griffith and Wallis chose to take this effect into account using an empirical coefficient placed in the first term of the right side of equation rather than through use of a second term.

Also in 1962, White and Beardmore³⁶ performed experimental work on large bubbles rising in tubes. They used glass tubes of diameters ranging from 0.5 to 3.87 cm. The fluids used had specific gravities ranging from 0.997 to 1.40, viscosities ranging from 0.87 to 20,900.00 cp, and surface tensions ranging from 30.8 to 77.7 dyne/cm. A correlation for velocity of rise of cylindrical bubbles in vertical tubes was presented using dimensionless groups. Their correlation is presented in Figure 2.12. The correlation is given in terms of (1) the diameter number N_d , (2) the Froude number, N_{Fr} ; and (3) a property group, or liquid viscosity number, N_L .

These groups are defined by

$$N_d = (\rho_L g d_t^2 / \sigma_L)^{0.5} \quad (2.47)$$

$$N_{Fr} = v_b^2 / g d_t \quad (2.48)$$

$$N_L = (g \mu_L^4 / \rho_L \sigma_L^3)^{0.25} \quad (2.49)$$

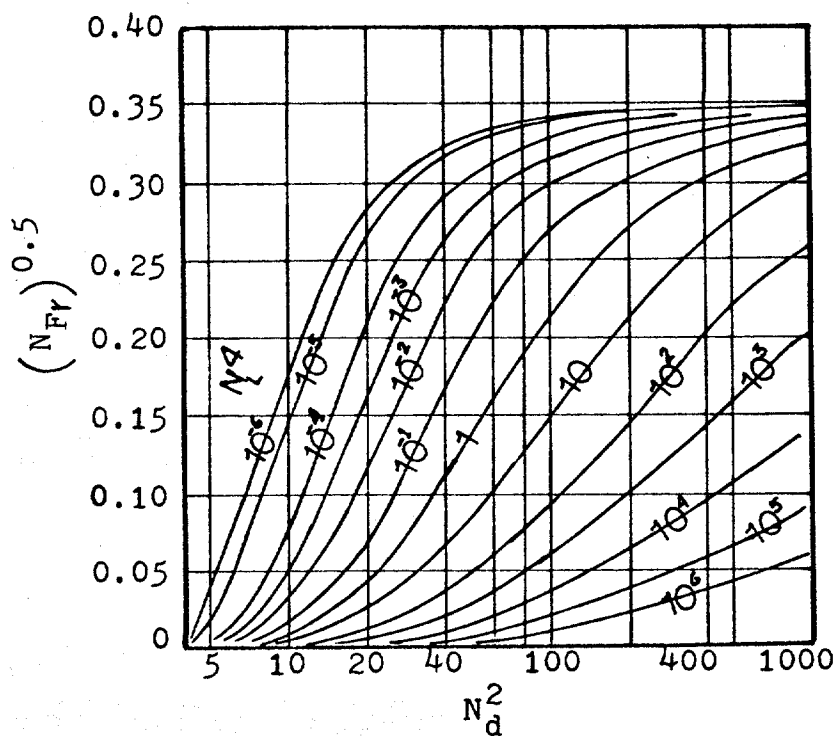


Figure 2.12 General correlation for velocity of rise of cylindrical air bubbles (After White and Beardmore³⁶).

where ρ_L = the density of the liquid
 g = gravitational acceleration
 d_t = internal tube diameter
 σ_L = interfacial tension between fluid and bubble
 v_{bo} = terminal velocity of the bubble, relative to undisturbed liquid
 μ_L = viscosity of the liquid

The correlation can be used in the following way.

(1) Calculate the property group, or liquid viscosity number, N_L , and the diameter number, N_d , which only are function of the continuous phase properties and the geometry of the tube. (2) With these two parameters, determine the maximum of the square root of the Froude number, from Figure 2.12. Solving this equation, the velocity of a cylindrical bubble in such a system will be determined.

Example 2.1

Determine the velocity of cylindrical bubbles v_{bo} in 1.18, 2.24 and 6 in diameter tubings which are filled with livestock oil. The fluid properties are:

$$\mu_L = 84.69 \text{ cp} = 56.91 \times 10^{-3} \frac{\text{lbm}}{\text{ft-sec}}$$

$$\rho_L = 54.88 \text{ lbm/ft}^3$$

$$\sigma_L = 34.07 \text{ dyne/cm} = 0.07496 \text{ lbm/sec}^2$$

1. Calculate the fourth power of the property group or liquid viscosity number, N_L

$$N_L^4 = \frac{\varepsilon \mu_L^4}{\rho_L \sigma_L^3} = \frac{32.17 (56.91 \times 10^{-3})^4}{54.88 (0.07496)^3} = 1.46 \times 10^{-2}$$

2. Calculate the square of the diameter number, N_d

$$N_d^2 = \frac{\varepsilon \rho_L}{\sigma_L} d_t^2 = \frac{32.17 (54.88)}{0.07496} d_t^2 = 23552 d_t^2$$

$$\text{if } d_t = 1.18 \text{ in, } N_d^2 = 227.7$$

$$d_t = 2.24 \text{ in, } N_d^2 = 820.7$$

$$d_t = 6.0 \text{ in, } N_d^2 = 5887$$

3. Determine, from Figure 2.12, the value of the square root of the Froude number, $v/(gd)^{0.5}$, for each tube diameter.

$$\text{if } d_t = 1.18 \text{ in, } \frac{v_{bo}}{(gd)^{0.5}} = 0.315$$

$$d_t = 2.24 \text{ in, } \frac{v_{bo}}{(gd)^{0.5}} = 0.333$$

$$d_t = 6 \text{ in, } \frac{v_{bo}}{(gd)^{0.5}} = 0.35$$

4. Calculate the cylindrical bubble velocity

$$\text{if } d_t = 1.18 \text{ in, } v_{bo} = 0.315 \left(\frac{32.17 \times 1.18}{12} \right)^{0.5} = 0.56 \text{ ft/sec}$$

$$d_t = 2.24 \text{ in, } v_{bo} = 0.333 \left(\frac{32.17 \times 2.24}{12} \right)^{0.5} = 0.82 \text{ ft/sec}$$

$$d_t = 6.0 \text{ in, } v_{bo} = 0.35 \left(\frac{32.17 \times 6.0}{12} \right)^{0.5} = 1.40 \text{ ft/sec}$$

These theoretical values obtained through the use of the White and Beardmore correlation are in good agreement with the measured values reported by O'Brian and Gosline³¹: 0.55, 0.75 and >1.28 ft/sec for 1.18, 2.24 and 6.0 in tubing respectively. The value >1.28 means that O'Brian and Gosline did not obtain completely developed cylindrical bubbles for the 6 in diameter tubing.

In their conclusions, White and Beardmore stated: "The velocity is unaffected by (1) viscosity if $\frac{\rho_L^2 g d^3}{\mu_L^2} > 3 \times 10^5$, (2) surface tension if $\frac{\rho_L g d^2}{\sigma_L} > 70$, and (3) inertial effects if $(v_{bo}^2/g d)^{0.5} < 0.05$."

Brown³⁷ also published a correlation of large bubbles rising in vertical tubes. The velocity of the bubble in a stagnant liquid was expressed as follows:

$$v_{bo} = 0.496 (g r_t)^{0.5} \left(1 - \frac{-1 + (1 + 2 Nr_t)^{0.5}}{Nr_t} \right) \quad (2.50)$$

where N = Dimensional property parameter, ft^{-1} ,

$$= (14.5 \rho_L^2 g / \mu_L^2)^{1/3}$$

ρ_L = liquid density, lbm/ft^3

μ_L = liquid viscosity, $lbm/ft\text{-sec}$

g = gravity acceleration, ft/sec^2

r_t = tubing radius, ft

The author limited this equation for the following conditions:

1) Surface tension parameter:

$$\frac{\rho_L g r_t^2}{\sigma_L} \left(1 - \frac{r_t - r_o}{r_t} \right) > 5.0$$

2) Viscosity parameter

$$2 N r_t > 60$$

In these expressions, $(r_t - r_o)$ is the equilibrium liquid film thickness falling past the large lenticular bubble of radius r_o in a tube of radius, r_t .

Example 2.2

Determine the velocity of cylindrical bubbles for the data of example 2.1.

1. Calculate the dimensional property parameter, N .

$$N = \frac{(14.5 \text{ g } \rho_L^2)}{\mu^2}^{1/3} = \frac{(14.5 \times 32.17 (54.88)^2)^{1/3}}{(56.91 \times 10^{-3})^2}$$

$$N = 756.99 \text{ ft}^{-1}$$

2. Check if the Brown's correlation is limited by viscosity:

$$2 N r_t = 2 (756.99) r_t$$

The minimum value for the above expression will be obtained for $d_t = 1.18 \text{ in}$, or $r_t = 0.0492 \text{ ft}$

$$2 N r_t = 2 (756.99) (0.0492) = 74.43$$

Since $74.43 > 60$ the Brown's correlation can be used.

3. Calculate the velocity of the cylindrical bubbles for each diameter.

d_t (in)	v_{bo} (ft/sec)
1.18	0.50
2.24	0.73
6.0	1.27

$$\text{where } v_{bo} = 0.496 (32.17 r_t)^{0.5} \left(1 - \frac{-1 + (1 + 756.99 d_t)^{0.5}}{756.99 (d_t/2)} \right)$$

The values of bubble velocity obtained with the Brown's correlation approaches the actual values given by O'Brian and Gosline.

Zukosky¹⁷ performed a series of experiments in order to determine the influence of viscosity, surface tension and tube inclination on motion of long bubbles in closed tubes. He defined a velocity v_o to normalize his results and determined two dimensionless parameters to assure similarity between two systems. These parameters are given by the following expressions:

$$v_o = (g r_t \frac{\rho_L - \rho_g}{\rho_L})^{0.5} \quad (2.51)$$

$$N_{Ro} = \frac{r_t v_o \rho_L}{\mu_L} \quad (2.52)$$

$$\Sigma = \frac{\sigma_L}{g (\rho_L - \rho_g) r_t^2} = \frac{4}{N_d^2} \quad (2.53)$$

He concluded that for bubble Reynold numbers greater than about 200, the velocities are substantially independent of viscous effects. He also pointed out that the surface

tension parameter Σ tended to increase with decreasing bubble Reynolds number so that it was difficult to ascertain if Σ or N_{R_0} is the controlling factor. However, Figure 2.13 was presented as evidence that the surface tension has very large effect for Σ values above 0.1. With respect to the tube inclination, Zukosky found that the velocity increases with the angle of inclination (measured from the vertical), and it reaches a maximum at around 45° . The effect of tube inclination is shown in Figure 2.14.

Example 2.3

Determine the velocity of cylindrical bubbles for the data of example 2.1

$$\Sigma = \frac{\sigma_L}{g(\rho_L - \rho_g) r_t^2} = \frac{4 \sigma_L}{g(\rho_L - \rho_g) r_t^2} = \frac{4}{N_d^2}$$

d_t (in)	N_d^2	Σ	$(v_{bo}/v_o)^*$	v_{bo} (ft/sec)
1.18	227.7	17.57×10^{-3}	0.44	0.553
2.24	820.7	4.874×10^{-3}	0.44	0.762
6.0	5887	0.6795×10^{-3}	0.44	1.25

* From Figure 2.13

$$v_{bo} = 0.44 \left(g r_t \frac{\rho_L - \rho_g}{\rho_L} \right)^{0.5} = 0.44 \left(g \frac{(54.88 - 0.0882)}{54.88} r_t \right)^{0.5}$$

$$v_{bo} = 0.44 (32.17 \times 0.9984 r_t)^{0.5}$$

$$v_{bo} = 0.44 (32.12 r_t)^{0.5}$$

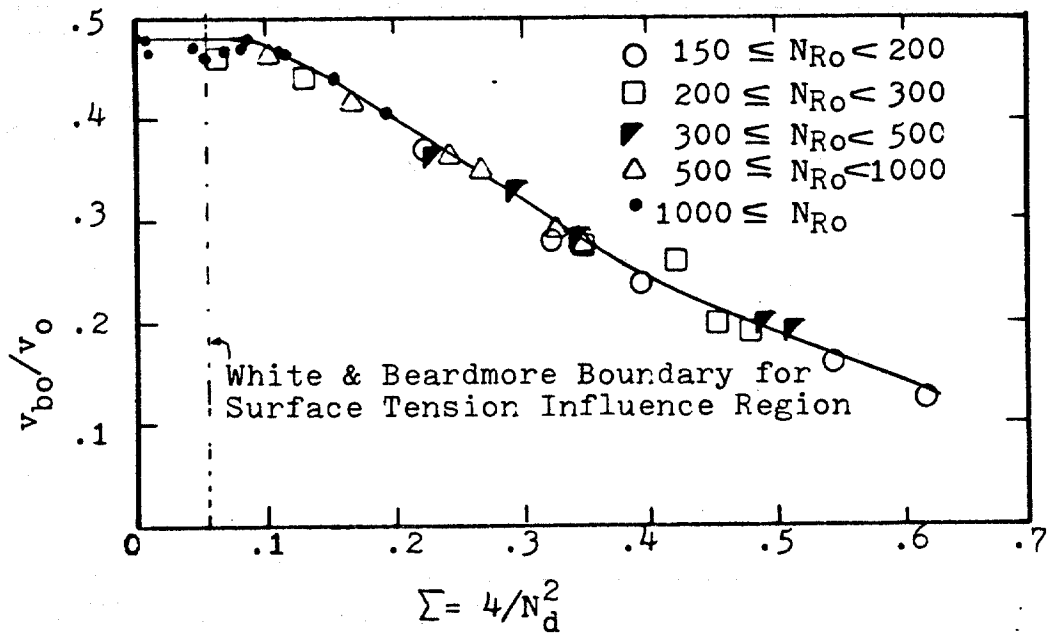


Figure 2.13 Bubble velocity vs. surface tension parameter for ranges of Reynolds numbers (After Zukoski¹⁷).

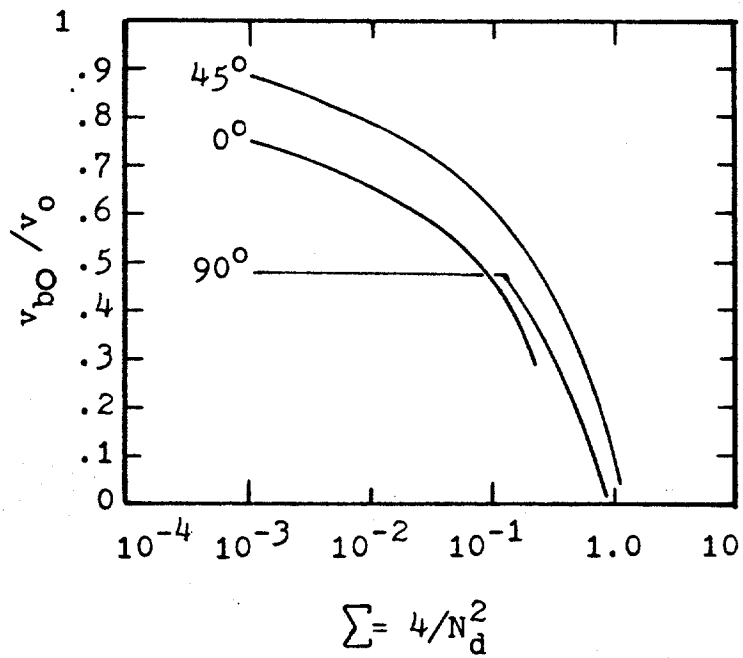


Figure 2.14 Variation of normalized velocity with diameter number for angles of inclination as measured with respect to a horizontal plane (After Zukoski¹⁷).

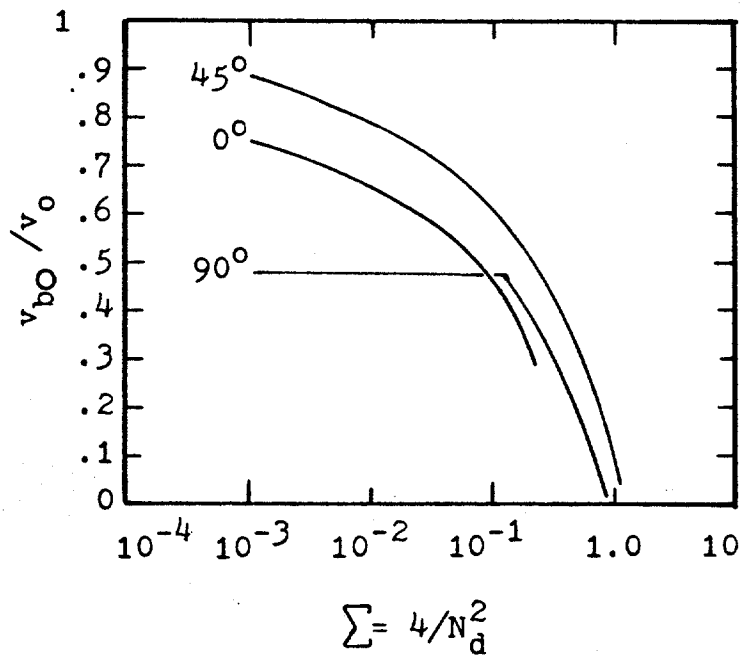


Figure 2.14 Variation of normalized velocity with diameter number for angles of inclination as measured with respect to a horizontal plane (After Zukoski¹⁷).

This equation gives the values reported in column 5.

In 1967, Collins³⁸ presented a work dealing with the effect of a cylindrical boundary on the velocity of large gas bubbles in a liquid. The solid lines in Figure 2.8 represent the theoretical solution found by the author. This theoretical solution is a function of the curvature radius of the bubble at the forward stagnation point of the bubble. Using the empirical relation derived by Davies and Taylor relating the bubble velocity with volume of lenticular bubbles, he arrived to the semi-empirical line shown in Figure 2.15. Here, v_{bo} is the bubble velocity in a restricted media and v_{∞} is the Davies-Taylor velocity of bubbles in an infinite media. Eq. (2.24). The geometry and the volume of the bubble were correlated by the equation

$$\frac{\bar{r}_c}{r_t} = 0.71 \tanh^{0.5} \left[4.25 (v_b^{1/3}/r_t)^2 \right] \quad (2.54)$$

where \bar{r}_c is the average curvature radius

r_t is the tube radius

2.2.3 Annuli

Only a very limited number of investigators have studied the rise of gas in an annular geometry. However, since the transversal section of annuli may be approximately as a rectangle, a review of bubbles rising in rectangular channels was also included in the literature review.

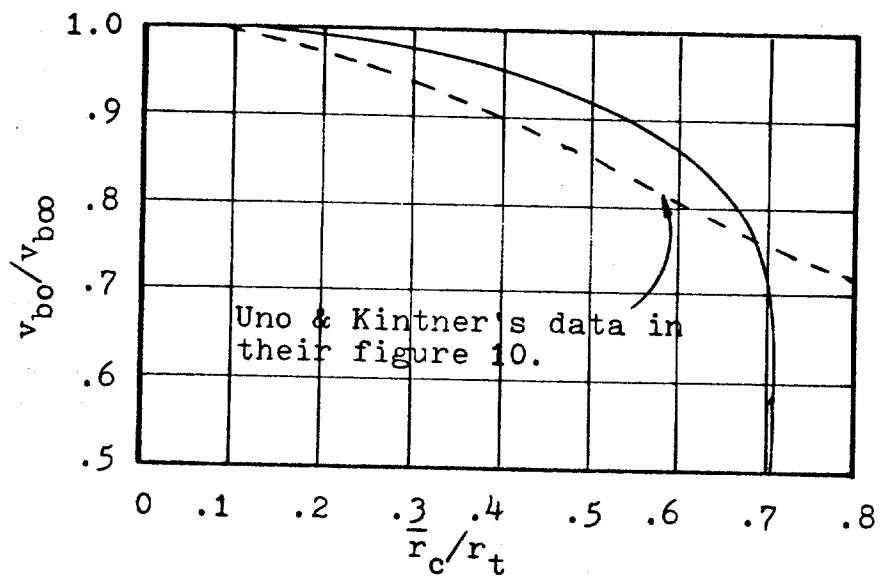


Figure 2.15 Variation of v_{bo}/v_{b00} with \bar{r}_c/r_t
(After Collins³⁸).

Griffith³⁹ determined experimentally that the limiting gas slug velocity, v_{bo} , is given by

$$v_{bo} = (0.23 + 0.065 \frac{2t}{w}) (gw)^{0.5} \quad (2.55)$$

where w is the channel width

t is the channel thickness

g is the gravity acceleration

If the channel is thought of as an annulus, (See Figure 2.6) the width and the thickness of the channel can be approximated by the following equations

$$\begin{aligned} 2t &= d_2 - d_1 \\ w &= \frac{\pi}{2} (d_2 + d_1) \end{aligned}$$

and the Equation (2.55) can be expressed by

$$v_{bo} = \left[0.2883 + 0.05186 \left(\frac{d_2 - d_1}{d_2 + d_1} \right) \right] [g (d_2 + d_1)]^{0.5} \quad (2.55a)$$

In 1965, R. Collins⁴⁰ derived the velocity of a two-dimensional gas bubble rising in liquid along the axis of a channel of finite width. He chose as asymptotes of the two-dimensional solution

$$v_{bo} = 0.5 (g r_c)^{0.5} \quad (2.56)$$

$$v_{bo} = 0.238 (g w)^{0.5} \quad (2.57)$$

where v_{bo} = velocity of lenticular plane bubbles between infinitely wide parallel plates.

v_{bo} = gas slug velocity in a rectangular channel of width w

g = acceleration due to gravity

r_e = curvature radius of a lenticular bubble

w = width of a rectangular channel

The equation (2.56) was also derived by Collins while the equation (2.57) is the Garabedian solution for the limiting velocity of a plane bubble. Normalizing his results with the first two equations, Collins gave the expressions:

$$\frac{v_{bo}}{v_{bo\Box}} = \left[\frac{3w}{2\pi r_c} \left(3 + \left(\frac{3w}{2\pi r_c} \right)^2 \right) \right]^{0.5} - \left(\frac{3w}{2\pi r_c} \right)^{1.5} \quad (2.58)$$

$$\frac{v_{bo}}{v_{bo\Box}} = \frac{w}{\pi r_c} \left[3 + \left(\frac{3w}{2\pi r_c} \right)^2 \right]^{0.5} - 6 \left(\frac{w}{2\pi r_c} \right)^2 \quad (2.59)$$

$$\text{where } \frac{r_c}{w} \leq \frac{3}{2}$$

If a channel is thought of as an annulus bounded by diameters d_1 and d_2 , equations (2.57), (2.58), and (2.59) become

$$v_{bo\Box} = 0.2987 \left[g (d_1 + d_2) \right]^{0.5} \quad (2.57a)$$

$$\frac{v_{bo}}{v_{bo\Box}} = \left[\frac{3 (d_1 + d_2)}{4 r_c} \left[3 + \left(\frac{3 (d_1 + d_2)}{4 r_c} \right)^2 \right] \right]^{0.5}$$

$$- \left[\frac{3 (d_1 + d_2)}{4 r_c} \right]^{1.5} \quad (2.58a)$$

$$\frac{v_{bo}}{v_{bo\infty}} = \frac{d_1 + d_2}{2 r_c} \left[3 + \left(\frac{3 (d_1 + d_2)}{4 r_c} \right)^2 \right]^{0.5}$$

$$- 6 \left(\frac{d_1 + d_2}{4 r_c} \right)^2 \quad (2.59a)$$

The theoretical curves and the experimental results given by Collins are plotted in Figure 2.16. Collins reported the actual values of bubble velocities to be 9% higher than the calculated with his equations. He explained that this difference was due to the three-dimensional nature of the real flow. The curvature radius, r_c , can be related to the volume of the bubble either through the equivalent radius concept given in Equation (2.28) or through the following relationship derived by Collins, $r_c = 2.695 r_e$.

Maneri and Mendelson⁴¹ wrote a paper in 1968. They used a wave theory analogy and arrived to the following equation for bubbles rising in rectangular channels:

$$\frac{v_{bo}}{v_{bo\infty}} = \left[\tanh \left(\frac{\pi C_3 (w/2 r_e)}{2 + t/r_e} \right) \right]^{0.5} \quad (2.60)$$

where

$$v_{bo\infty} = \left[\frac{\pi \sigma_L}{(2 r_e + t) \rho_L} + \frac{g (2 r_e + t)}{\pi} \right]^{0.5} \quad (2.61)$$

$$C_3 = \left(\frac{2 + (2t/w)}{\pi} \right) \tanh^{-1} \left\{ \frac{2 \pi [0.23 + 0.065 \times 2t/w]}{2 + (2t/w)} \right\}^2 \quad (2.62)$$

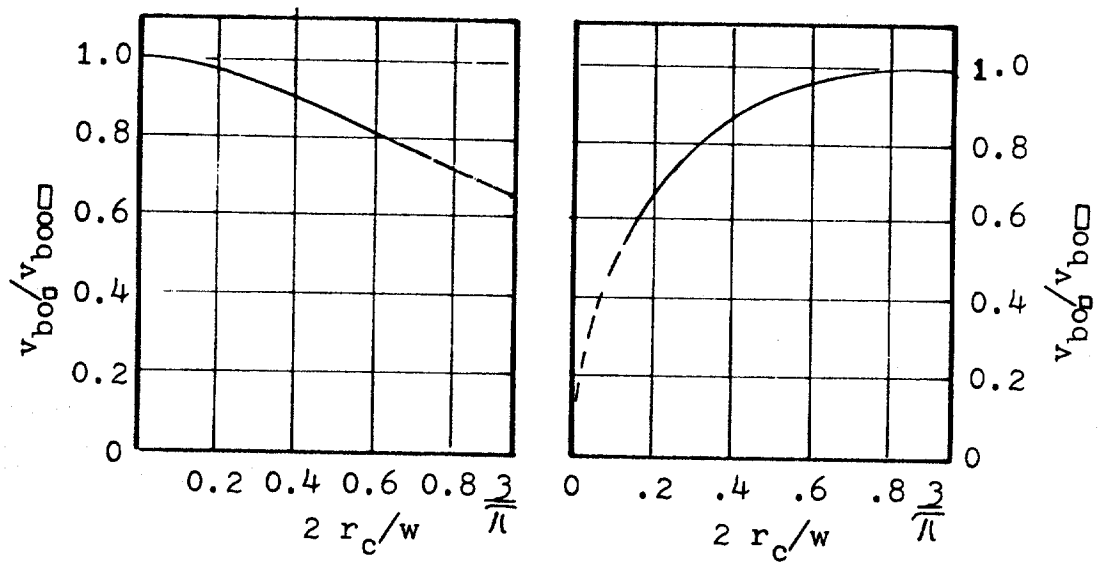


Figure 2.16 Variation of bubble velocity with $2 r_c/w$. (After Collins⁴⁰)

Here, the equivalent radius, r_e , describes that of one plane bubble having a thickness t and a curvature radius, r_c . The transformation from r_c to r_e given by the authors is illustrated in Figure 2.17. The relationship between r_c and r_e is given either by equation (2.28) or by that presented by Collins. The former equations adapted for an annular space limited by radii r_1 and r_2 , can be expressed:

$$\frac{v_{bo}}{v_{bo\infty}} = \left[\frac{\tanh \left(\frac{\pi^2 c_3 \left(\frac{r_2 + r_1}{r_e} \right)}{4 + 2 \left(\frac{r_2 - r_1}{r_e} \right)} \right)}{r_e} \right]^{0.5} \quad (2.60a)$$

$$v_{bo\infty} = \left[\frac{2 \sigma_L}{(2 r_e + (r_2 - r_1)) \rho_L} + \frac{g (2 r_e + (r_2 - r_1))}{\pi} \right]^{0.5} \quad (2.61a)$$

$$c_3 = \frac{2}{\pi} + \frac{2}{\pi^2} \left(\frac{r_2 - r_1}{r_2 + r_1} \right) \tanh^{-1}$$

$$\left\{ \frac{2\pi \left[0.23 + \frac{0.065 \times 2}{\pi} \left(\frac{r_2 - r_1}{r_2 + r_1} \right) \right]^2}{2 + \frac{2}{\pi} \left(\frac{r_2 - r_1}{r_2 + r_1} \right)} \right\} \quad (2.62a)$$

In 1975, D.W. Rader, A.T. Bourgoyne, and R.W. Ward¹⁸ introduced a correlation to calculate annular bubble rise velocity. Their experimental work was performed in small laboratory models. The parameters experimentally studied were (1) annular geometry, (2) liquid viscosity, (3) gas and

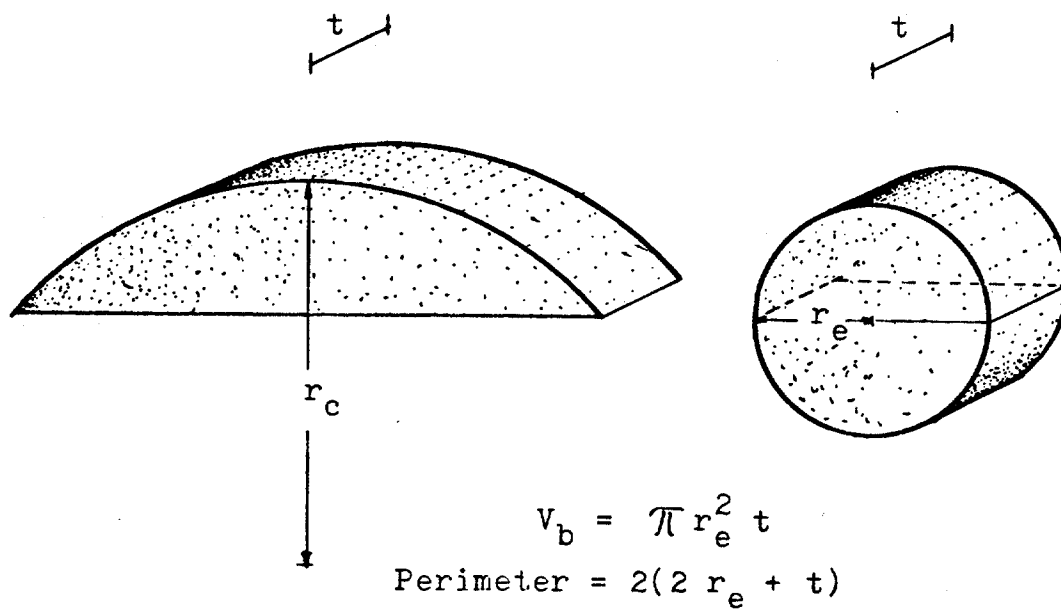


Figure 2.17 Definition of equivalent radius and perimeter for plane bubble.

liquid densities, (4) gas expansion, (5) liquid velocity, (6) slanted wells, (7) bubble length, (8) the interface tension between gas and liquid, (9) eccentricity of the annulus. They showed that the first six parameters affect significantly the raise velocity of a simple continuous bubble whereas the remaining three parameters have little or no effect on the slip velocity of a continuous bubble. Furthermore, they arrived to the following conclusions:

1. A gas bubble rising in a vertical annulus will travel up on side of the annulus with liquid backflow occupying an area opposite to the bubble.

2. The fractional area of liquid backflow increases as the viscosity of the fluid increases.

Their experimental work covered annular spaces bounded by inner diameters, d_1 , from 0.2 in to 7.94 in and by outer diameters, d_2 , from 0.58 in to 9.58 in. Both newtonian and non-newtonian fluids were used as liquid phase. The viscosity range of Newtonian fluids was from 1 to 1050 cp. Non-Newtonian fluids covered the following range of rheologic characteristics: (1) yield point from 1.3 to 129 lb/100 ft², and (2) plastic viscosity from 11 to 111 cp.

Rader, Bourgoyne and Ward arrived to the following correlation for gas slug velocity.

$$v_{b/L} = \left[0.163 + 0.0920 \log N_{Rb} \right] (d_1 + d_2)^{.5} \left[\frac{\rho_1 - \rho_g}{\rho_L} \right]^{.5} \quad (2.63)$$

$$1 \leq N_{Rb} \leq 100\,000$$

$$N_{Rb} = \frac{928 \rho_L v_{b/L} (d_2 - d_1)}{\mu_L} \quad (2.64)$$

where $v_{b/L}$ = relative velocity of the slug respect the liquid, ft/sec

d_1 = outside diameter of the inner tube of the annulus, in

d_2 = inside diameter of the outer tube of the annulus, in.

ρ_L = liquid density, lb/gal

ρ_g = gas density, lb/gal

μ_L = liquid viscosity, cp

When expressed in a set of consistent units, Equation (2.63) becomes

$$v_{b/L} = \left[2.395 \times 10^{-3} + 1.352 \times 10^{-3} \log N_{Rb} \right] \left(g (d_1 + d_2) \frac{(\rho_L - \rho_g)}{\rho_L} \right)^{0.5} \quad (2.63a)$$

2.3 Liquid Holdup Correlations

An important parameter needed in the quantitative characterization of two phase flow patterns is the average fractional volume of the conduit which is occupied by gas,

Q , or conversely, the fractional volume occupied by liquid, H_L . The fractional liquid volume is commonly called the liquid holdup. Many previous investigators who have

presented empirical correlations for determining flow patterns also have presented liquid holdup correlations.

The liquid holdup can be related to the average slip velocity of the gas bubbles relative to the liquid

$$\bar{v}_s = \bar{v}_g - \bar{v}_L \quad (2.65)$$

The average upward gas flux called the gas superficial velocity is given by

$$\bar{v}_{sg} = \frac{q_g}{A} \quad (2.66)$$

The true upward average gas velocity is given by the gas volume flow rate divided by the average area available to the gas. Thus

$$\bar{v}_g = \frac{q_g}{A \alpha} = \frac{\bar{v}_{sg}}{\alpha} = \frac{\bar{v}_{sg}}{1 - H_L} \quad (2.67)$$

Similarly, the upward liquid superficial velocity is given by

$$\bar{v}_{sL} = \frac{q_L}{A} \quad (2.68)$$

and the true upward average liquid velocity is given by

$$\bar{v}_L = \frac{q_L}{A H_L} = \frac{\bar{v}_{sL}}{H_L} \quad (2.69)$$

A convenient grouping of terms called the mixture velocity is defined by

$$\bar{v}_m = \bar{v}_{sg} + \bar{v}_{sL} \quad (2.70)$$

Employing Equations (2.65) - (2.70) it can be shown that:

$$H_L = \left[(\bar{v}_s - \bar{v}_m) + \sqrt{(\bar{v}_m - \bar{v}_s)^2 + 4 \bar{v}_s \bar{v}_{sL}} \right] \frac{1}{2\bar{v}_s} \quad (2.71)$$

It must be remembered in employing Equation (2.71) that an upward direction was assumed for both the gas and liquid flow.

Hagedorn and Brown⁴² published a correlation to find a theoretical liquid holdup. Their correlation requires the calculation of four dimensionless numbers. These numbers depend on the liquid phase properties, the geometry of the tube and the superficial velocity of the fluids. Three of the dimensionless numbers are defined by Equations 2.1b, 2.1c, and 2.1d; the fourth number, N_L , is defined

$$N_L = \mu_L \sqrt[4]{\frac{g}{\rho_L \sigma_L^3}} \quad (2.72)$$

where μ_L = viscosity of the liquid
 σ_L = surface tension of the liquid
 ρ_L = liquid density
 g = gravity acceleration

The holdup in Hagedorn and Brown's correlation was determined as that required to make the calculated pressure losses to fit with the measured pressure losses. The measured pressure losses were obtained from tests performed in small diameter tubings of 1500 ft of length.

Duns and Ross¹⁴ measured directly the liquid holdup. They published correlations of dimensionless functions against the viscosity number, N_L , defined by Equation 2.72. The dimensionless functions determine the slip velocity number, N_s , which is defined

$$N_s = v_s \left(\frac{\rho_L}{\sigma_L g} \right)^{0.25} \quad (2.73)$$

The slip velocity obtained from this equation is substituted in Equation 2.71 to obtain the liquid fraction. Griffith and Wallis⁷ defined the gas fraction as

$$\alpha = \frac{v_{sg}}{v_m + v_{bo}} \quad (2.74)$$

where α , v_{sg} and v_m are defined as above, and v_{bo} is the bubble rise velocity with respect to the liquid. This velocity includes a correction factor to take into account the compressibility of the gas phase. The expression to obtain v_{bo} is the Equation (2.40) already discussed.

$$v_{bo} = C_1 C_2 (g r_t)^{0.5}$$

the authors published two correlations to determine the constants C_1 and C_2 .

Nicklin, Wilkes and Davidson³⁵ derived the following expression to determine the "equivalent" length of liquid around a gas slug:

$$L_{eL} = 0.495 (d_t L_s)^{0.5} \quad (2.75)$$

where d_t = tube diameter, in.

L_s = gas slug length, in.

L_{eL} = equivalent length of liquid around a slug, in.

The equivalent length of liquid is the volume of liquid around a slug divided by the area of the tube.

The authors showed experimentally that Equation (2.75) holds for short slugs.

Nicklin et al, also published an equation to determine the gas slug velocity in non static liquids:

$$v_b = 1.2 \left(\frac{q_g + q_L}{A} \right) + 0.35 (g d_t)^{0.5} \quad (2.76)$$

The authors reported that this equation was successfully tested for predicting the voidage or gas fraction defined as follows:

$$\alpha = \frac{v_{sg}}{v_b} \quad (2.77)$$

where v_{sg} is the superficial gas velocity

v_b is the rising velocity of the slug with respect to the tube.

They extended the use of the Equation (2.76) to bubble flow pattern. By analogy, they proposed the following equation for bubble flow.

$$v_b = \frac{q_g + q_L}{A} + v_{bo} \quad (2.78)$$

where v_{bo} is the rising bubble velocity in a stagnant liquid
 v_b is the rising velocity of the bubbles with respect
to the tube.

The gas fraction for bubble flow is also predicted by
Equation (2.77). Notice that the only difference between
bubble flow and slug flow equations is a coefficient of 1.2.

Brown and Govier⁴³ proposed the following correlation
for single bubble velocity in moving liquid streams

$$\frac{v_b}{v_{bo}} = f \left(C_o \frac{\bar{v}_L}{v_{bo}} \right) \quad (2.79)$$

\bar{v}_L is the average liquid velocity ahead of bubble, relative
to tube. C_o was empirically determined and presented as
Figure 2 in their work⁴³. The bubble velocity, v_b was
tested for predicting the gas voidage through the use of
Equation (2.77). The authors reported excellent results
even for flow pattern other than slug or bubble flow.

Some investigators have worked out theoretical
calculations for a single flow pattern.

Marrucci²⁸ proposed an expression relating the
velocity of rise of a swarm of spherical bubbles to the
velocity of a single bubble. Based in an analysis of a
cellular spherical model, he derived the following equation

$$v_{\text{swarm}} = v_{bo} \frac{(H_L)^2}{1 - \alpha^{5/3}} \quad (2.80)$$

$$1 < N_{Rb} < 300$$

where v_{swarm} = velocity of a swarm of bubbles with respect

to the liquid.

v_{bo} = velocity of a single bubble with respect to the liquid above or below the bubble.

α = volume fraction occupied by the gas.

$$H_L = 1 - \alpha$$

Equation 2.80 is restricted to the range of high but sub-critical Reynolds numbers, and pure, ideal fluids.

Bhatia⁴⁵ derived a method to predict the gas holdup or gas fraction of a swarm of bubbles based on the bubble velocity in a restricted media as developed by Mendelson and Maneri⁴¹. Therefore, this method is applicable to pure inviscid liquids. The relationship between volumetric gas fraction and bubble velocity given by Bhatia is

$$v_{bo} = v_{bo\infty} \sqrt{\tanh (0.25 (1/\alpha)^{1/3})} \quad (2.81)$$

where v_{bo} = relative velocity of a bubble or a swarm of bubbles in a bounded system with respect to the upstream liquid.

$v_{bo\infty}$ = velocity of the bubble in an infinite media as defined by Equation (2.30)

α = volumetric gas fraction

The gas fraction, α , is in turn defined by

$$\alpha = \left(\frac{r_e}{r_t} \right)^3 \quad (2.82)$$

where r_e = equivalent radius of a gas bubble based on a
sphere of equal volume

r_t = tube radius

Equation (2.81) does not apply for slug flow.

CHAPTER III

EXPERIMENTAL APPARATUS AND PROCEDURE

After completing a review of the previous investigations related to the determination of flow patterns, gas slip velocity, and gas concentrations in a well during pressure control operations, it was felt that considerable additional experimental work would be required before any major improvements in the accuracy of computer simulations of pressure control operations could be achieved. As was noted in the previous Chapter, most of the previous work was done in tubes or extended liquids rather than in an annulus. Also, essentially all of the flow pattern work was done for steady state conditions involving the continuous injection of gas and liquid into the bottom of the tubular section. This previous flow pattern work was directed towards an understanding of producing wells, especially those producing by means of artificial gas injection using gas lift valves. Almost no previous work towards an improved understanding of two phase flow patterns occurring during pressure control operations was found. Thus, the next phase of this study involved the design and construction of an experimental apparatus for modeling an annular well

geometry. After construction of the model was completed, several types of experiments were conducted. This chapter describes the apparatus and experimental procedures used.

3.1 Apparatus

A diagram of the model constructed is shown in Figure 3.1. The main feature of the model is the 32 ft vertical tube having an internal diameter of 6.375 and an external diameter of 6.625 . This tube simulates the casing or bore hole of a well. The casing consists of four sections of transparent, PVC pipe joined by flanges. The lower end of the casing is attached to a pressure vessel by means of a ball valve. This vessel has a pressure relief valve to prevent the pressures in excess of 80 psig, the working pressure of the PVC tube. The upper end of the casing is connected to a gas/liquid separator vessel by means of a tube having the same diameter as the casing.

In order to simulate drill pipe within the casing a 2 inches diameter tube of PVC with a check valve attached to its lower extreme could be placed in the casing.

Liquid could be circulated down the drill string and up the annulus by means of a centrifugal pump. Gas could be injected into the bottom of the model either from the pressure vessel by means of a quick open ball valve or in a continuous manner by means of a pressure regulated gas supply.

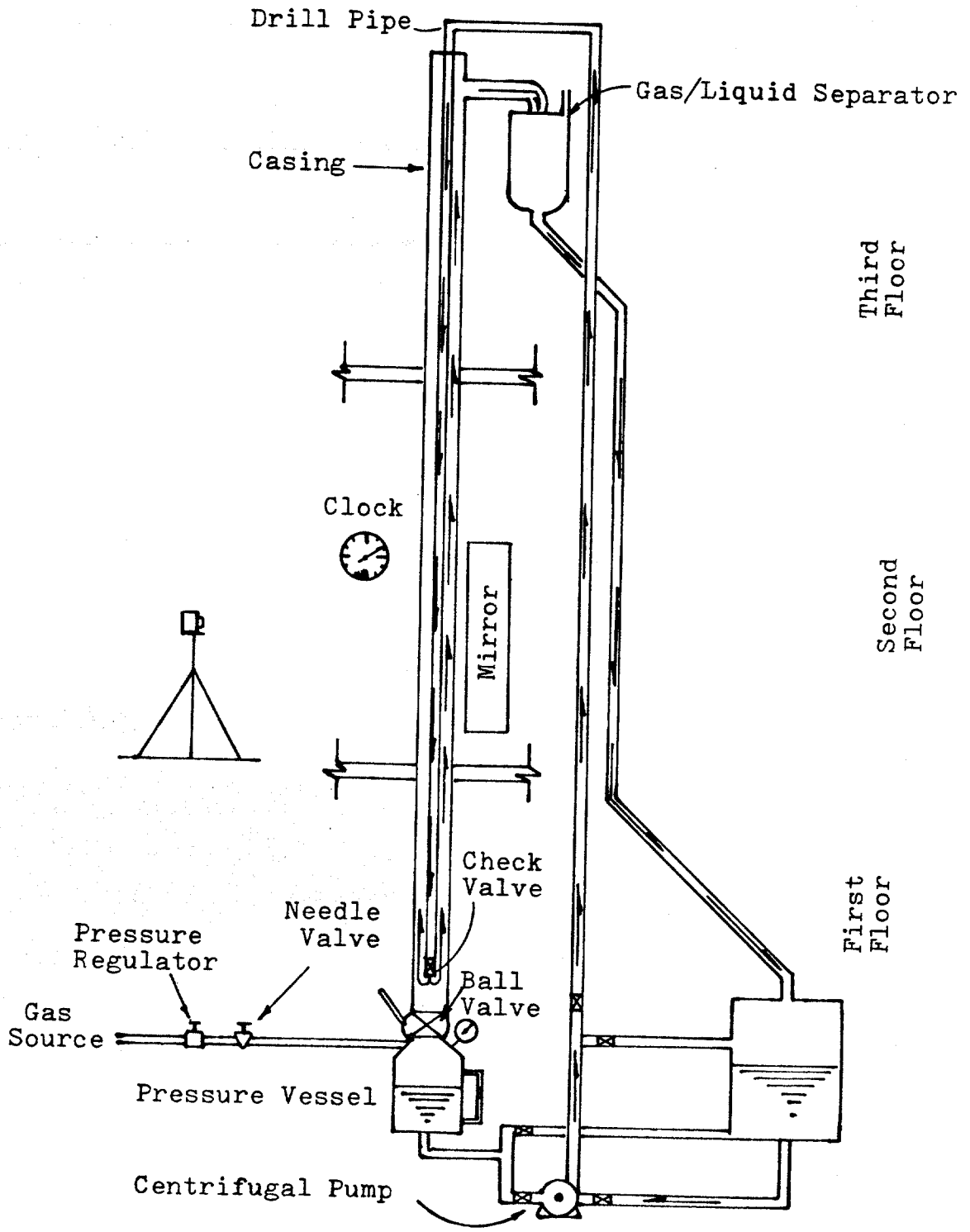


Figure 3.1 Diagram of the Model.

Mixtures of water and glycerine were used to investigate the effect of the viscosity on the flow patterns. The range of liquid viscosities was from 1 to 146 cp, and the range of liquid densities was from 1 to 1.231 gr/cc, measured at 29°C, respectively. The liquid phase was colored with green food dye to obtain contrast in the photographs of the bubbles. A 35 mm camera loaded with Kodak Tri-X pan film was used. Two neon-tubes and two flooding lamps were used to light the casing section of interest. A mirror was arranged near a section of the vertical column to allow opposite sides of the column to be simultaneously photographed. The negatives were analyzed in an enlarger. Finally, to analyze whether the small gas bubbles are incorporated to the main initial bubble, a movie camera was used.

3.2 Experimental Procedure

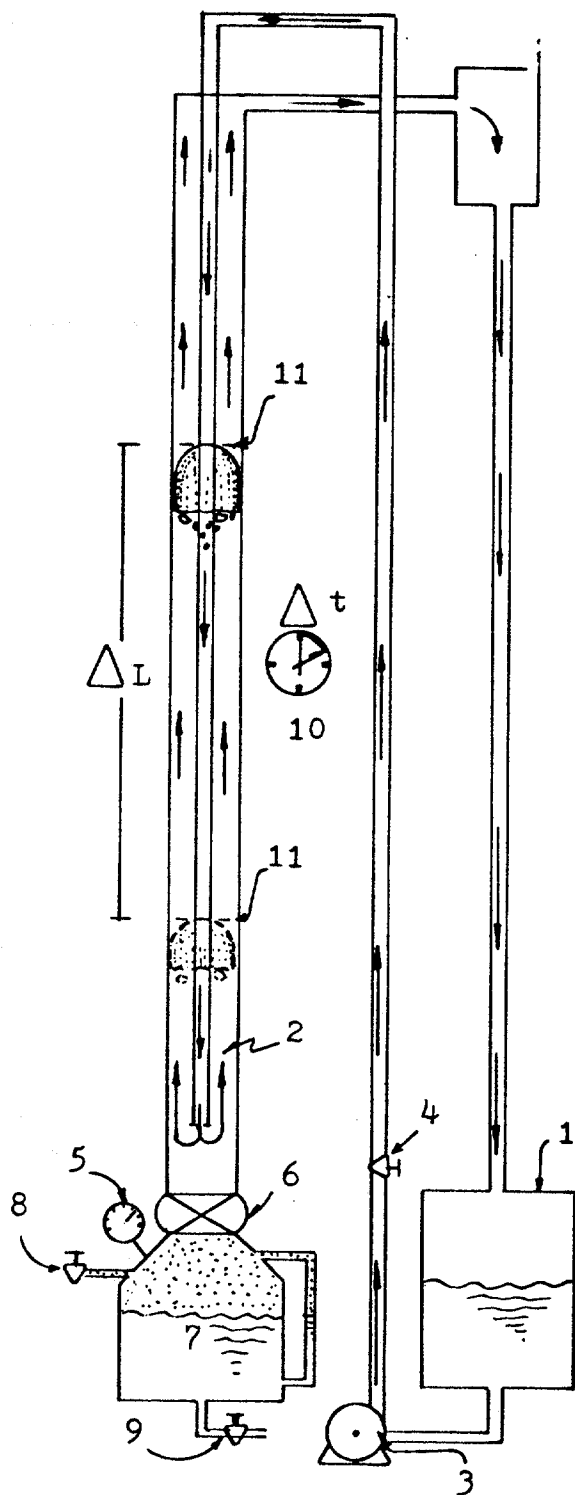
The initial experimental procedures used in the new apparatus were designed to test the Bourgoyne-Rader gas slip velocity correlation that had been developed in a prior LSU study based on data collected by Rader⁴⁶, by Ward⁴⁷, and by Koederitz⁴⁸. The experimental apparatus used in these previous studies were inferior to the new apparatus in that (1) circulation was possible only in very small, 0.58 in diameter models and (2) the large diameter models were relatively short, having a maximum length of 12 ft. Also, the previous studies included only a fully developed slug flow pattern which occurs for very high gas injection rates.

Application of the Bourgoyne-Rader correlation to tests conducted in a 6000 ft well by Mathews⁴⁹ indicated that real well behavior could not be adequately described using this correlation. Mathews concluded that the difference in predicted and observed well behavior was probably due to the presence of smaller gas bubbles in the 6000 ft well during simulated pressure control operations. The observed pressure behavior of the well indicated a lower gas migration velocity than obtained through use of the Bourgoyne-Rader correlation.

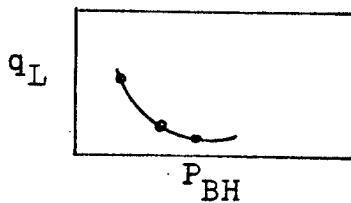
3.2.1 Bubble Rise Velocity Measurements

The first set of experiments were conducted to measure the slip velocity of a wide range of gas bubble sizes for several different liquid flow rates and liquid viscosities. The experimental procedure followed is illustrated in Fig.3.2.

The desired liquid was placed in the holding tank (1). The liquid was pumped into the wellbore (2) using the centrifugal pump (3). A throttle valve (4) was fixed at the desired setting during model fill-up and the effective pump characteristics were defined during fill-up by plotting the change in fluid height in the model wellbore with time versus the bottom hole pressure (5). After fill-up, the ball valve (6) was closed and the desired gas volume was placed in the pressure chamber (7) by pressurizing the upper portion of the chamber using a pressure regulated gas supply (8) and draining liquid from the lower portion of the chamber through the drain valve (9). Gas



1. Store desired gas volume in pressure vessel (7).
2. Set pump throttle valve (4).
3. Note fill-up time to various heights and plot pump flow rate, q_L , versus bottom hole pressure.



4. Estimate final flow rate at P_{BH} .
5. Open ball valve (6).
6. Measure ΔL and Δt .
7. Photograph the gas bubble.

Figure 3.2 Experimental Procedure Followed in Bubble Rise Velocity Measurements.

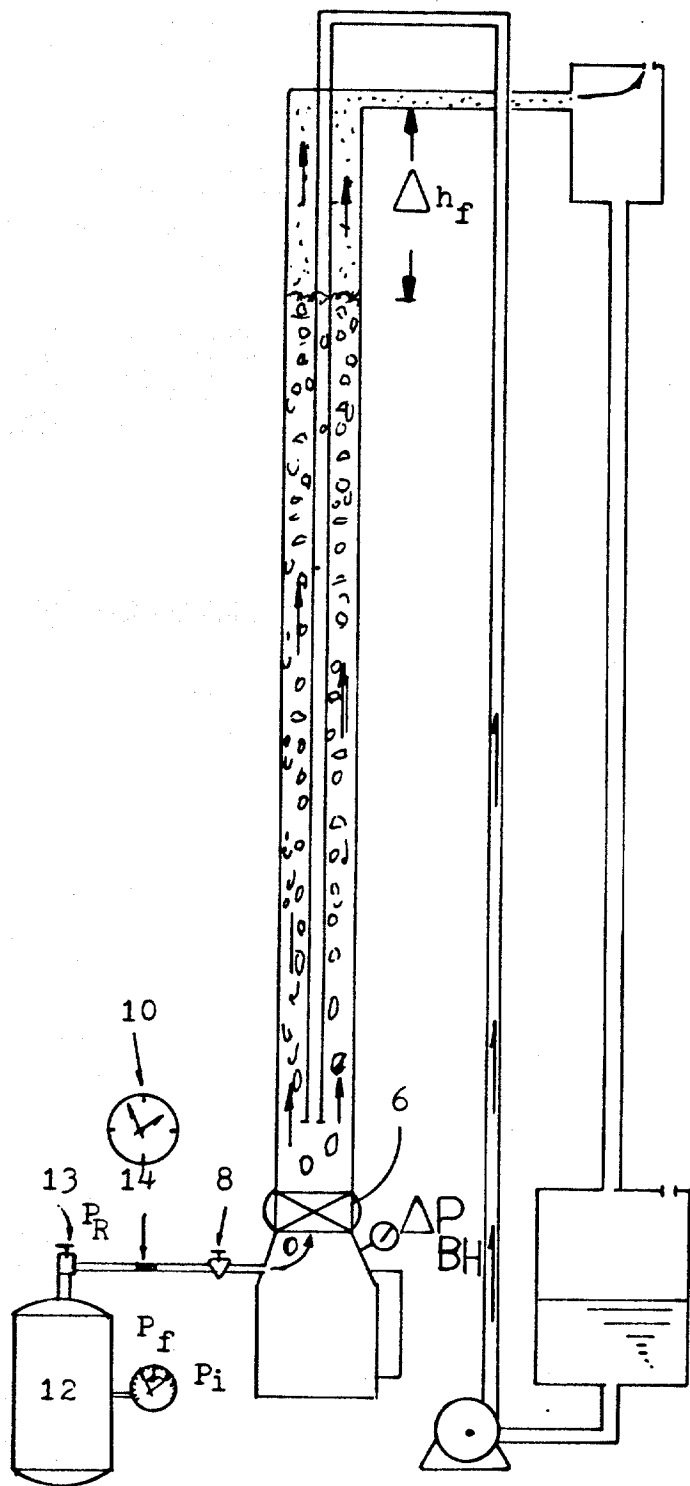
injection was accomplished by rapidly opening the ball valve (6). The velocity of the gas slug or bubble was obtained by noting the elapsed time (10) for the top of the slug to pass between two markers (11) at the second floor level. The gaseous region was photographed using both a 35 mm camera and a 16 mm movie camera. Slug length was estimated from the photographs.

3.2.2 Flow Patterns Observations

The second set of experiments were conducted to determine the effect of constant flow rate on the flow pattern of a gas kick, and particularly, on the initial gas distribution. These experiments were made for different fluid rates and liquid viscosities. The experimental procedure followed is illustrated in Figure 3.3.

The model fill-up was made as it was described above. The ball valve (6) remained open. The gas tank (12) was filled to a pressure P_i and the regulator (13) was set to obtain a reduced pressure P_R . The gas flow rate was controlled by setting the needle valve (8) at a desired opening. The quick opening valve (14) was opened suddenly and simultaneously the time counter (10) was turned on. Both the leading edge of the gas and the developed flow pattern were photographed. The time elapsed for the tank pressure (12) to fall from P_i to P_f was noted. The ball valve (14) was closed. The final static bottom hole pressure was recorded to obtain the change in bottom hole pressure and/or

the change on the liquid level was recorded.



1. Fill column with liquid and adjust liquid flow rate as described previously.
2. Fill gas tank to P_i .
3. Set regulator (13) to P_R .
4. Set needle valve (8) and open ball valve (6).
5. Photograph the initial slug formed (leading edge) and state flow pattern achieved
6. Note time for tank to fall to Pressure P_f .
7. Close valve and record ΔP_{BH} and/or Δh_f .

Figure 3.3 Flow Pattern Observations.

CHAPTER IV

EXPERIMENTAL RESULTS

Before presenting the results, it is convenient to describe the relations between the parameters used in developing the present work. Figure 4.0 illustrates the nomenclature and describes the velocities and their relationships. The velocities are presented by vectors and are scaled to show their relationship. The definition of the terms is as follows:

- A is the fixed observation point or reference point.
- v_{L-} is the average velocity of the liquid flowing behind the gas contaminated region.
- v_{L+} is the average velocity of the liquid flowing ahead of the gas contaminated region.
- v_b is the measured velocity of the leading edge of the gas contaminated region.
- v_E is the component of the gas velocity caused by gas expansion.
- $v_b - v_{L-}$ is the slip velocity of the leading edge of the gaseous region with respect to the liquid below.
- $v_b - v_{L+}$ is the slip velocity of the leading edge of the

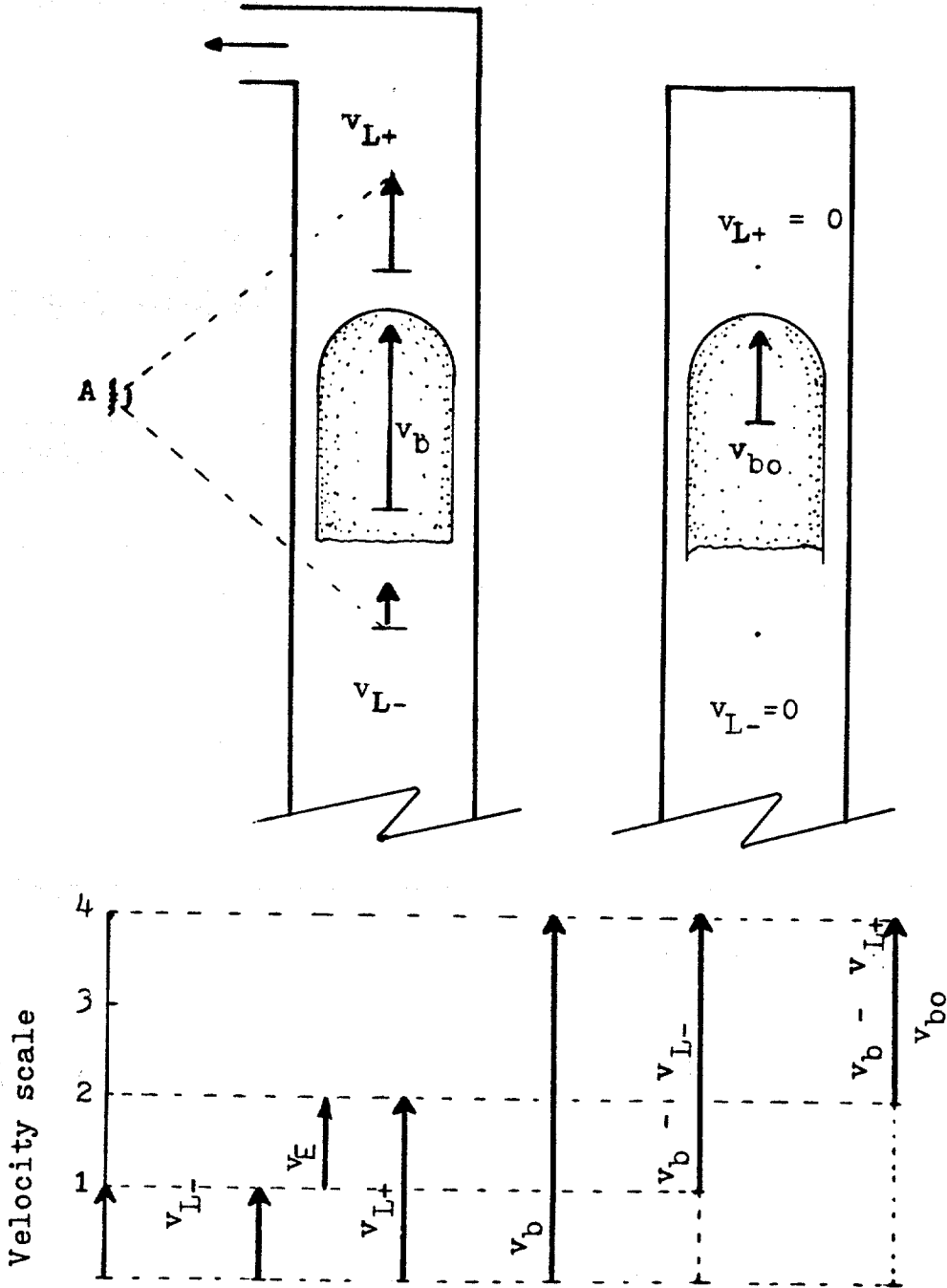


Figure 4.0 Definition of Velocities and Its Relationships.

gaseous region with respect to the liquid above. When slug flow develops at the top of the gaseous region and v_{L-} is zero, this relative velocity is equal to the limiting gas slug velocity v_{bo} as it is defined by Dumitrescu's equation, or as it is measured in a closed end tube.

4.1 Bubble Rise Velocity Measurements

4.1.1 Tube

The first runs were performed in the 6.375 in internal diameter tube. These runs were aimed at determining the effect of the liquid viscosity on the limiting velocity of gas bubbles in a large vertical tube. Previous experimental data were not available for tube diameters greater than about 2 in. Tap water and a 146 cp solution of glycerine were used as liquid phases. All measurements were obtained in static liquids, i.e., with v_{L-} equal to zero. The obtained data are presented in Table 4.1 and were plotted in Figure 4.1 after correcting for gas expansion effects. The correction for the gas expansion effect was made using the last term of Equation (2.44) with the liquid velocity v_L taken as v_{L+} , the liquid velocity above the bubble. The cylindrical bubble velocities, corrected by gas expansion effect were in good agreement with the velocity predicted by Dumitrescu's theory.

Based on the Dumitrescu's velocity and the data of

TABLE 4.1 Velocity of Cylindrical Bubbles in a 6.375 in. Tube

FLUID	Measured Velocity v_b (ft/sec)	Bubble Length Theoretical ¹ (ft)	Actual ² (ft)	Non-Expanding Bubble Velocity $v_{b-KLy} \bar{v}_{L+}$ (ft/sec)	Eq. 4.1 (ft/sec)
Water	1.475	1.18	-	1.427	1.44
	= 1.0 cp 1.519	1.76	-	1.445	1.44
	= 1.0 1.506	1.50	1.08	1.444	1.45
	1.521	2.00	1.33	1.437	1.44
	1.567	2.50	1.69	1.458	1.46
	1.580	3.12	1.94	1.445	1.45
1.740	6.17	-	1.442	1.52	
Glycerine	1.553	1.67	-	1.449	1.467
	= 146 cp 1.565	1.43	1.50	1.475	1.493
	= 1.231 1.583	1.91	1.97	1.462	1.48
	1.614	2.38	2.38	1.460	1.49
	1.613	2.96	-	1.422	1.47
	1.983	5.86	-	1.517	1.73

¹ Gas volume injected, corrected for average gas pressure during the velocity determination, divided by the cross sectional area of the tube.

² The overall length of the leading slug determined photographically.

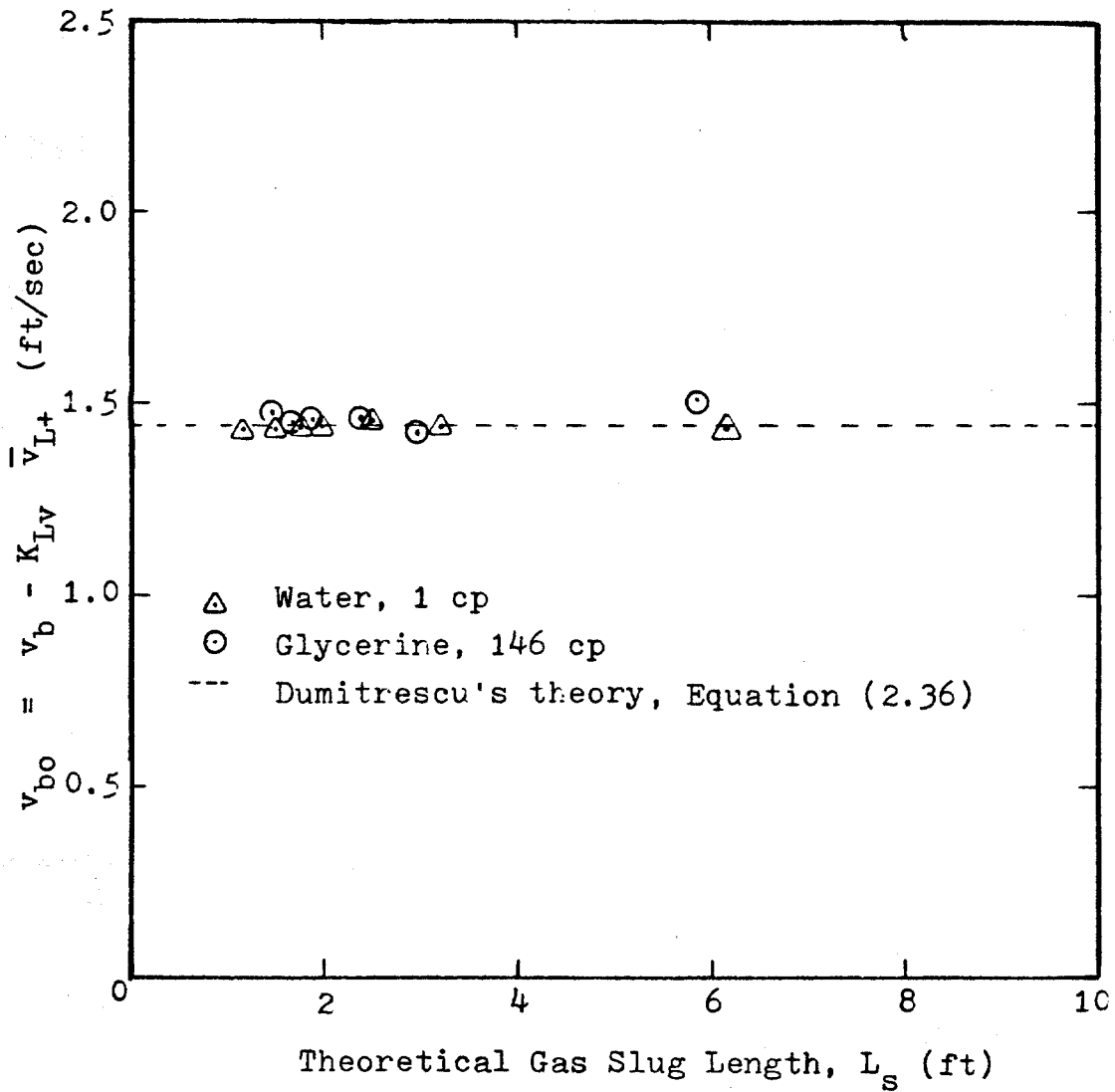


Figure 4.1 Velocity of Cylindrical Bubbles Versus Slug Length for Low and High Viscosity Liquids. Tube Diameter 6.375 in.

Table 4.1 the plot presented in Figure 4.2 was prepared using a new approach. This plot shows the bubble slip velocity, $v_b - v_{L-}$, as a function of the cylindrical bubble velocity v_{bo} predicted by Equation (2.36). Use of the liquid velocity above of the cylindrical bubble accounts for the departure of the Dumitrescu's potential theory and apparently provides a generalized correlation given by Equation 4.1.

$$\frac{v_b - v_{L-}}{v_{L+}} = 1.27 \left[\frac{v_{bo}}{v_{L+}} \right]^{0.9457} \quad (4.1)$$

Note that this equation can be solved for the slip-velocity in an ideal slug flow pattern. Note that there is good agreement between the experimental data and the velocities computed using either Equation (2.44) or (4.1), with Equation (4.1) being slightly better.

As a result of this new data, it can be seen that the viscosity does not greatly influence the slip velocity $v_b - v_{L+}$ in large diameter tubes. It appears that the velocity predicted by Dumitrescu's equation correctly predicts the velocity of a gas slug in a closed tube, regardless of liquid viscosity. However, the viscosity does affect the absolute velocity of a rising gas slug in an open tube. The liquid viscosity must be taken into account in correcting the Dumitrescu velocity to the

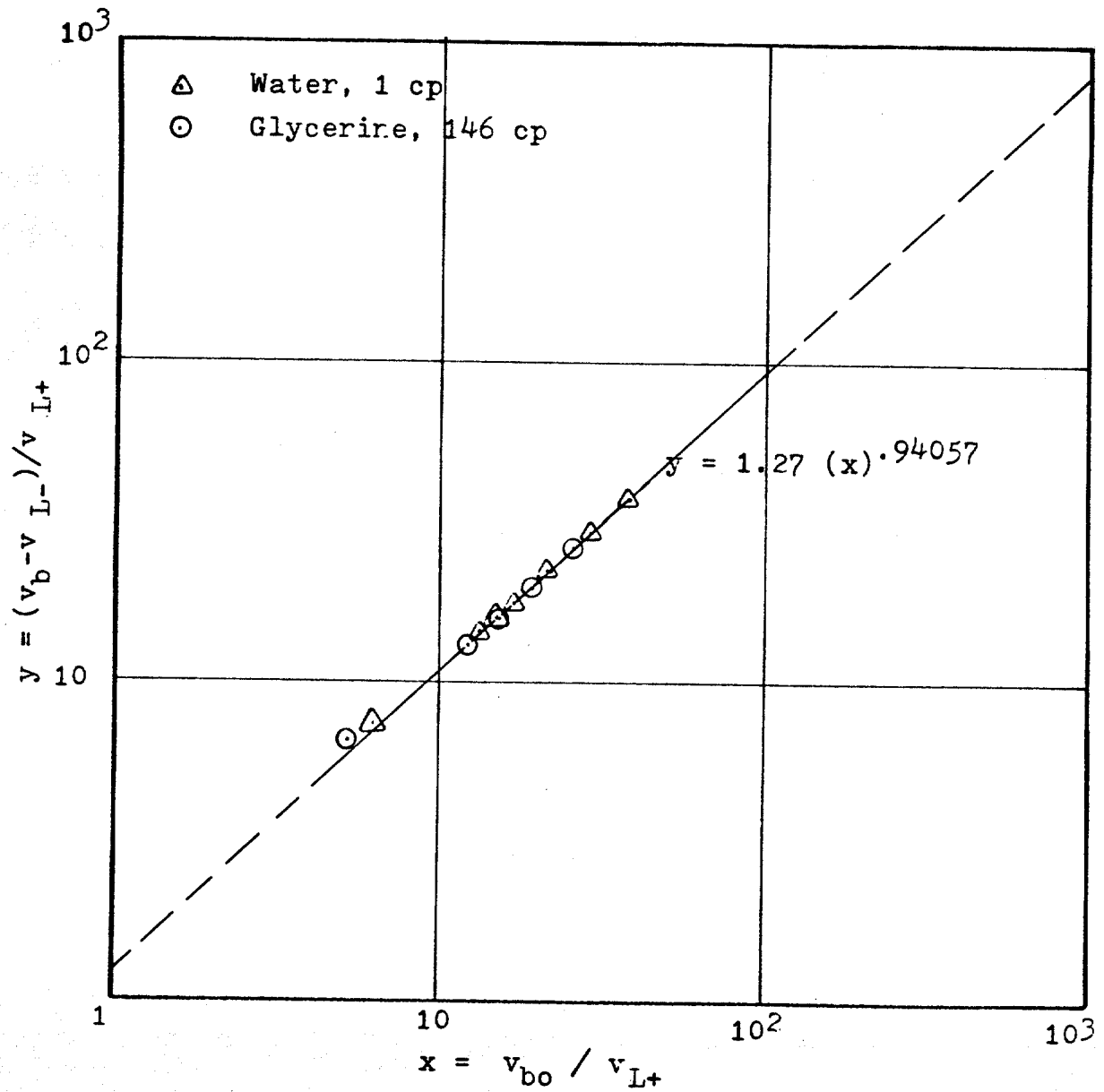


Figure 4.2 Relationship Between v_b and v_{bo} for Ideal Slug Flow.

TABLE 4.2a Velocity of Air Bubbles in an 6.375 in
by 2.375 in Annulus through Quiescent Water

Equivalent Diameter ¹ , d_e (inches)	Measured Velocity, v_b (ft/sec)	Eq. 2.63 $v_b - K_L v_{L+}$ (ft/sec)	Non-Expanding Bubble Velocity Eq. 4.2 v_{L+} (ft/sec)	Bubble Length ² Theoretical (ft)
1.66	1.28	-	-	.007
2.01	1.41	-	-	.013
2.15	1.41	-	-	.015
2.45	1.42	-	-	.023
2.61	1.47	-	-	.028
2.95	1.45	-	-	.041
9.70	1.55	-	-	1.450
10.01	1.56	-	-	1.590
10.51	1.57	1.471	-	1.850
10.85	1.57	1.472	1.41	2.020
11.22	1.57	1.463	1.40	2.240
11.57	1.56	1.468	1.39	2.460
11.84	1.57	1.465	1.40	2.640
12.22	1.58	1.466	1.40	2.890
12.41	1.59	1.468	1.41	3.030
12.80	1.58	1.450	1.40	3.330
12.92	1.61	1.464	1.42	3.430
13.33	1.61	1.460	1.42	3.760
14.27	1.62	1.455	1.42	4.610
14.72	1.63	1.425	1.42	5.070
16.24	1.69	1.457	1.47	6.800
	1.74	1.410	1.50	

1 Gas volume injected, corrected for average gas pressure during the velocity determination, expressed as the diameter of sphere which would contain this volume.

2 Gas volume injected, corrected for average gas pressure during the velocity determination, expressed as the length of annulus which would contain this volume.

TABLE 4.2b Velocity of Air Bubbles in an 6.375 in by 2.375 in Annulus through a Quiescent 80 cp Glycerine Solution.

Equivalent ¹ Diameter, d _e (inches)	Measured Velocity, v _b (ft/sec)	Eq. 2.63 (ft/sec)	Non-Expanding Bubble v _b -K _L v̄ _L + (ft/sec)	Bubble Velocity Eq. 4.2 (ft/sec)	Bubble Length ² Theoretical (ft)
0.75	1.27	1.235	-	-	-
0.74	1.03	1.235	-	-	-
0.77	1.15	1.235	-	-	-
0.91	1.12	1.235	-	-	-
0.97	1.20	1.235	-	-	-
1.29	1.32	1.235	-	-	-
1.60	1.38	1.235	-	-	-
1.71	1.37	1.235	-	-	-
2.19	1.44	1.235	-	-	-
2.77	1.49	1.235	-	-	-
3.45	1.53	1.235	1.52	1.51	.033
4.68	1.54	1.235	1.49	1.49	.065
5.82	1.56	1.235	1.53	1.47	.163
7.44	1.57	1.235	1.53	1.45	.326
9.30	1.61	1.235	1.53	1.46	.652
10.79	1.65	1.235	1.52	1.42	1.275
12.00	1.67	1.235	1.49	1.47	1.993
12.85	1.73	1.235	1.50	1.51	2.742
					3.365

1 Gas volume injected, corrected for average gas pressure during the velocity determination, expressed as the diameter of sphere which would contain this volume.

2 Gas volume injected, corrected for average gas pressure during the velocity determination, expressed as the length of annulus which would contain this volume.

TABLE 4.2c Velocity of Air Bubbles in an 6.375 in by
2.375 in Annulus through a Quiescent 146 cp
Glycerine Solution.

Equivalent ¹ Diameter, d_e (inches)	Measured Velocity, v_b (ft/sec)	Non-Expanding Bubble Velocity		Bubble Length Actual ³ (ft)	Bubble Length Theoretical ² (ft)
		Eq. 2.63 (ft/sec)	Eq. 4.2 (ft/sec)		
1.28	1.26	1.157	-	-	-
1.74	1.34	1.157	-	-	-
2.16	1.47	1.157	-	-	-
2.73	1.60	1.157	-	-	-
3.45	1.57	1.157	-	-	-
4.66	1.68	1.157	-	-	-
5.86	1.59	1.157	1.67	0.23	0.16
7.39	1.59	1.157	1.57	0.50	0.32
9.44	1.65	1.157	1.55	0.88	0.64
10.71	1.73	1.157	1.57	1.63	1.33
10.69	1.73	1.157	1.60	2.41	1.94
11.77	1.75	1.157	1.60	2.46	1.94
		1.157	1.57	2.67	2.59

1 Gas volume injected, corrected for average gas pressure during the velocity determination, expressed as the diameter of sphere which would contain this volume.

2 Gas volume injected, corrected for average gas pressure during the velocity determination, expressed as the length of annulus which would contain this volume.

3 Slug length determined from photographs.

velocity of an expanding gas slug in an open tube.

4.1.2 Annulus

The velocities of both lenticular bubbles and large slugs in quiescent fluids were determined in a 6.375 in by 2.375 in annulus. The obtained data for water, 80 cp glycerine solution and 146 cp glycerine solution are presented in Table 4.2a to Table 4.2c. Shown in Figure 4.3 are the measured velocities as a function of the equivalent diameter of the bubbles. The dashed line is the theoretical bubble velocity in a pure extended liquid predicted by Equation (2.30) and the continuous line is the bubble velocity predicted by Equation (2.29). The actual velocities of the bubbles were in agreement with the theoretical values up to an equivalent diameter of around 1.8 inches. From 1.8 to 3 inches of equivalent diameter the bubble velocities were in the range of 66% of the theoretical bubble velocity for lenticular bubbles. The boundary effects caused by the annular walls became more pronounced as the bubble size was increased.

From around 3.5 to 9 inches of equivalent diameter the bubbles appeared to reach a limiting slug velocity of about 1.55 ft/sec. However, the gas slugs were not well defined. Fully developed slugs ($d_e > 9$ in) increased their velocities up to 2 ft/sec. The phenomenon was believed to be due to the expansion of the bubble as it rose in the open tube. The more pronounced effect in the

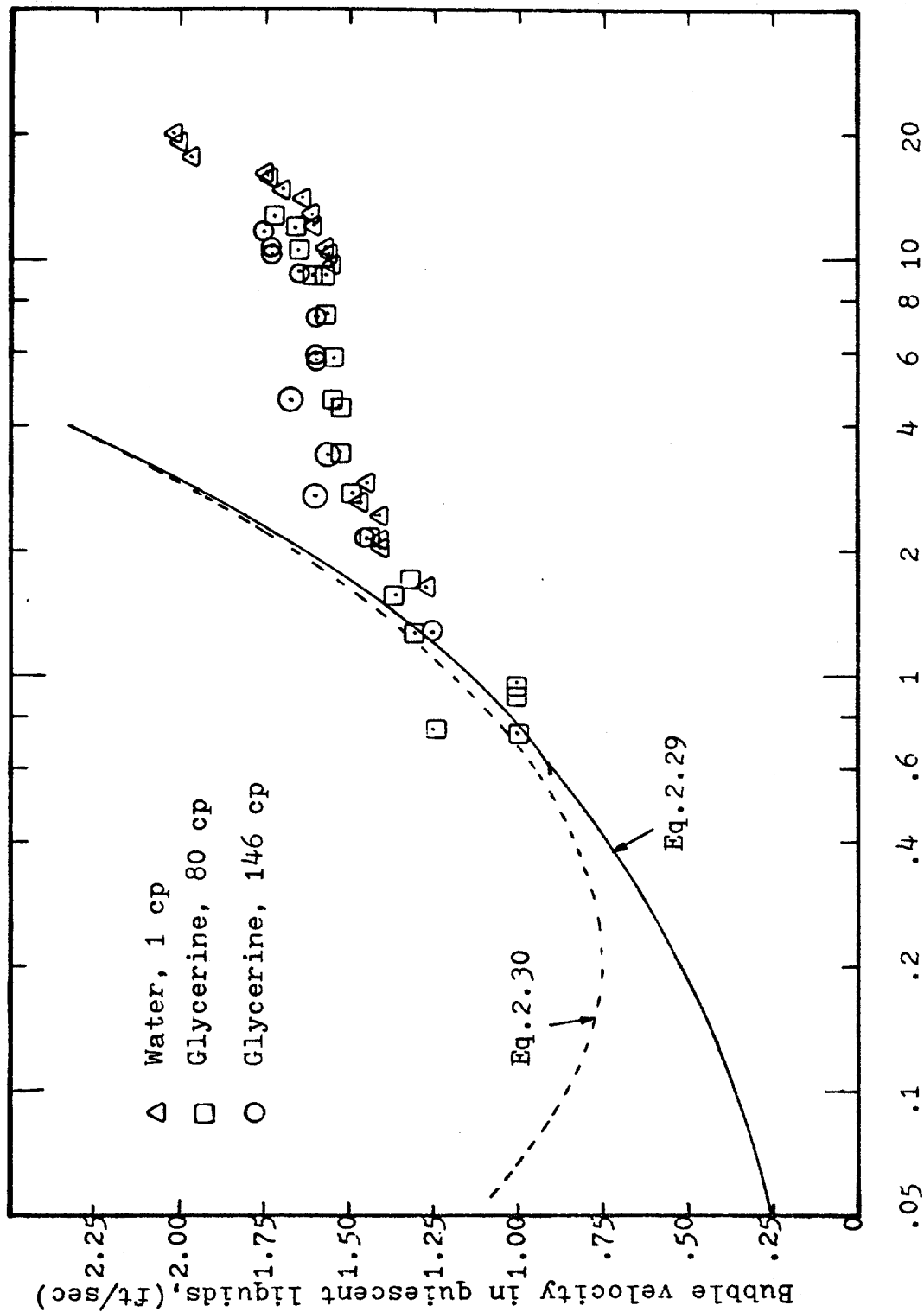


Figure 4.3 Measured Bubble Velocity Versus Equivalent Diameter of the Bubbles in a 6.375 in by 2.375 in Annulus (Zero Liquid Velocity).

high viscosity fluid is explained by the closer agreement between the theoretical slug length and observed slug length. The injected gas was indeed traveling as a single cylindrical bubble and gas expansion occurred at a higher rate. However, in water, bubble fragmentation was observed to occur due to turbulence, and only a fraction of the injected gas traveled in the main gas body. Unfortunately, the pictures of gas bubbles in water lack good definition and no actual slug length was reported.

The measured velocity of the gas slugs was corrected for expansion effects by computing bubble expansion using the theoretical slug length and using the last term of Equation 2.44 with the liquid velocity, v_L , taken as the liquid velocity above the gas, v_{L+} . The corrected bubble velocity is plotted in Figure 4.4. The limiting velocity appeared to be 1.51 ft/sec which is in good agreement with the value predicted by Equation 2.55 for a non expanding bubble.

Also shown in Tables 4.2a-c are values of bubble rise velocity computed using Equation (2.63) developed by Rader, Bourgoyne and Ward. Note that values predicted by Equation (2.63) tended to be in agreement with the values obtained for fully developed gas slugs in water (Table 4.2a). However, this equation predicted velocities around 33% lower for the fully developed gas slugs flowing in high viscosity fluids (Tables 4.2b and 4.2c).

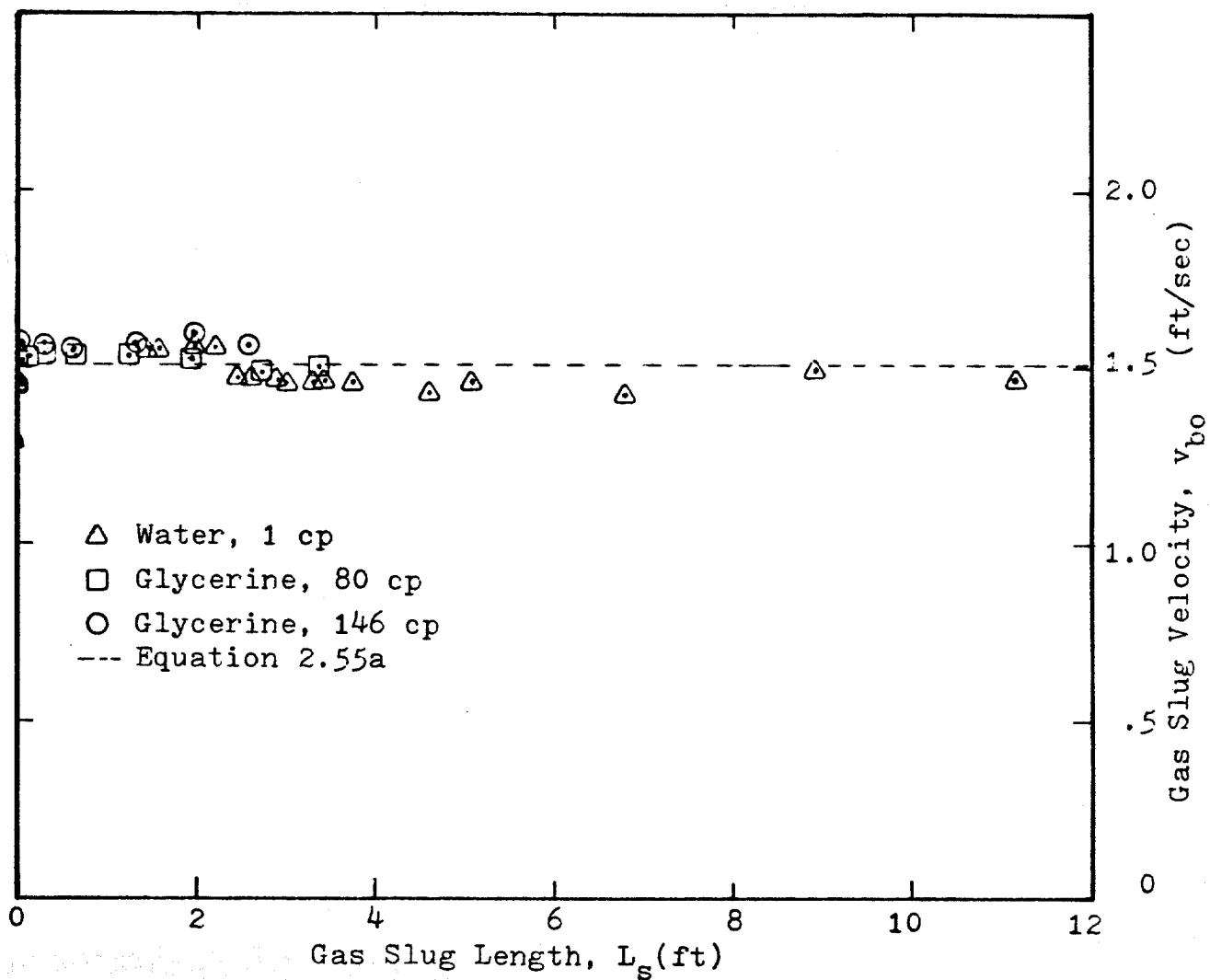


Figure 4.4 Velocity of Large Bubbles in a 6.375 in by 2.375 in Annulus. Zero Liquid Velocity.

Some measurements of bubble velocity in a 6.375 in by 2.375 in annulus were also made in flowing glycerine. These data are given in Table 4.2d. The data of Table 4.2d for gas slug velocity in a 146 cp liquid stream were plotted in Figure 4.5 as a function of the gas slug length. Again the velocities were corrected using the last term of Equation (2.44). However, the resulting limiting slug velocity, v_{bo} , was around 2 ft/sec. This is 30% higher than the value predicted for quiescent liquids, 1.511 ft/sec. Apparently the factor, K_{Lv} , of 1.48 (laminar flow) developed for gas slug rising in water was not adequately correcting the effect of both a moving liquid and gas expansion in the high viscosity fluid. Again, a plot of bubble slip velocity ($v_b - v_{L-}$) as a function of the limiting bubble velocity v_{bo} was constructed. The velocity predicted by Equation 2.55, 1.511 ft/sec, was taken as the limiting velocity. Figure 4.6 points out that the slip velocity ($v_b - v_{L-}$) is a function of the limiting bubble velocity v_{bo} . The new equation obtained that governs the relationship between ($v_b - v_{L-}$) and v_{bo} is:

$$\frac{v_b - v_{L-}}{v_{L+}} = 1.22 \left[\frac{v_{bo}}{v_{L+}} \right]^{0.9712} \quad (4.2)$$

This equation can be solved for the slip-velocity in an ideal slug flow pattern.

TABLE 4.2d Velocity of Gas Slugs in a 6.375 in by
2.375 in Annulus through a 146 cp Glycerine
Solution Having an Upward Flow of 0.26 ft/sec.

Equivalent ¹ Diameter, d_e (inches)	Measured Velocity, v_b (ft/sec)	Non-Expanding Bubble Velocity		Bubble Length	
		Eq. 2.63 (ft/sec)	$v_b - K_L v \sqrt{L^+}$ (ft/sec)	Eq. 4.2 (ft/sec)	Actual } Theoretical ² (ft)
3.75	2.27	1.157	1.88	1.50	0.13
3.47	2.29	1.157	1.90	1.52	0.17
4.68	2.24	1.157	1.83	1.51	0.33
5.87	2.24	1.157	1.82	1.51	0.50
7.37	2.38	1.157	1.94	1.51	0.88
	2.40	1.157	1.90	1.51	1.54
	2.43	1.157	1.90	1.51	2.04
	2.41	1.157	1.93	1.51	2.75
					2.590

1 Gas volume injected, corrected for average gas pressure during the velocity determination, expressed as the diameter of sphere which would contain this volume.

2 Gas volume injected, corrected for average gas pressure during the velocity determination, expressed as the length of annulus which would contain this volume.

3 Slug length from photographs.

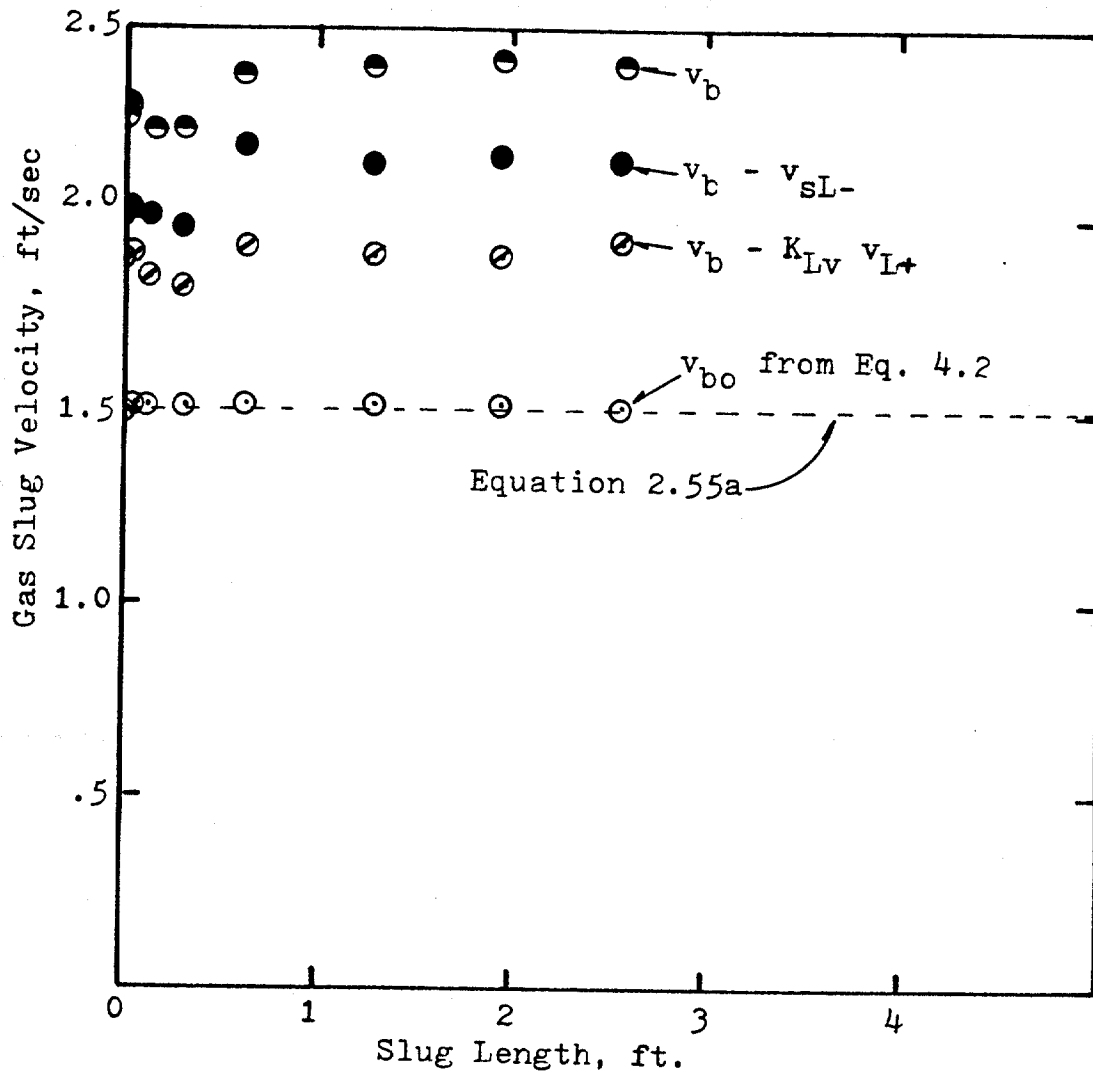


Figure 4.5 Bubble Velocity in a 6.375 in by 2.375 in Annulus through 146 cp Glycerine Solution with an Upward Flow of 0.26 ft/sec

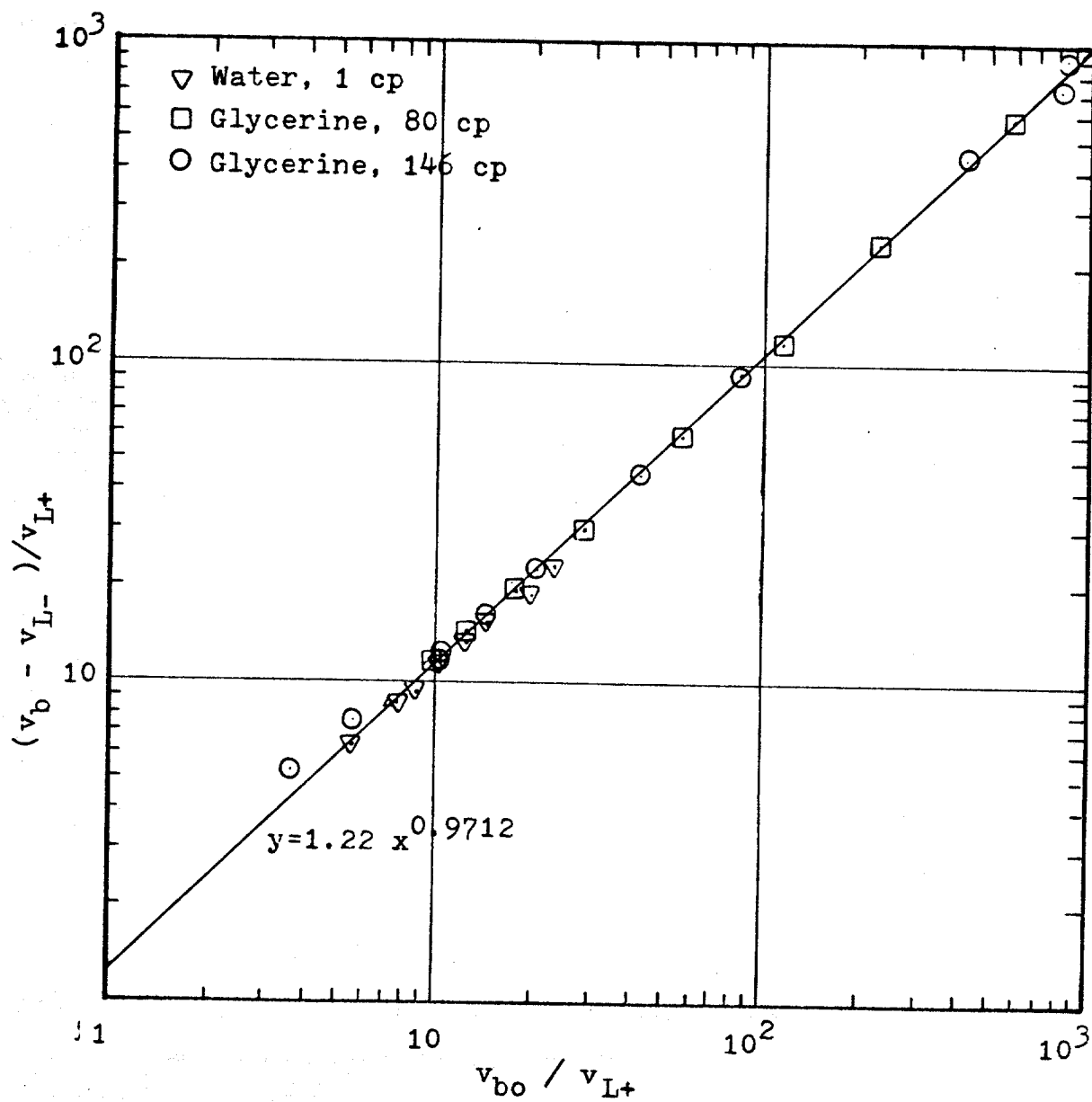


Figure 4.6 Relationship Between v_b and v_{bo} for Ideal Slug Flow in a 6.375 in by 2.375 in Annulus.

4.2 Flow Pattern Observations

In the former section, it was shown that the basic velocity of gas slugs or limiting velocity of cylindrical bubbles is around 1.5 ft/sec for the tubes and annulus dimensions of actual wells. On the other hand, Rehm⁵⁰ states that it is generally accepted that gas in the annulus will rise at about 0.28 ft/sec. Such a velocity would require a very small equivalent bubble diameter of around .026 inches, rising in water, and further indicate a gas migration in bubble flow pattern.

In an attempt to determine what flow pattern will rule the migration of a given gas kick, a quantitative series of tests were run in the laboratory equipment previously described.

4.2.1 Tube

Gas flow rates to simulate kick rates from a fraction of barrel per minute to two barrels per minute at bottom hole conditions were used. The length of the leading gas bubble or slug was determined in a photograph enlarger and reported as initial slug length, L_{si} , in Table 4.3. This data was felt to give some indication of the tendency to form slugs at the given gas injection rate. However, this data is not felt to be totally representative of field conditions because of the short length of the column and the technique used to inject the gas.

TABLE 4.3 Initial Slug Length and Gas Fraction for
Constant Gas Flow Rates in a Static Column
of Water (6.375 in I.D. Tube).

Gas Feed Rate, v_{sg} (ft/sec)	Initial Bubble Length, L_{si} (ft)	Average Gas Fraction, α	Average ¹ Bubble Velocity, v_b (ft/sec)	Equivalent ² Bubble Diameter (inches)	Comments
.085	-	.048	1.786	2.074	Lenticular bubbles leading the gas. Bubble flow. Ibid.
.246	.17	.136	1.808	1.674	
.502	.96	.214	2.343	2.216	Gas slug leading the gas. Bubble flow. Ibid. Resembles churn flow.
.802	.75	.279	2.876	2.678	
Static Column of 146 cp Glycerine					
.102	.42	.033	3.063	6.201	Large lenticular bubbles leading the gas. Bubble flow. Ibid.
.248	.93	.061	4.059	9.968	
.502	1.75	.156	3.226	4.509	Small Taylor bubbles leading the gas. Slug/churn flow. Ibid. Churn flow.
.815	2.08	.217	3.761	4.773	

¹ Average bubble velocity computed from gas fraction, α , using Equation(2.67).

² Computed using $v_b = 1.01 (g r_e)^{0.5} + K_{Lv} \bar{v}_{L+}$

Figure 4.7 shows the observed relationship between initial slug length and gas injection rate. From this figure it can be seen that, at relatively low gas flow rates, it is easier to generate slugs or Taylor bubbles in the more viscous fluid. For a kick rate of .75 bbl/min, an initial gas slug of 1.3 ft (2.6 times the tube diameter) is generated in the 146 cp liquid whereas in the water practically no slug is generated.

Further increase in gas flow rate resulted in large initial slugs. At a kick rate of 1.5 barrels per minute, the slug lengths are 3 and 4 times the diameter of the casing for water and glycerine respectively. Apparently, if the kick rate is high enough, it will cause essentially the bubble coalescence in both fluids or the same initial size of slugs.

The continuous injection of gas resulted in two-phase flow patterns along the entire tube. These flow patterns were observed to be related to the initial slug sizes as follows:

1. Bubble flow occurred with vanishing sizes of initial slug or lenticular bubbles.
2. Slug flow occurred with fully developed initial cylindrical bubbles which filled most of the available cross sectional area.
3. Churn flow occurred with large initial cylindrical bubbles having a length of at least two outer

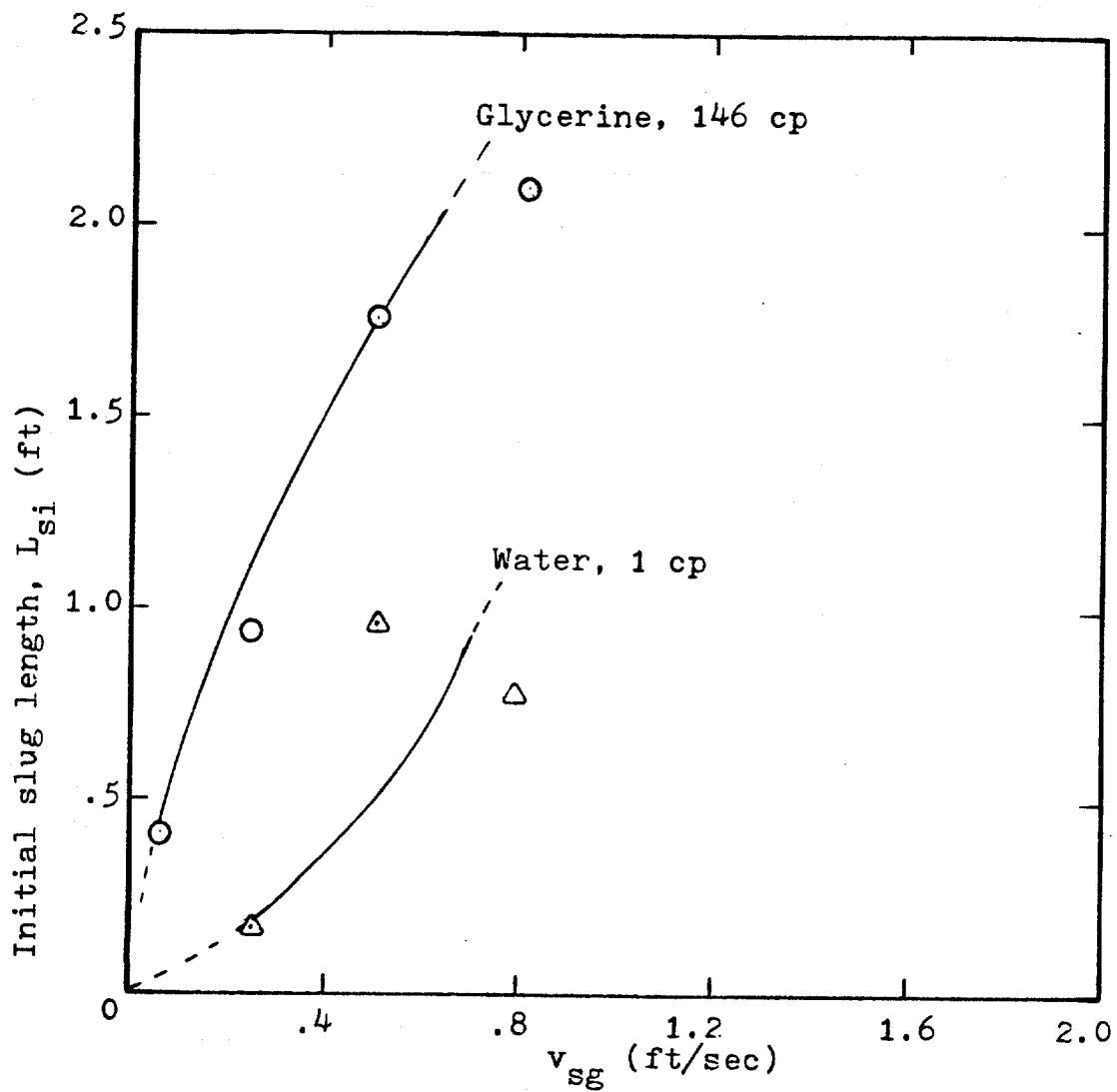


Figure 4.7 Initial Slug Length Versus Superficial Gas Velocity in a 6.375 in Tube and Quiescent Liquids.

tube diameters.

These relationships are based on observations in the laboratory model and are not necessarily valid for field conditions. A small initial slug could become a very large slug in a well high above the injection point. Gas availability and gas expansion would increase the size of the gas slug if bubble fragmentation does not occur. Similarly, the steady flow of gas in liquid for long time intervals may not accurately model the condition under which gas kicks are generated and the two phase flow pattern could change as the gas contaminated region propagates to the surface. Under rather short times, the formation gas flows into the wellbore and then normally the gas flow is controlled by closing the well. From this instant the gas will travel upward as a disturbance through a continuous body of liquid.

4.2.2 Annulus

Constant gas flow rates ranging from a fraction of barrel per minute to around 4 barrels per minute were fed to the annulus limited by a 6.375 in casing and a 2.375 in drill pipe. The results are presented in Tables 4.4 - 4.5. A plot constructed from this data for quiescent liquid is presented in Figure 4.8.

The high viscosity liquids again showed a tendency to facilitate the generation of initial slugs; for the range of flow rates studied, the initial slug length was

TABLE 4.4a Initial Slug Length and Gas Fractions for Constant Gas Flow Rates in Static Column of Water (6.375 in by 2.375 in Annulus).

Gas Feed Rate, v _{sg} (ft/sec)	Initial Bubble Length, l _{si} (ft)	Average Gas Fraction, α	Average Bubble Velocity, v _b (ft/sec)	Bubble Diameter Equivalent ² (inches)	Comments
.293	.26	.119	2.462	3.257	Bubble flow.
.440	.36	.170	2.588	3.104	Bubble flow.
.548	.43	.195	2.810	3.388	Bubble flow.
.795	.54	.252	3.155	3.542	Bubble flow.
.895	.60	.275	3.255	3.477	Ibid. Occasional slugs.
.972	.63	.292	3.329	3.419	Agitated bubble flow.
1.230	.69	.370	3.324	2.498	Ibid.
1.597	.89	.446	3.581	2.026	Resembles churn flow.
1.520	1.50	.453	3.355	1.715	Ibid.
1.780	1.50	.480	3.708	1.808	Ibid.

1 Average bubble velocity computed from gas fraction, α , using Equation (2.71)

2 Computed using $v_b = 1.01 (g r_e)^{0.5} + K_{Lv} \bar{v}_{L+}$

TABLE 4.4b Initial Slug Length and Gas Fractions for Constant Gas Flow Rates in Static Column of 80 cp Glycerine (6.375 in by 2.375 in Annulus).

Gas Feed Rate, v_{sg} (ft/sec)	Initial Bubble Length, L_{si} (ft)	Average Gas Fraction, α	Average ¹ Bubble Velocity, v_b (ft/sec)	Equivalent ² Bubble Diameter (inches)	Comments
.014	.08	.011	1.273	1.146	Lenticular bubbles.
.049	.38	.023	2.130	3.097	Ibid.
.072	.08	.034	2.118	2.958	ibid.
.111	.46	.034	3.265	7.030	ibid.
.197	.92	.045	4.378	12.210	Larger bubbles than the former ones.
.281	1.17	.073	3.849	8.621	Ibid.
.560	1.83	.152	3.684	5.963	Apparently churn flow.

1 Average bubble velocity computed from gas fraction, α , using Equation (2.71).

2 Computed using $v_b = 1.01 (g r_e)^{0.5} + K_{Lv} \bar{v}_{L+}$

TABLE 4.4c Initial Slug Length and Gas Fraction for Constant Gas Flow Rates in Static Column of 146 cp Glycerine (6.375 in by 2.375 in Annulus).

Gas Feed Rate, v_{sg} (ft/sec)	Initial Bubble Length, L_{si} (ft)	Average Gas Fraction, α	Average ¹ Bubble Velocity, v_b (ft/sec)	Equivalent ² Bubble Diameter (inches)	Comments
.028	0.17	.017	1.647	1.885	Large lenticular bubbles. Occasional larger bubbles.
.087	0.48	.027	3.222	6.998	Ibid. Lenticular bubbles.
.192	0.88	.039	4.923	15.737	Ibid. Turbulence and stream lined slugs.
.313	1.29	.081	3.864	8.459	Developed slug flow.
.453	1.79	.120	3.775	7.049	Ibid.
.538	2.25	.139	3.871	6.912	Wavy slug. Slug or churn flow.

1 Average bubble velocity computed from gas fraction, α , using Equation (2.71).

2 Computed using $v_b = 1.01 (g r_e)^{0.5} + K_{Lv} \bar{v}_{L+}$

TABLE 4.5 Initial Slug Length and Gas Fraction for Constant Gas Flow Rates in a Flowing Column of 146 cp Glycerine (6.375 in by 2.375 in Annulus with $v_{SL} = .10$ ft/sec).

Gas Feed Rate, v_{sg} (ft/sec)	Initial Bubble Length, L_{si} (ft)	Average Gas Fraction, α	Average ¹ Bubble Velocity, v_b (ft/sec)	Equivalent ² Bubble Diameter (inches)
.101	0.42	.025	4.040	10.243
.262	0.88	.036	7.278	33.241
.415	1.29	.072	5.764	18.295
.453	1.42	.072	6.292	21.907
.582	1.71	.122	4.771	10.345

1 Average bubble velocity computed from gas fraction, α , using Equation (2.71).

2 Computed using $v_b = 1.01 (g r_e)^{0.5} + K_{Lv} \bar{v}_{L+}$

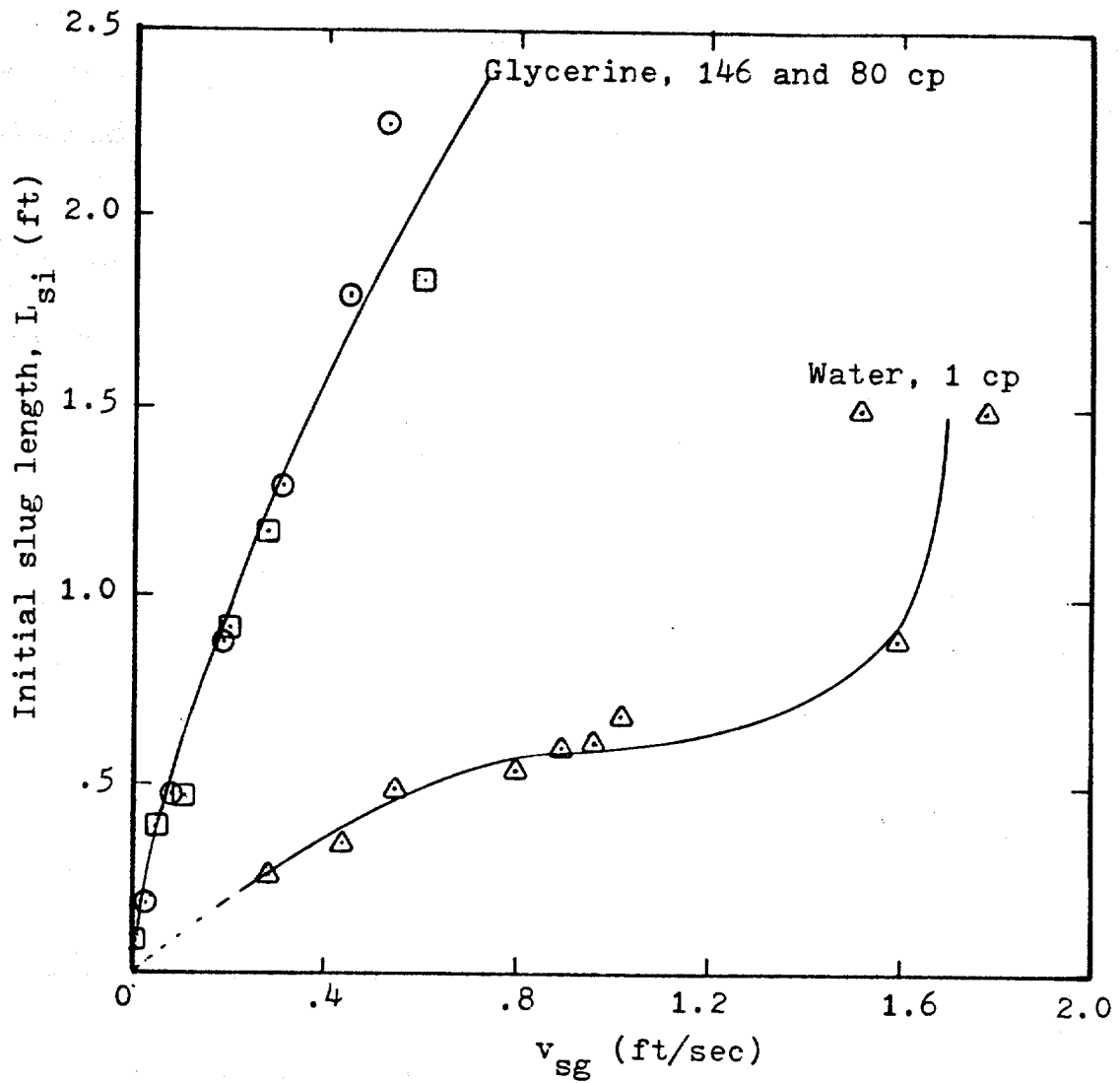


Figure 4.8 Initial Gas Slug Length Versus Superficial Gas Velocity (6.375 in by 2.375 in Annulus and Quiescent Liquid).

almost proportional to the increase of flow rate. Practically, there was no difference in the observed behavior of the 80 cp fluid and the 146 cp fluid. A single curve describes the trend of both fluids. The low viscosity fluid (water) showed a different profile. Even when there is an increase in initial slug size with increase in gas velocity, the change is a gradual one. The gas slug increases slowly with the gas flow rate up to around 1.2 ft/sec superficial gas velocity. Further increment in gas flow rate, resulted in a sharply increase of the slug length. The inflexion point corresponds to flowing gas fraction of 0.36 (See Figure 4.14). This points out that higher coalescence of bubbles resulting in slugs occurred above a gas fraction of 0.36. The flow patterns were observed to be related to the initial slug sizes in the same way that was described in the previous section.

Finally, a test was run to simulate a gas kick entering the annulus while the fluid is circulating through the hydraulic system of the well. Figure 4.9 shows the obtained results. A moderate liquid velocity, 0.1 ft/sec, was used to allow time for observation of the leading edge of the gas. For these conditions, the relationship between gas flow rate and initial slug length becomes a linear one. The sizes of the generated slugs were slightly lower than those obtained with static liquid for the same gas flow rates. This was to be expected since the effect of the

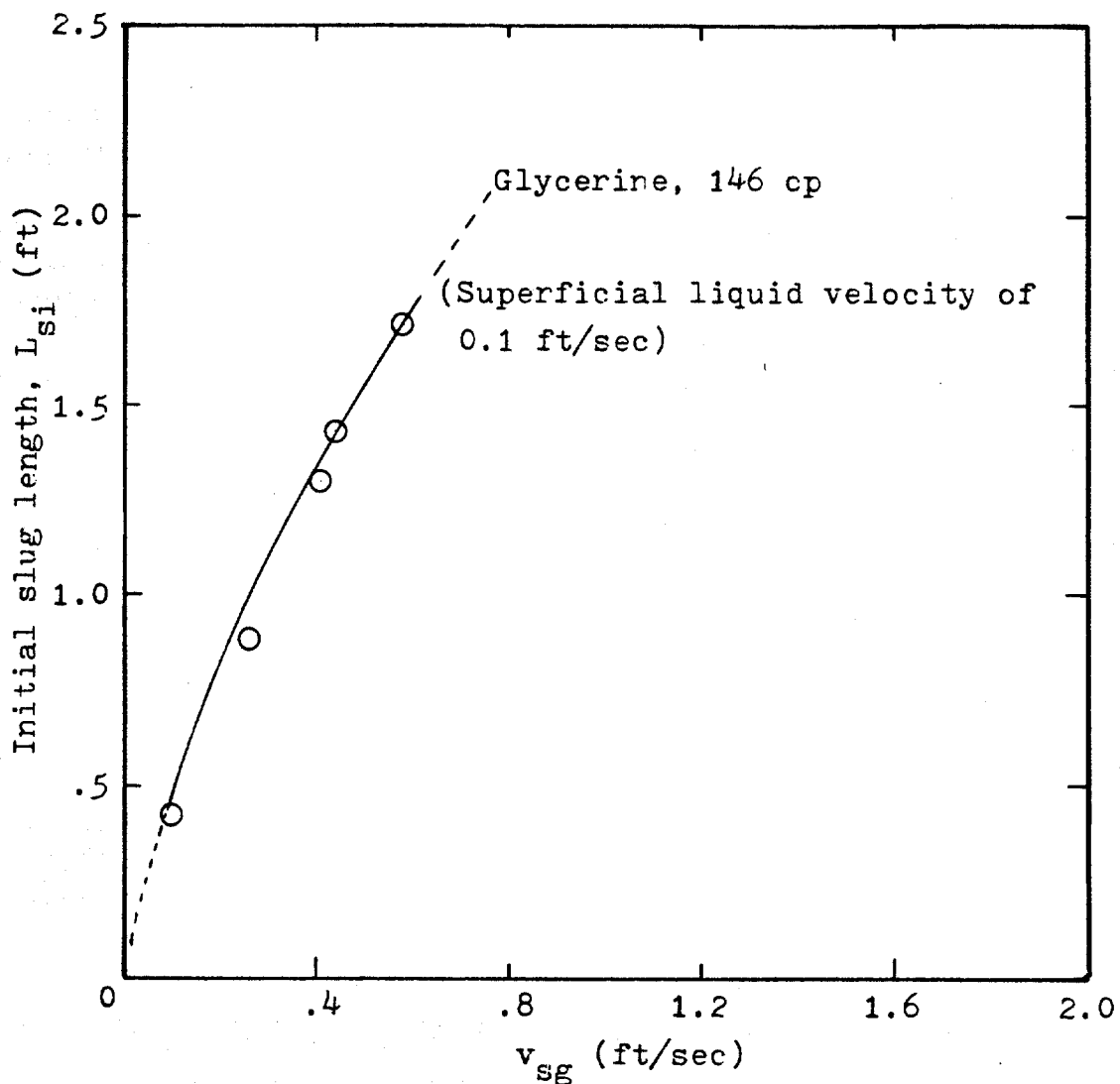


Figure 4.9 Initial Gas Slug Length Versus Superficial Gas Velocity (6.375 in by 2.375 in Annulus and Liquid Velocity of 0.1 ft/sec).

liquid flow rate is to diminish the flowing gas fraction. Under these circumstances a decrease in the coalescence of the bubbles was indicated.

All of the data on initial gas slug length obtained in both the tube and the annulus is presented in Figure 4.10. For all practical purposes the high viscosity fluid shows the same trend for both the tube and annulus. However, a sharp difference between annulus and tube tests can be seen for the tests obtained using water. Whereas in the annulus the slugs were difficult to form, in the tube the slugs were easily generated. For example, at 1.0 ft/sec of superficial gas velocity, the initial slug length in the annulus is 0.5 ft while in the tube the slug length is 1.5 ft. Apparently a gas kick occurring while the pipe is off the bottom will travel as a slug or Taylor bubble easier than in an annulus. On the other hand, gas kicks occurring while drilling with low viscosity fluid will have more opportunities of traveling as swarm of bubbles. Furthermore, the liquid flow rates will promote bubble fragmentation. This would appear to be true at least at the lower sections of the well.

The flow patterns were bubble flow for the two lower flow rates reported in Table 4.3 either for both water and for 146 cp glycerine. The two high flow rates were in churn flow pattern. The gas fractions for this series of tests was plotted in Figure 4.11. The theoretical gas

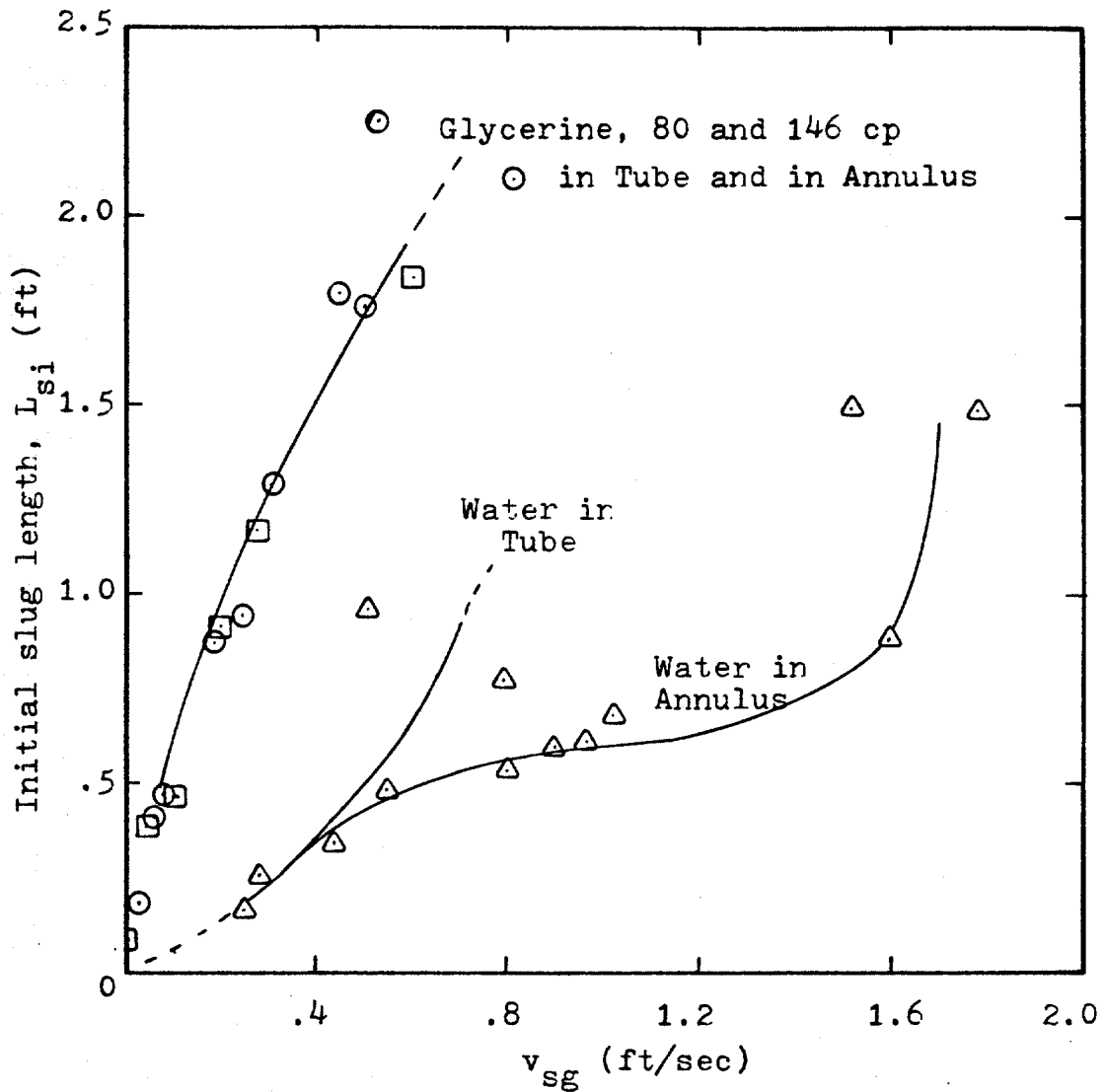


Figure 4.10 General Plot of Initial Gas Slug Length Versus Superficial Gas Velocity. (6.375 in by 2.375 in Annulus and 6.375 in Tube).

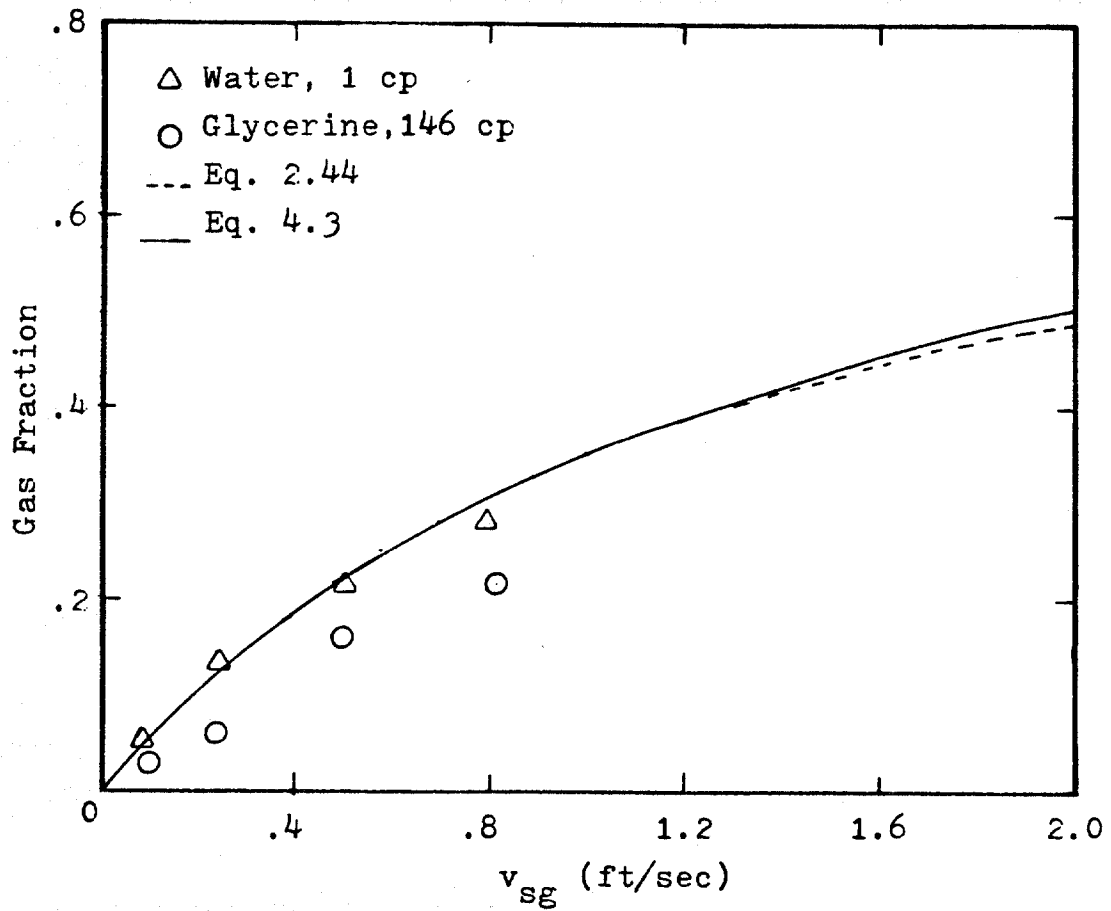


Figure 4.11 Gas Fraction Versus Superficial Gas Velocity (Tube of 6.375 in I. D.)

fraction is also presented in this Figure. The expression for obtaining the theoretical gas hold-up, α , was based on the correlation presented in Figure 4.2, and it is as follows

$$\alpha = \frac{v_{SG}}{1.27 \left(\frac{v_{bo}}{v_{L+}} \right)^{0.94057} v_{L+} + v_{L-}} \quad (4.3)$$

where v_{bo} and v_L are in any set of consistent units. This equation gave good agreement with the measured gas fraction for water, even in the region of bubble flow. However, Equation (4.3) overpredicted the gas hold-up for the high viscosity fluid. Apparently this is mainly due to that the equation was developed for slug flow. The former implies flow rates high enough to reach gas fractions greater than around 0.25. Also, the correlation does not take into account the viscosity of liquid which can be important in bubble flow.

Equation (2.44) of Nicklin et al³⁵ was also used to obtain the theoretical gas fraction. This equation practically predicted the same gas voidage as Equation (2.44); however, for superficial gas velocities higher than 1.2 ft/sec, the values predicted by this equation fell below of those predicted by Equation (4.3).

Superficial gas velocities from 0.293 ft/sec to 1.78 ft/sec were injected into the annulus filled with static column of water. Gas fractions from 0.119 to 0.473 were measured for these runs and they are plotted in Figure 4.12. The results for a flowing stream of 146 cp glycerine are also included in this Figure. For low flow rates, only bubble flow patterns were obtained. For high gas flow rates apparently churn flow was the ruling pattern. In this case, long bodies of gas travelled frequently through the agitated gas-liquid mixture. Slug flow pattern was not obtained for the range of gas flow rates studied.

In the case of 80 and 140 cp solutions of glycerine, superficial gas velocities from 0.014 ft/sec to 0.56 ft/min were injected into the annulus. The gas hold-up varied from 0.0112 to 0.1517 for the 80 cp liquid and from 0.139 to 0.119 for the 146 cp liquid. The gas fraction was always lower for the more viscous fluid at equal gas flow rates. As the gas flow rate was increased, the flow pattern passed from large lenticular bubbles to churn flow.

A test made with a 0.1 ft/sec stream of high viscosity liquid (146 cp) also resulted in bubble flow and "churn" flow patterns. However, the resulting gas voidage was lower than those obtained in the non-flowing tests.

The gas fractions for this series of tests were plotted in Figure 4.12. The theoretical gas fraction for zero liquid flow rate is also included in this figure.

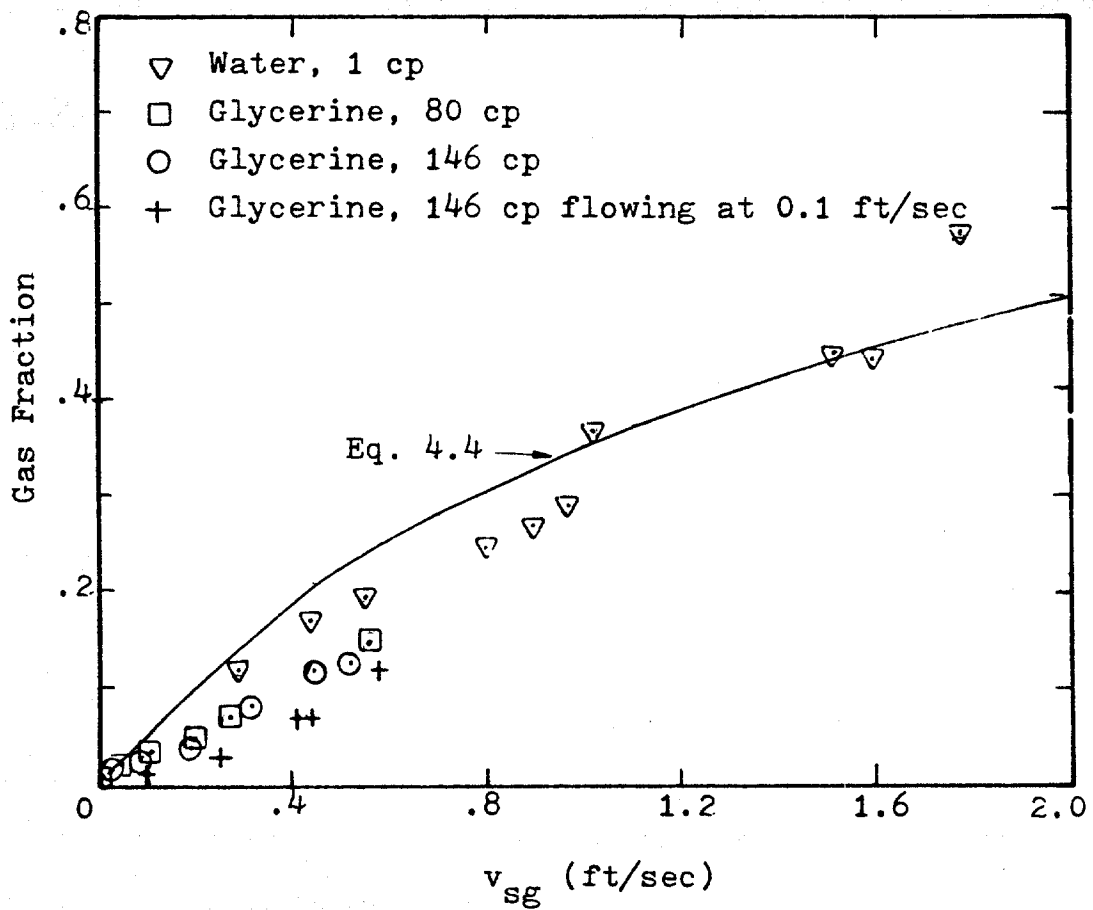


Figure 4.12 Gas Fraction Versus Superficial Gas Velocity (6.375 in by 2.375 in Annulus).

The expression for obtaining the gas hold-up, α , was obtained from the correlation presented in Figure 4.2. Upon assuming that all of the gas will travel in slugs, the following equation is obtained

$$\alpha = \frac{v_{sg}}{1.22 \left(\frac{v_{bo\Box}}{v_{L+}} \right)^{0.94057} v_{L+} + v_{L-}} \quad (4.4)$$

where $v_{bo\Box}$ is the limiting bubble velocity in an annulus.

v_{L+} is the average liquid velocity ahead of the gas slug.

v_{L-} is the average liquid velocity behind of the gas slug.

The predicted gas voidage reasonably agrees with the measured gas fraction for water. Equation 4.4 overpredicted the gas hold-up for the high viscosity fluids and, especially, for the stream of 146 cp glycerine. The explanation given in the former section applies in this case, too.

The theoretical gas voidage predicted by Equation 4.4 for superficial liquid velocities of 0, 1, 2, 5, and 10 ft/sec were plotted in Figure 4.13. The equation predicts the observed trend that the gas voidage decreases when the liquid flow rate increases. Also, it can be seen from Figure 4.13 that this effect is more important for the

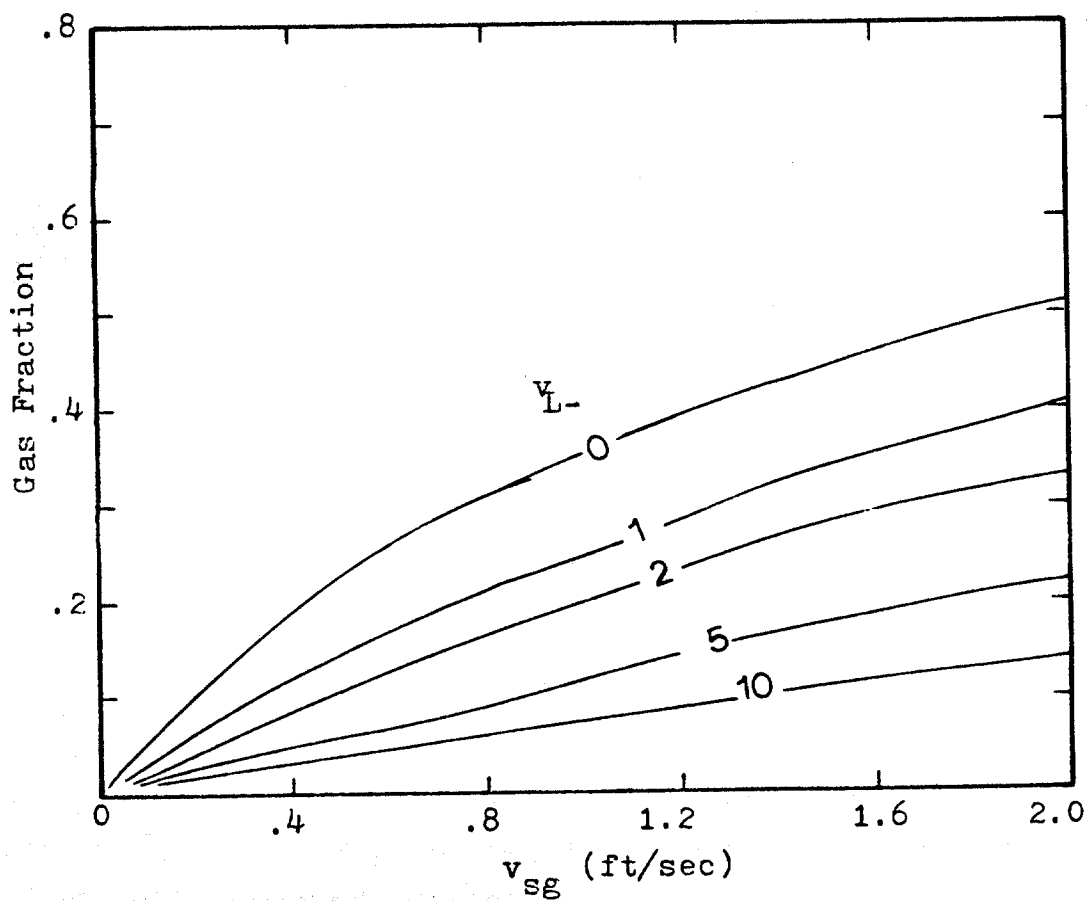


Figure 4.13 Theoretical Gas Fraction for Annular Geometries as Predicted by Eq. 4.4.

lower liquid velocities.

4.2.3 Annulus with Restriction

A few experimental runs were made to determine the effect of a restriction on the flow pattern of gas traveling through the annulus. To accomplish this, a 3 ft long section of pipe having a 4.0 in of internal diameter was inserted in the casing of 6.375 inches. This simulated a flow restriction as it is indicated in Figure 4.14. Small Taylor bubbles passed the restriction easily. As the size of the bubble increased, a change in shape from lenticular to fully developed Taylor bubbles occurred while passing the 4 in by 2.375 in annular restriction. (See Figure 4.15) Leaving the restriction, the bubbles tended to return to their original shape. Finally totally developed Taylor bubbles filled the restriction, and the remaining gas of the bubble collected below the restriction while the leading gas passed through the 4 in by 2.375 in annulus. The gas rate through the restriction was controlled by the reduced slip velocity in the restriction. The bubble size leaving the restriction appeared to be the size bubble having a slip velocity equal to the slip velocity through the restriction.

Table 4.6 shows the trend of the size of slugs leaving the restriction. A maximum size of around 0.8 ft is indicated by this figure. This appeared to correspond to the bubble size having a slip velocity equal to the slip

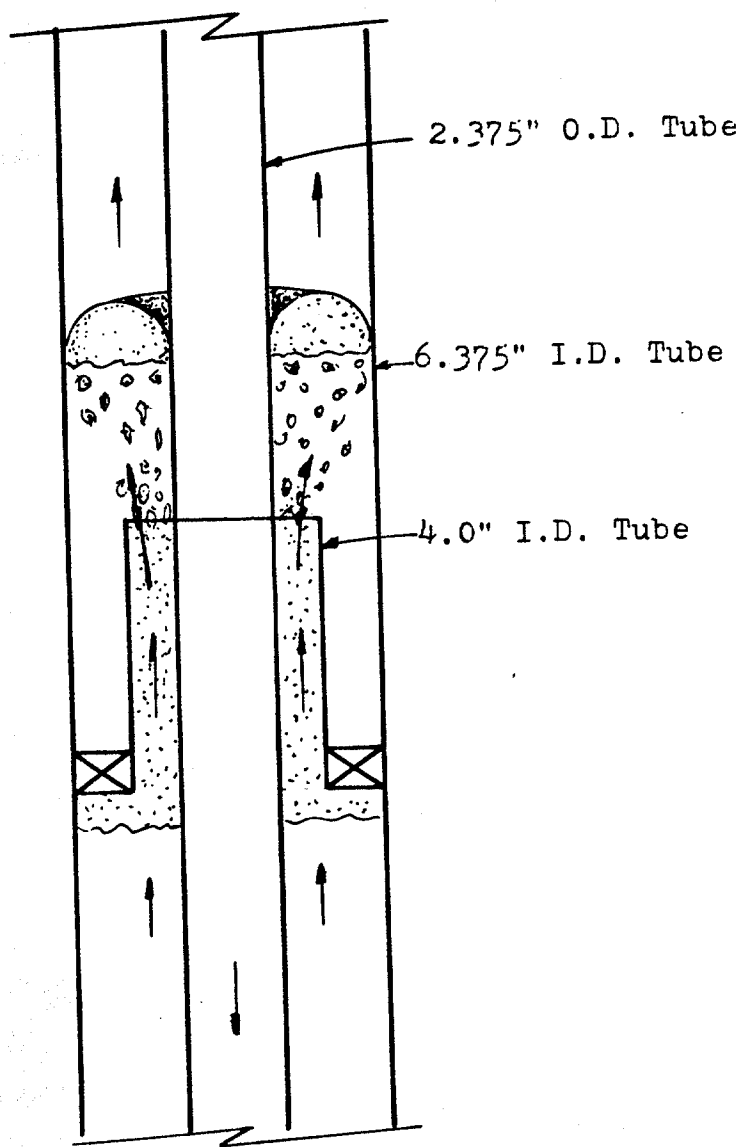
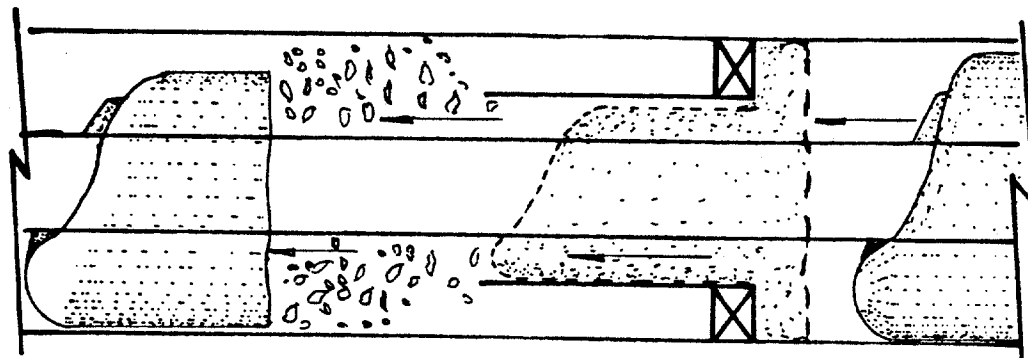
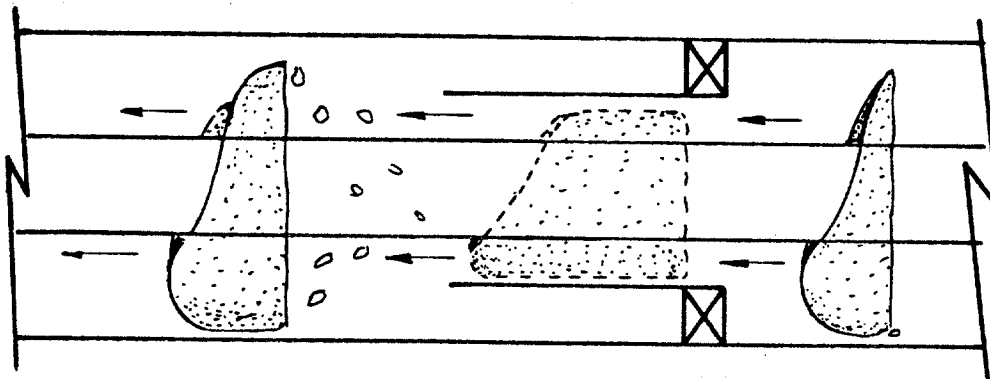


Figure 4.14 Flow Restriction in the 6.375 in by 2.375 in Annulus.



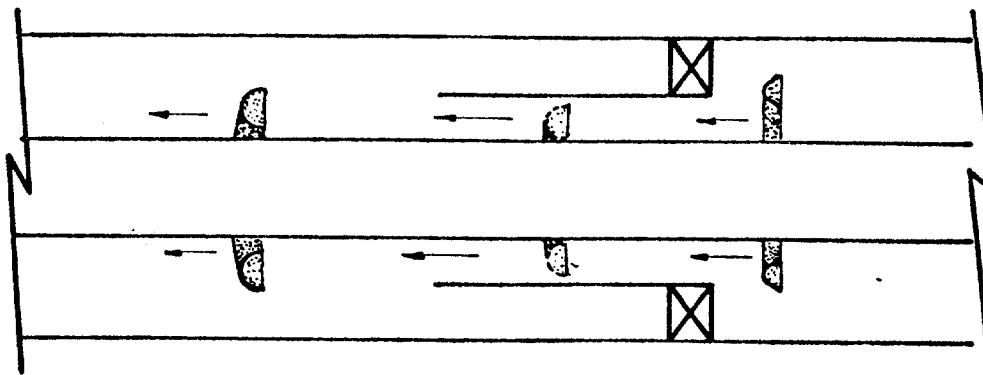
(c)

Annular "Taylor" Bubbles.



(b)

Large Lenticular Bubbles.



(a)

Small Lenticular Bubbles.

Figure 4.15 Bubbles Passing Through Annular Restriction.

TABLE 4.6 Initial Slug Length Leaving a 4 in
Restriction in an 6.375 in by 2.375 in
Annulus (Static Column of 80 cp
Glycerine).

Injected Air Volume @ 17.08 psig. (l)	L_{si} (inches)	Comments
.10	1.5	
.25	2.4	
.50	3.9	
1.00	6.3	
2.10	9.0	
3.81	9.0	High volumes of air
5.52	6.8	make some turbulence
5.52	8.5	in the trailing edge
5.52	9.5	of the slug leaving
5.52	7.5	the restriction. The
7.50	8.0	gas behind the main slug
3.81	8.0	travels in lenticular
3.81	9.0	bubble shapes.
3.81	8.0	
3.81	8.0	
3.81	8.0	

velocity in the restriction. For the area below and above the choke, a maximum slip velocity of 1.511 ft/sec was indicated from previous experimental runs, whereas for the annular restriction of 4 by 2.375 inches, a maximum slip velocity of only 1.25 ft/sec was calculated. The sizes of the slugs formed at a restriction continues to change as the gas moves up the column. For example, pictures taken near the top of the column at a point 2.164 ft below of the discharge to the atmosphere showed a slug size greater than 2.8 ft against the 0.66 ft reported near of the restriction. Thus, as the pressure on the gas changes, the observed flow pattern may also change.

The limited results obtained in this study may prove useful in understanding the role of restrictions in complex configurations. A gas kick, traveling in a slug flow pattern will have a greatly reduced slip velocity as it enters a small diameter choke line. This may cause the gas to collect below the choke line and enter the choke line at much higher gas concentrations than was present in the well. The change will depend on the size and frequency of the bubbles arriving to the choke line.

In a well as that described in Figure 1.2, a continuous gas flow observed in the surface, does not necessarily mean that the gas has travelled all the well length as a single body. The limiting cylindrical bubble of a $3\frac{1}{2}$ in choke line is around 1 ft/sec while the limiting

velocity in the annulus is around 2.0 ft/sec, but most important, lenticular bubbles ($r_e > 0.3600$ in) in the annulus will travel faster than the gas in the $3\frac{1}{2}$ choke line; an accumulation of gas as that described in Figure 4.15c will occur at the choke line entrance.

CHAPTER V

CONCLUSIONS

As result of the experimental work done in this thesis, the following conclusions are drawn:

1. The velocity of large gas slugs relative to the liquid above the slug is not significantly influenced by viscosity for tubes and annuli in the size range present in well control operations.
2. For low viscosity liquids, the correlation of Rader, Bourgoyne, and Ward gave good agreement with the measured gas slug velocities.
3. For high viscosity liquids, the correlation of Rader, Bourgoyne, and Ward tended to predict values of gas slug velocity that were lower than those observed.
4. Based on the experimental data obtained, a new approach was developed for computing the velocity of large gas slugs.
5. The predominant flow patterns present during well control operations is bubble flow, especially in low viscosity fluids.

NOMENCLATURE

A = Area of tube, L^2

C_1 = Coefficient, function of the bubble Reynolds number.

C_2 = Coefficient function of both bubble and mixture Reynolds number.

d_{bi} = initial diameter of the bubble, L .

d_N = nozzle diameter, L .

d_t = internal diameter of tube, L .

d_1 = outer diameter of the internal tube, L .

d_2 = inner diameter of the external tube, L .

E_k = kinetic energy, FL .

$F(\infty)$ = void function

F_D = drag force, F

f_D, f'_D = drag coefficients

$F(n), F_1(n)$ = function of the pseudoplasticity index

g = acceleration due to gravity, L/T^2

g_c = gravitational constant, ML/FT^2

H_L = Liquid holdup

- K = Consistence index of the liquid
- K_{Lv} = Coefficient of the liquid velocity ahead of the bubble.
- L_B = parameter for bubble flow/slug flow transition defined by Equation (2.2b).
- L_{eL} = equivalent length of liquid around a gas slug, in.
- L_S = slug length, in.
- L_x = parameter defined by Equation (2.2c)
- L_1, L_2 = parameter defined by N_D and Figure 2.5
- l_E = maximum length of the system above the entrance in which churn flow can exist, L.
- N = Dimensional property parameter, ft^{-1} .
- N_d = pipe diameter number
- N_{fr} = Froude number
- N_{Frm} = modified Froude number
- N_{gv} = gas velocity number
- N_L = Liquid viscosity number
- N_{Lv} = Liquid velocity number
- N_{ps} = Poiseville number
- N_{Rb} = Reynolds number of a bubble

- N_{Rf} = fluid Reynolds number
 N_{Rbm} = modified Reynolds number of a bubble
 N_{Ro} = Reynolds number defined by Equation (2.52)
 n = pseudoplasticity index
 q_g = upward gas volume flow rate at existing conditions,
 L^3/T
 q_L = Upward liquid volume flow rate at existing
conditions, L^3/T .
 \bar{r}_c = average curvature radius
 r_c = curvature radius of the top portion of a bubble,
 L .
 r_{cr} = critical sphere radius, L .
 r_e = equivalent radius of a sphere having the same
volume of the gas bubble, L .
 r_{ef} = critical equivalent radius at which bubble
fragmentation occurs or maximum radius of a
lenticular bubble
 r_o = equilibrium radius of a large lenticular
bubble, ft .
 r_t = tube internal radius
 r_1 = outer radius of the internal tube
 r_2 = inner radius of the external tube

- t = channel thickness
 V_b = volume of the bubble
 v_b = bubble velocity with respect to the ground
 v_{bo} = velocity of a bubble with respect to the liquid ahead of the bubble.
 $v_{b\infty}$ = terminal velocity of the bubble in an extended liquid
 $v_{bo\Box}$ = velocity of a bubble in a rectangular channel with respect to the liquid ahead of the bubble
 $v_{b\infty\Box}$ = velocity of lenticular bubbles between infinitely wide parallel plates
 v_E = component of the gas velocity caused by gas expansion
 \bar{v}_g = average gas velocity
 v_{gN} = gas velocity through nozzle
 \bar{v}_L = average liquid velocity
 v_{L+} = average liquid velocity ahead of the gas contaminated region
 v_{L-} = Ibid. behind the gas contaminated region
 v_m = non-slip mixture velocity or two phase velocity
 v_o = reference cylindrical bubble velocity defined by Equation (2.51)
 \bar{v}_s = average slip velocity of the gas
 v_{sg} = superficial gas velocity
 v_{sL} = superficial liquid velocity

v_{swarm} = velocity of a swarm of bubbles with respect
to the liquid

W = weight of the bubble

w = channel width

GREEK SYMBOLS

α = voidage or volumetric fraction of pipe occupied
by gas

μ_L = liquid viscosity

ρ_g = gas density

ρ_L = liquid density

σ_L = interfacial tension

Σ = reciprocal of the radius number as defined by
Equation (2.53)

λ = wave length

REFERENCES

1. Harris, L.M.: "Design for Reliability in Deepwater Floating Drilling Operations". The Petroleum Publishing Company. Tulsa, Oklahoma.
2. Haberman, W.L. and Morton, R.K.: "An Experimental Study of Bubbles Moving in Liquids", Trans. ASCE (1954) 227.
3. Levich, V.L., "Physicochemical Hydrodynamics", p.395 (1962), Prentice-Hall, N.Y.
4. Taitel, Y., Bornea, D., and Dukler, A.E.: "Modeling Flow Pattern Transitions for Upward Gas-Liquid Flow in Vertical Tubes", AIChE Journal (May, 1980) V26, N3, 345.
5. Chierici, G.L., Ciucci, G.M., Schlocci, G.: "Two-Phase Vertical Flow in Oil Wells-Prediction of Pressure Drop", Journal of Petroleum Technology (August, 1974) 927.
6. Davies, R.M. and Taylor, G.: "The Mechanics of Large Bubbles Rising Through Extended Liquids and Through Liquids in Tubes". Proc. Royal Society, London (1950) 200, series A, 375-390.
7. Griffith, P., and Wallis, G.B.: "Two Phase Slug Flow", J. Heat Trans., (1961) 83, 307.
8. Sternling, V.C. "Two Phase Flow Theory and Engineering Decissions", AIChE Annual Meeting (December 1965).
9. Wallis, G. B.: "One Dimensional Two-Phase Flow", McGraw Hill (1969).
10. Hewitt, G.F. and Roberts, D.N.: "Studies of Two Phase Flow Patterns by Simultaneous X-Ray and Flash Photography" UK Atomic Energy Authority Report AERE-M 2159 (1969).
11. Govier, G.W. and Aziz, : "The Flow of Complex Mixtures in Pipes" Van Nostrand Reinhold Co. (1972)

12. Gould, T.L. "Vertical Two-Phase Steam-Water Flow in Geothermal Wells". *Journal of Petroleum Technology* (1974) 26, 833.
13. Oshinawa, T. and Charles, M.E. "Vertical Two-Phase Flow Part II" *Can. J. Chem. Eng.* (1974) 56, 438.
14. Duns, Jr. H., and Ross, N.C.: "Vertical Flow of Gas and Liquid Mixtures from Boreholes", Proc. 6th. World Petroleum Congress. Frankfurt (June, 1963).
15. Orkiszewski, J. "Predicting Two-Phase Pressure Drops in Vertical Pipes", *Journal of Petroleum Technology* (June, 1967) 829-838.
16. Bailey, R.V., Zmola, P.C., Taylor, F.M., and Planchet, R.J.: "Transport of Gases Through Liquid-Gas Mixtures" Available from P.C. Zmola, Combustion Engineering, Windson, Conn.
17. Zukoski, E.E. "Influence of Viscosity, Surface Tension, and Inclination Angle on Motion of Long Bubbles in Closed Tubes", *Fluid Mech.* (1966), Vol. 25, Part 4 pp. 821-837.
18. Rader, Bourgoyne, and Ward: "Factors Affecting Bubble -Rise Velocity of Gas Kicks", *Journal of Petroleum Technology* (May, 1975) 571-584.
19. Nicklin, D. J.: "Two-Phase Bubble Flow", *Chemical Engineering Science*, (1962) Vol. 17, 693-702.
20. Acharya, A., Mashelkar, R.A., Ulbrecht, J.J.: "Bubble Formation in Non-Newtonian Liquids", *Industrial Engineering Chemical Fundamentals* (1978) Vol. 17, No. 3. 230-232.
21. Sada, E., Yasinishi, A., Katoh, S., and Nishioka, M.: "Bubble Formation in Flowing Liquid". *The Canadian Journal of Chemical Engineering*. (December, 1978) Vol. 56, 669-672.
22. Hadamard, : *Comp. Rend.* (1911) 154-1735.
23. Rybezynski, : *Bill. Intern. Acad. Science Cracovie (A)* (1911), p. 40.
24. Peebles, F.N., and Garber, H.J.: "Studies on the Motion of Gas Bubbles in Liquids", *Chemical Engineering Progress* (February, 1953), 88-97.

25. Mendelson, H.D.: "The Prediction of Bubble Terminal Velocities from Wave Theory", AIChE Journal (March, 1967), 250-252.
26. Acharya, A., Mashelkar, R.A., Ulbrecht, J.: "Mechanics of Bubble Motion and Deformation in Non-Newtonian Media", Chemical Engineering Science (1977) 863-872.
27. Ishii, T., and Pei, C.T.: "Drag Coefficient of Relatively Contaminated Gas Bubbles", The Canadian Journal of Chemical Engineering, (February, 1980), Vol. 58, 25-32.
28. Marrucci, G.: "Rising Velocity of a Swarm of Spherical Bubbles", Industrial Engineering Chemical Fundamentals (May, 1965), Vol. 4, No. 2, 224-225.
29. Lewis, E.W., and Bowerman, E.W.: Ind. Eng. Chem., (1952), Vol. 48, 603.
30. Bryn, T.: Forsch. Gabiete Ingenieurw., (1933), Vol. 4 No. 1, 27.
31. O'Brien, M.P., and Gosline, J.E.: "Velocity of Large Bubbles in Vertical Tubes", Industrial and Engineering Chemistry (December 1935) V. 27, N. 12, 1436-1440.
32. Dumitrescu, D.T., "Stromungan einer Luftblase imsenkrechten Rohr". Z. Angew, Math. Mech. (June 1943) V. 23, 139-149.
33. Laird, A.D.K., and Chisholm, D.: "Pressure and Forces Along Cylindrical Bubbles in a Vertical Tube", Ind. Eng. Chem. (August, 1956) V. 48, N.8, 1361-1364.
34. Uno, S., and Kintner, R.C.: "Effect of Wall Proximity on the Rate of Rise of Single Air Bubbles in a Quiescent Liquid", A.I.Ch. Journal (September, 1956) V. 2, N. 3, 420-425.
35. Nicklin, D. J., Wilkes, J.O., and Davidson, J.F.: "Two-Phase Flow in Vertical Tubes", Trans. Instn. Chem. Engrs. (1962) V.40, 61-68.
36. White, E. T., and Beardmore, R.H.: "The Velocity of Rise of Single Cylindrical Air Bubbles Through Liquids Contained in Vertical Tubes", Chem. Eng. Sc. (1962) V.17, 351-361.
37. Brown, R.A.S.: The Mechanics of Large Gas Bubbles in

- Tubes", The Canadian Journal of Chemical Eng. (October, 1965) 217-223.
38. Collins, R: "The Effect of a Containing Cylindrical Boundary on the Velocity of a Large Gas Bubble in a Liquid", J. Fluid Mech. (1967) V. 28, Part 1, 97-112.
 39. Griffith, P.: American Society of Mechanical Engineers Paper No. 63-HT-20.
 40. Collins, R.: "A Simple Model of the Plane Gas Bubble in a Finite Liquid", J. Fluid Mech. (1965) V. 22 Part 4, 763-771.
 41. Manevi and Mendelson: "The Rise Velocity of Bubbles in Tubes and Rectangular Channels as Predicted by Wave Theory", AIChE Journal (March, 1968) V. 14, N. 2, 295-300.
 42. Hagedorn, A. R. and Brown, K. E.: "Experimental Study of Pressure Gradients Occurring During Continuous Two-Phase Flow in Small-Diameter Vertical Conduits", Journal of Petroleum Technology. (April, 1965) 475-484.
 43. Brown, R.A.S., and Govier, G.W.: "The Mechanics of Large Gas Bubbles in Tubes", The Canadian Journal of Chemical Engineering, (October, 1965) 224-230.
 44. Marrucci, G.: "Rising Velocity of a Swarm of Spherical Bubbles", Industrial Engineering Chemical Fundamentals (May, 1965), Vol. 4, No. 2, 224-225.
 45. Bhatia, V.K.: "Gas Hold-Up of a Bubble Swarm in Two-Phase Vertical Flow", A.I.Ch.E Journal (May, 1969) V.15, N3, 466-469
 46. Rader, D.W.: "Movement of Gas Slugs Through Newtonian and Non-Newtonian Liquids in Vertical Annuli", MS Thesis, Louisiana State University, Baton Rouge, LA. (May, 1973)
 47. Ward, R.H.: "Movement of Gas Slugs Through Static Liquids in Large Diameter Annuli", MS Thesis, Louisiana State University, Baton Rouge, LA. (August, 1974)
 48. Koederitz, W.L.: "The Mechanics of Large Bubble Rising in an Annulus", MS Thesis, Louisiana State University Baton Rouge, LA. (May, 1976)

49. Mathews, J.L.: "Upward Migration of Gas Kicks in a Shut-In Well", MS Thesis, Louisiana State University, Baton Rouge, LA. (May, 1980)
50. Rehm, B.: "Pressure Control in Drilling". Petroleum Publishing Co., Tulsa, Oklahoma (1970).

VITA

Son of Mr. and Mrs. Manuel Casariego, Vicente Casariego G. was born in Yautepec, Mor., Mexico, February 9, 1944.

He graduated in Petroleum Engineering, October, 1969 at the Universidad Nacional Autonoma de Mexico (Mexico).

From 1968 to 1978 he was hired by the Instituto Mexicano del Petroleo, working in the following areas:

1. Collaborator in the Reservoir Department, during one year.
2. Collaborator in the Production Department where he was involved in the following projects: (a) Pressure profiles in vertical tubes for multiphase flow; (b) Evaluation of fluids for completion and workovers of wells; (c) Study on foams and their application as circulating fluids for workovers and drilling operations. As part of this project, he constructed laboratory models for evaluation of foam and foaming agents. Also, he developed a computer model for designing foam operations. He designed and integrated an experimental equipment to generate foam. This equipment was used to realize pilot tests on the use of foam as circulation fluid on workover operations in depleted oil wells in the Southern oil fields of Petroleos Mexicanos.

He developed a foaming agent, for which the Instituto Mexicano del Petroleo obtained the licensed patent. He was assigned to Petroleos Mexicanos for training field personnel in the use of foam as a circulation fluid in workover operations, and he was in charge of the first experimental applications of foams in Mexico. The computer model and the field operations procedures were compiled in reports of the Instituto Mexicano del Petroleo.

In 1978 he began working towards his MS degree in Petroleum Engineering at Louisiana State University.

He is married to the former Ma. Teresa Hefferan and they have a four-year old daughter, Carla.